N64-28517
(ACCESSION NUMBER)
151
(PAGES)
Nasa CR 58543
(NASA CR OR TMX OR AD NUMBER)
(THRU)
1
(CODE)
24
(CATEGORY)
FACILITY FORM 602

MHD research, inc.

POST OFFICE BOX 1815, NEWPORT BEACH, CALIFORNIA

DESIGN AND PERFORMANCE STUDY ON A 500 KILOWATT LINEAR CROSSED-FIELD AIR-PLASMA ACCELERATOR FOR A RE-ENTRY SIMULATION FACILITY

Report on Twelve Month Program
to
Ames Research Center
NASA
Moffett Field, California
on
Contract NAS2-1170
Control No. 37680001

by
MHD RESEARCH, INC.
P.O. Box 1815
Newport Beach, California
and
NORTHROP SPACE LABORATORIES
The Northrop Corporation
3401 West Broadway
Hawthorne, California

OTS PRICE
XEROX $ 11.50 ph
MICROFILM $

18 March 1964

MHD Report No. 648

SGY 11445

ACKNOWLEDGEMENT

This report was prepared on the basis of information generated at MHD Research, Inc. and the Northrop Corporation, operating on sub-contract to MHD Research, Inc. The following individuals participated in the report preparation:

R. C. Brumfield, Principal Investigator, MHD Research, Inc.

S. Demetriades, Consultant to MHD Research, Inc.

P. D. Lenn, Principal Investigator, Northrop Corporation

D. L. Ward, Engineer, Northrop Corporation

G. Bedjai, Engineer, Northrop Corporation, formerly with MHD Research, Inc.

The early phases of the program at the Northrop Corporation were directed by S. Demetriades.

28517

ABSTRACT

The design and performance of two models of 500 kw linear crossed-field air-plasma accelerators is described. The electromagnetic design, materials selections and configuration are included. The results of seven full-scale operating tests on the two accelerator configurations are given. The performance requirements are to accelerate an air stream of 0.01 pounds per second to a velocity of 25,000 feet per second with a steady, uniform velocity to within 5 percent over a core flow area of 0.2 square feet for a period of five minutes and with less than 1 percent contamination.

Experiments were run by heating and accelerating with an arc plasma generator and de Laval nozzle. The resulting supersonic jet was fired into an expanding accelerator channel with transverse, serial electrode discharges and a perpendicular applied magnetic field. Good success was obtained with all accelerator components except the sidewalls near the accelerator entrance. These were repeatedly destroyed by arc attachment, preventing steady-state operation with high Lorentz forces. Destruction was probably induced by the application of excessively high B fields at the first electrode pair.

Suggestions for avoiding the problem and recommendations for further work are outlined. The report discusses supporting experiments on the plasmajet, nozzles, electrodes, electrode holders, sidewalls, supersonic nozzle and the instrumentation used or studied for use on the program.

Significant success was obtained in the design of electrodes and other critical accelerator components. Further work is required to integrate these components into a successful accelerator.

Author

Preliminary studies of a 10 Mw linear crossed-field accelerator indicates that such an accelerator is presently feasible. This accelerator would accelerate 0.1 pounds per second of air at 40,000 feet per second.

TABLE OF CONTENTS

TABLE OF CONTENTS (continued)

LIST OF ILLUSTRATIONS

LIST OF ILLUSTRATIONS (cont'd)

LIST OF ILLUSTRATIONS (cont'd)

LIST OF TABLES

1. INTRODUCTION

1.1 BACKGROUND

This report describes the results of a twelve-month program on the development of a 500 kw linear crossed field (electromagnetic) air plasma accelerator for use in simulating atmospheric re-entry in a flow facility. The primary objective has been to accelerate 0.01 pounds per second of unseeded air to a velocity of 25,000 feet per second with a velocity ratio of at least two across the accelerator. A run duration of at least five minutes is specified, with contamination held below 0.1 percent by weight in the core flow. The core flow was to be expanded to an area of at least 0.2 square feet at a pressure altitude below 300,000 feet. The velocity variation with time or distance in the test core was to be less than 5 percent. These requirements are summarized in Table 2.1. Written recommendations for the development of an accelerator system with a minimum mass flow of 0.1 pounds per second of air and an exit velocity of 40,000 feet per second are required.

1.2 RELATION TO NASA PROGRAM

This program has provided information on the design, operation and performance of accelerators for use in facilities for simulating high velocity atmospheric re-entry, an integral part of NASA program requirements. The linear crossed-field accelerator is the most promising device for producing the plasma flow velocities required for a substantial period of time in the pressure range of interest here.

1.3 METHOD OF APPROACH

Both free-jet and confined accelerators have been operated extensively. The confined type with uniform cross section does not operate efficiently due to wall and electrode viscous drag and shock and heat losses to the walls and electrodes. Free-jet configurations have been successfully built in the velocity regime of interest, but test section pressure and velocity cannot be adequately controlled in the free jet. For most applications a closed, expanding channel configuration is probably the best compromise. The present program was devoted to designing, building and testing a closed, expanding accelerator to power and mass flow requirements described above. The development was based on pre-acceleration with a plasma jet, acceleration by crossed fields in an expanding channel, and post-expansion of the supersonic flow to achieve the test condition (Figure 1.1).

1.4 ORGANIZATIONAL RELATIONSHIP

Northrop Space Laboratories undertook the design, fabrication and testing of a linear crossed-field accelerator sub-system for MHD Research, Inc. on a best effort basis to meet the objectives outlined above. MHD Research, Inc. undertook to supply the plasma generator and associated instrumentation, magnet, materials required for accelerator fabrication, and diagnostic instrumentation and to provide overall supervision and direction for the program.

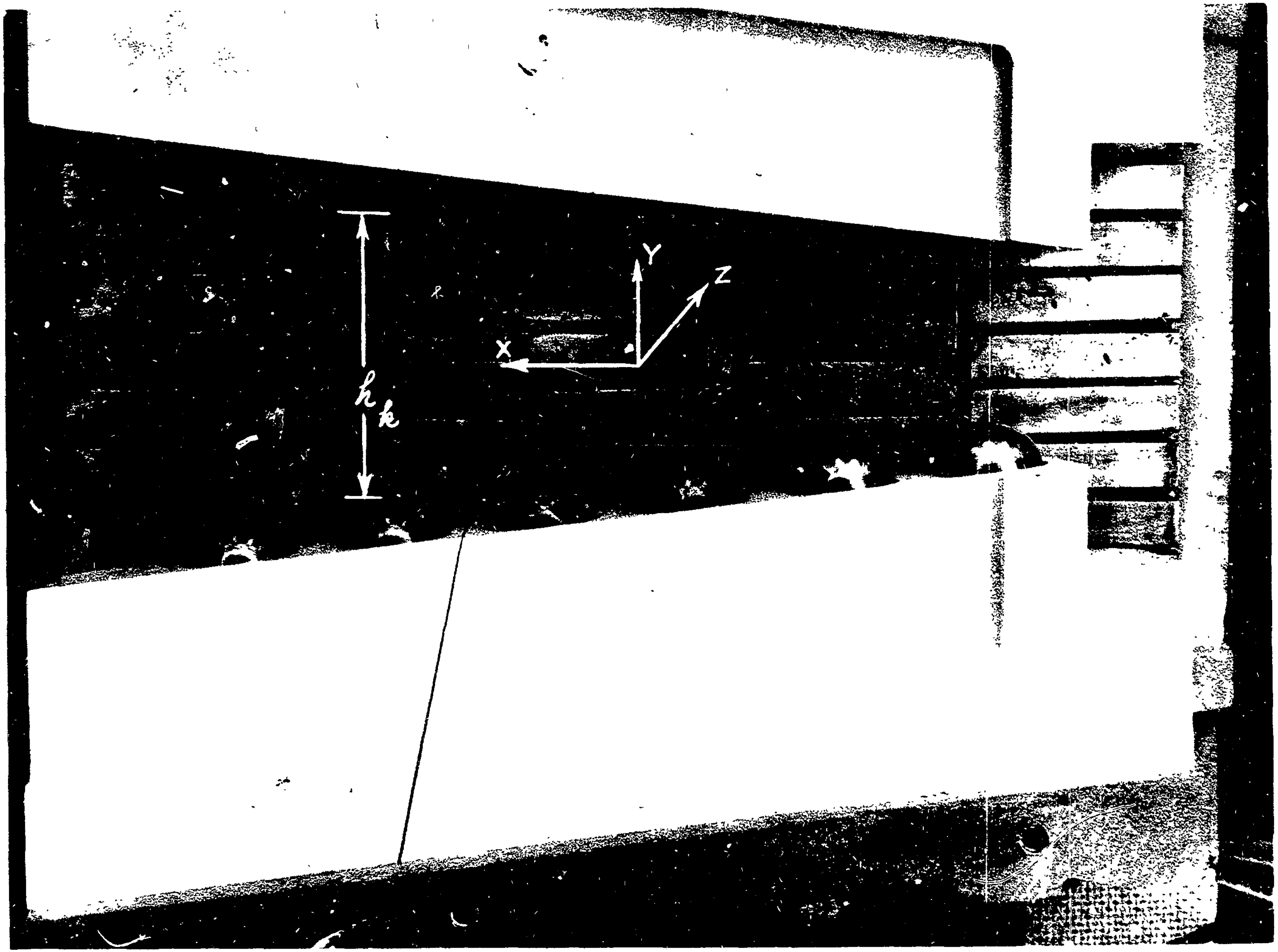

Figure 1.1 Photograph of the CA-2 linear crossed-field accelerator

2. SUMMARY OF RESULTS AND CONCLUSIONS

A one-dimensional idealized analysis of accelerator performance was performed to select operating conditions under which the goals of the program could be reached. The analysis is described in detail in Section 3. The analysis formed the basis for the selection of values for the electrode gaps, the applied currents and the applied magnetic field which it was estimated would lead to the required acceleration of the stream. The most involved calculation in the analysis is that leading to a prediction of the resistance losses between electrodes in the accelerator (see also References 1, 2 and 3).

On the basis of the analysis and previous experience the following ranges for the design variables were chosen:

Magnetic field	$0 \leq B \leq 2000$ gauss
Current per electrode pair	$0 \leq I_k \leq 500$ amperes
Channel pressure	$1 \leq p \leq 10$ mm Hg
Electrode gap	$h_i \approx 0.05$ m

Figure 2.1 shows the scalar conductivity of air as a function of temperature. Figure 2.2 shows the ion slip coefficient for air as a function of temperature at a pressure of 4.55 mm Hg. Figure 2.3 shows the ion slip coefficient for air as a function of temperature at a pressure of 15.2 mm Hg. Figure 2.4 shows the enthalpy of air at equilibrium as a function of equilibrium temperature. The data in these figures were used to make subsequent computations.

Calculations of the operating characteristics of the accelerator were performed for several sets of conditions which would lead to attainment of the performance goals given in Table 2.1. The results are given in Tables 2.2 through 2.7. These calculations of the resistive drop across the first electrode-pair are compared with experimental results in Figure 2.5. A comparison of predicted velocity increments is given in Figure 2.6.

The theoretical calculations and the selected ranges of the independent parameters of accelerator operation were used as a guide for determining the major features of an experimental device for the program. The specific design problem areas for the accelerator were divided into the following groupings: anodes, cathodes, electrode holders, sidewalls and exit nozzle, and the selection of materials. These are discussed in Section 4. To test possible solutions to these problems a series of component tests were performed. First, tests with a single pair of electrodes operating in an unconfined channel were performed to select the best anode materials. It was found that sintered mixtures of tungsten and copper and of tungsten and silver performed satisfactorily. No evidence was found of the formation of oxides on the electrodes. The anode configuration shown in Figures 2.7 and 2.8 was selected on the basis of previous experimental experience. In the electrode tests, an uncooled block of tungsten was used as the cathode. The cathode also performed satisfactorily until melting of the uncooled block occurred. Thus, it was decided that thoriated tungsten caps mounted on a water-cooled copper base would be used in CA-1. The cathode design is shown in Figure 2.9. The operating conditions for the electrode tests are given in Table 2.8.

Since the sidewall of a confined accelerator is subjected to extreme heat loads, it appeared that the use of water-cooled metallic elements would be necessary to keep the sidewall from ablating during operation of the accelerator. The specific problems of sidewall design are discussed in Section 4.7. The presence of metallic elements on the sidewall introduces the possibility of arc attachment to the wall. To reduce the voltage drop which could drive current through conducting paths in the sidewall and thus to prevent arc attachment, it is necessary to electrically isolate each of the metallic elements. The initial sidewall design concept was tested using the single electrode-pair accelerators shown in Figures 2.10 through 2.16. The operating conditions under which those sidewalls were tested are given in Tables 2.8 and 2.9. The success of these sidewalls, particularly of those used in the confined channel accelerator shown in Figures 2.12 through 2.16, indicated that enough confidence could be placed in the design to justify its incorporation into the first accelerator.

The electrode holders and the adapter between the arc jet nozzle and the accelerator channel were made of boron nitride. This material had been used in previous accelerators and found to behave rather well for such applications. A water-cooled exit nozzle for the accelerator was designed. The major consideration in the exit nozzle design was to avoid the presence of continuous conducting paths which might enhance arc attachment to the cooling elements.

The components and the final assembly of the accelerator model CA-1, are shown in Figures 2.8, 2.9 and 2.17 through 2.21. The accelerator was installed in the test facility shown in Figure 2.22. Four tests were performed with the accelerator model CA-1. The tests were at power levels below the design point and are described in detail in Section 6.

While the tests of CA-1 were being performed, the design and construction of a second accelerator, CA-2, was begun. Minor changes from the CA-1 design were introduced by Northrop Space Laboratories into the CA-2 design on the basis of the data available at the time. Among the changes were the use of six electrode-pairs, the reduction of the sidewall element height to one-half inch, the use of parallel sidewalls and the use of pointed rather than rounded tungsten caps for the cathodes. The CA-2 accelerator is shown in Figures 2.23 and 2.24. The tests performed with CA-2 are described in detail in Section 6.3.

The experimental results for accelerator operation obtained during the present program are given in Tables 2.10, 2.11 and 2.12. Salient features of these results are the following:

(a) The anode design and choice of materials was entirely satisfactory.

(b) The short rounded thoriated tungsten cathode caps permitted the discharge to attach at the solder joint between the cap and the copper base, which caused two of the caps to become detached during the fourth test. Conically-pointed cathode caps were used in Model CA-2 and found to be satisfactory under the conditions tested.

(c) The boron nitride adapter between the arc jet and the accelerator inlet performed satisfactorily under all conditions tested.

(d) The erosion of the boron nitride electrode holders was fairly severe at first but the rate of erosion decreased markedly once they had been worn in. The arc attachment at the upstream side of the cathodes and at the downstream side of the anodes causes the electrode holder to ablate so as to form wells at those locations. The wells appear to reach a stable depth after just a few minutes of operation.

(e) The accelerator exit nozzle performed satisfactorily under all conditions tested.

(f) The experimental facility including the pendulum-type thrust dynamometer performed satisfactorily after early difficulties were overcome.

(g) The velocity increments produced by the accelerator were lower than those corresponding to the total Lorentz force but were greater than fifty percent of the values predicted on the basis of the idealized theory.

(h) In the fourth test a velocity increment of 4500 feet per second was obtained with the accelerator. The results of the fifth test in which the dynamometer reading indicated a velocity increment of 22,600 feet per second were questionable because arc attachment to the sidewall occurred almost simultaneously with the application of a magnetic field strength of 2000 gauss.

(i) The major obstacle to systematic testing of the linear crossed-field accelerator was the problem of arc attachment to the water-cooled, metallic elements forming the channel sidewall. The sidewall elements were apparently adequately cooled for normal operation, although full-power operation was not achieved. They were not sufficiently well cooled to withstand arc attachment. This could probably be done, but would not solve the arc-attachment problem, only reduce the damage. The basic problem should be avoided or solved.

On the basis of the present investigation it is not possible to demonstrate conclusively the feasibility of using a crossed-field accelerator as a wind tunnel driver for steady-state operation. It was demonstrated that an increase of the impulse function of the stream corresponding to a velocity increment of 4500 feet per second could be achieved and that steady-state operation at an applied power level of 200 kw could be achieved in an air accelerator using a mass flow rate of 0.01 pounds per second. The calculated velocity-increments are, however, questionable because adequate pressure measurements were not made or used in correcting the thrust measurements to determine the momentum flux and average velocity increment.

Arc attachment to the sidewall near the entrance to the channel was the major operational problem. The rapid failure induced prevented refined measurements and a conclusive demonstration of adequate acceleration.

Two corrective actions are feasible:

(a) Refinement of sidewall design

(b) Reduction of the B field at the accelerator entrance

Although the former would constitute a valuable development, the latter approach is adequate and more practical at this stage of the development. Unfortunately, time did not allow the second to be tried.

A close scrutiny of Figures 2.27 through 2.29 reveals that it is most likely that the exit nozzle was not completely filled during Test No. 2, i.e. that the jet was overexpanded and the tank pressure of 0.7 mm Hg was probably higher than the nozzle exit design pressure for that test. As a consequence the thrust measured during that test was probably all due to a velocity increase of the stream. It is impossible to make a conclusive statement about the other tests (which involved higher power levels) since no similar pictures were taken at the conclusion of the other tests and the exit static pressures were not measured. No pressure measurements were taken at the exit of the accelerator channel or the nozzle exit to ascertain whether the measured thrust increment was entirely the result of an increase in air plasma velocity in all the tests. These measurements were scheduled but not accomplished because of sidewall failure.

Recommendations for a research and development program for an accelerator system with a minimum mass flow of unseeded air of 0.10 pounds per second and velocity of 40,000 feet per second are presented in Section 9 of this report.

In addition to this recommended program and design, Reference 5 entitled "Method for Optimizing the Design of Linear Crossed Field Accelerators" accompanies this report. It is felt that Reference 5 satisfies a pressing need for a tractable analytical model of cross-field plasma accelerators for use in the design and development of such equipment intended for hyperthermal wind tunnels and space propulsion.

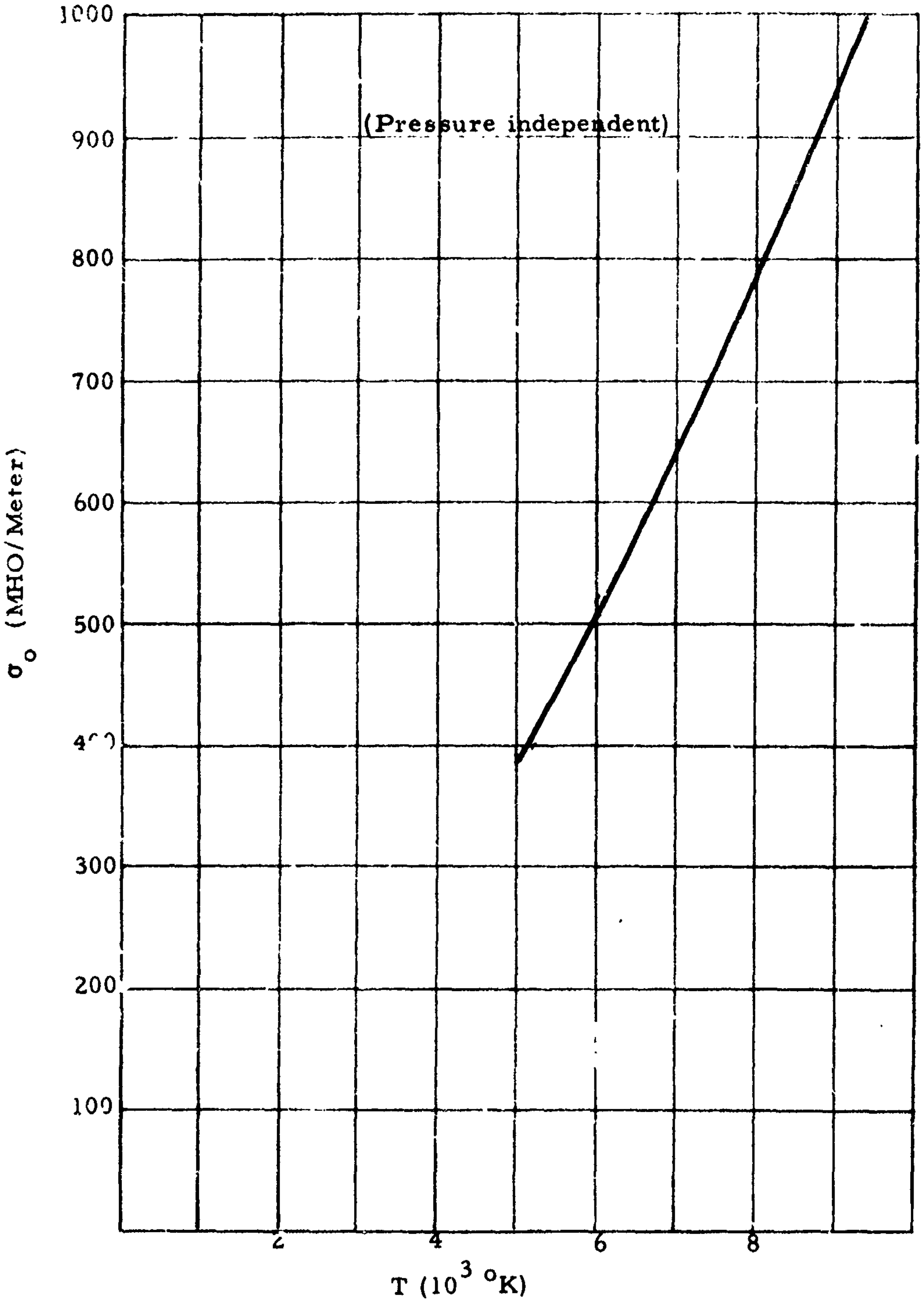

Figure 2.1. Scalar electrical conductivity of air vs. temperature.

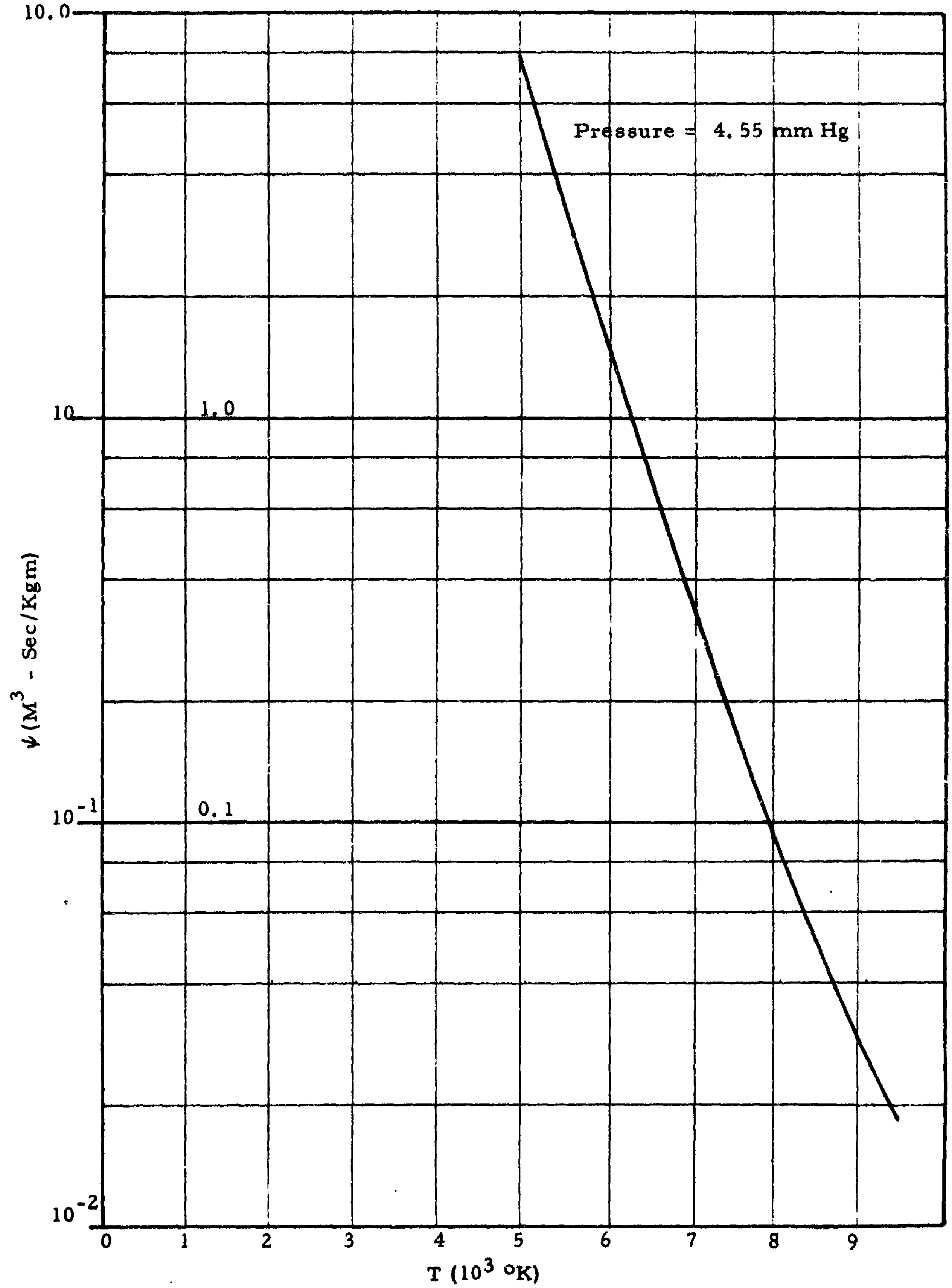

Figure 2.2. Ion slip coefficient of air vs. temperature.

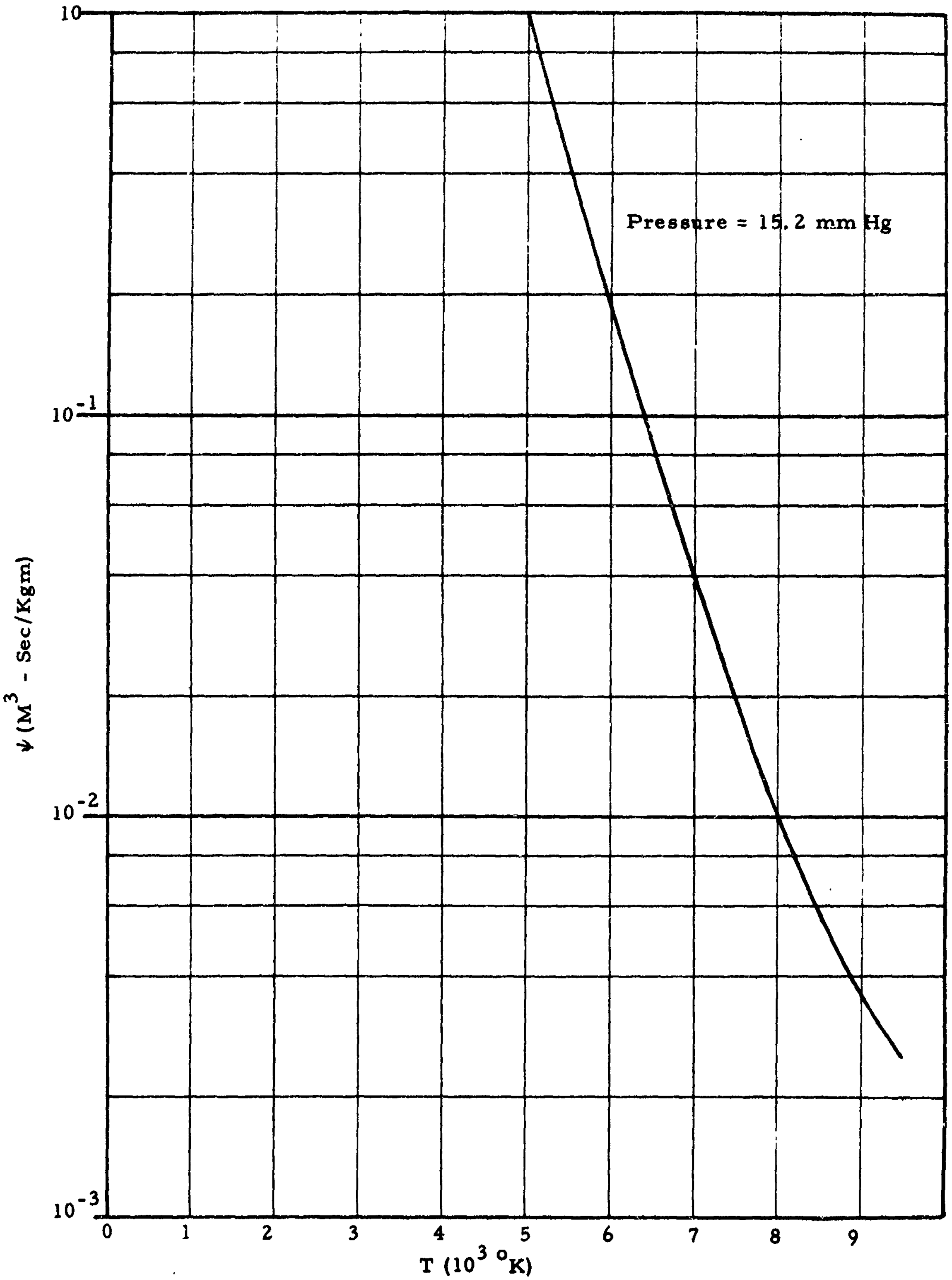

Figure 2.3. Ion slip coefficient of air vs. temperature.

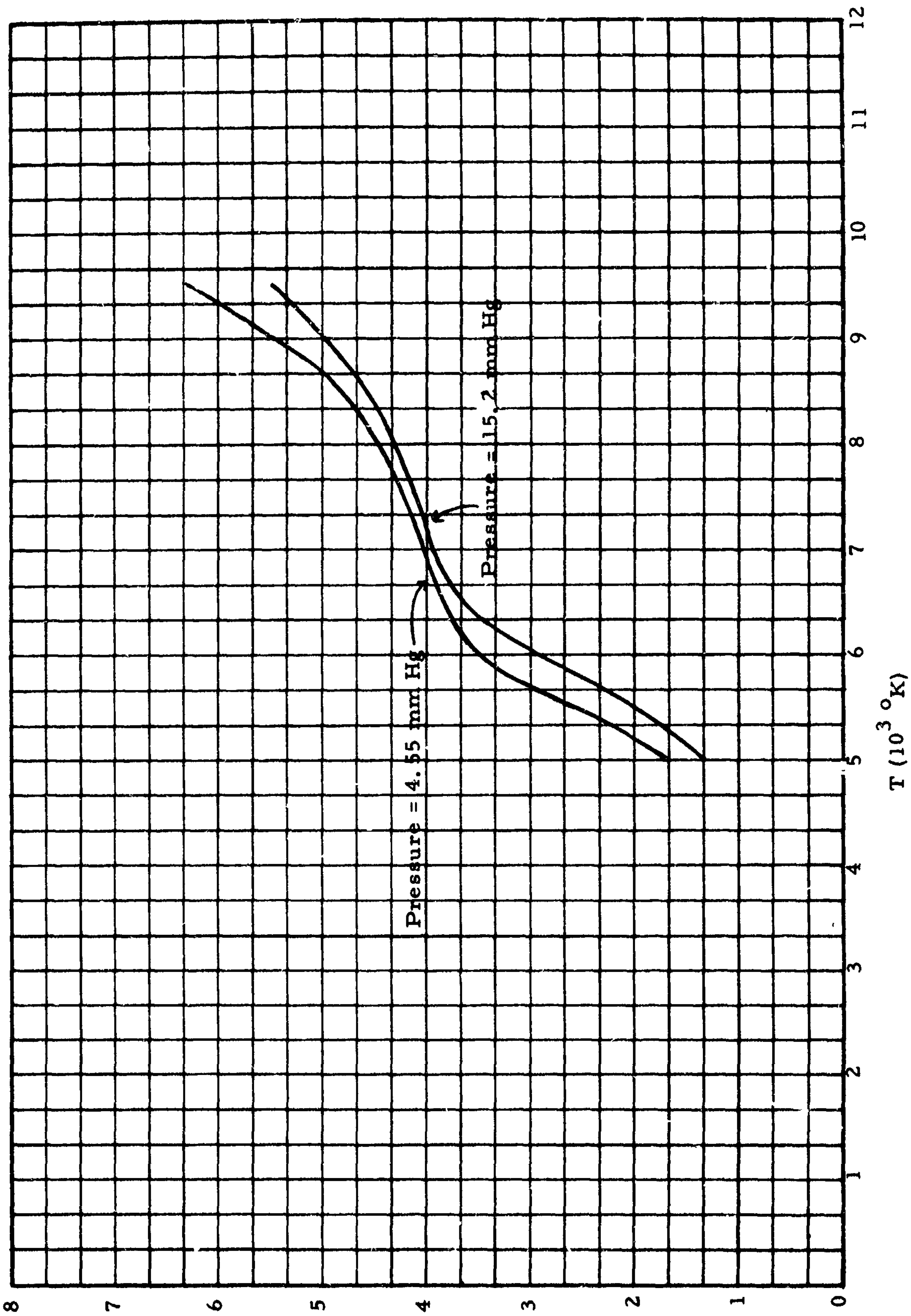

Figure 2.4. Enthalpy of air vs. temperature

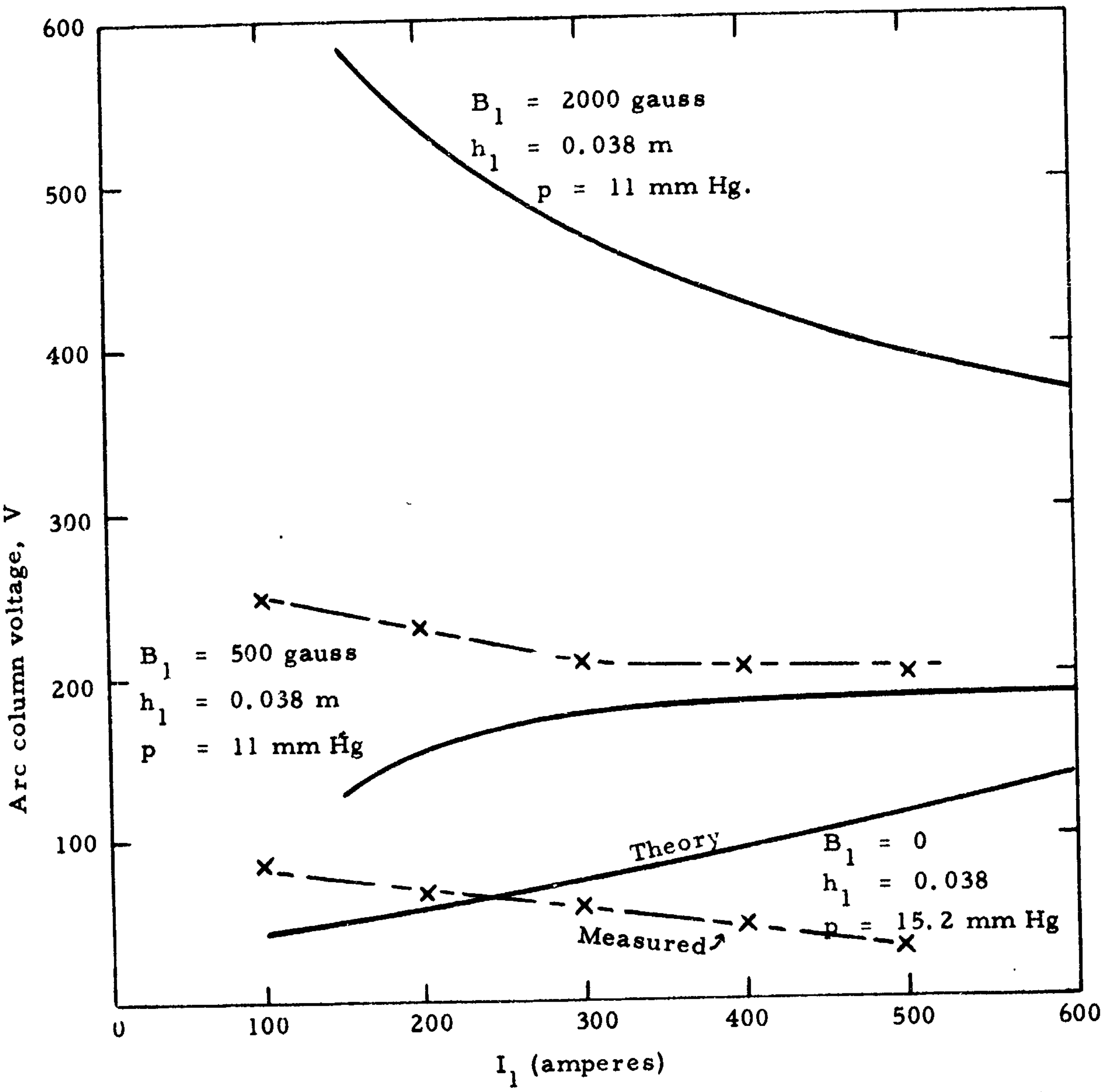

Figure 2.5. Voltage - current characteristics of an accelerator with one electrode pair.

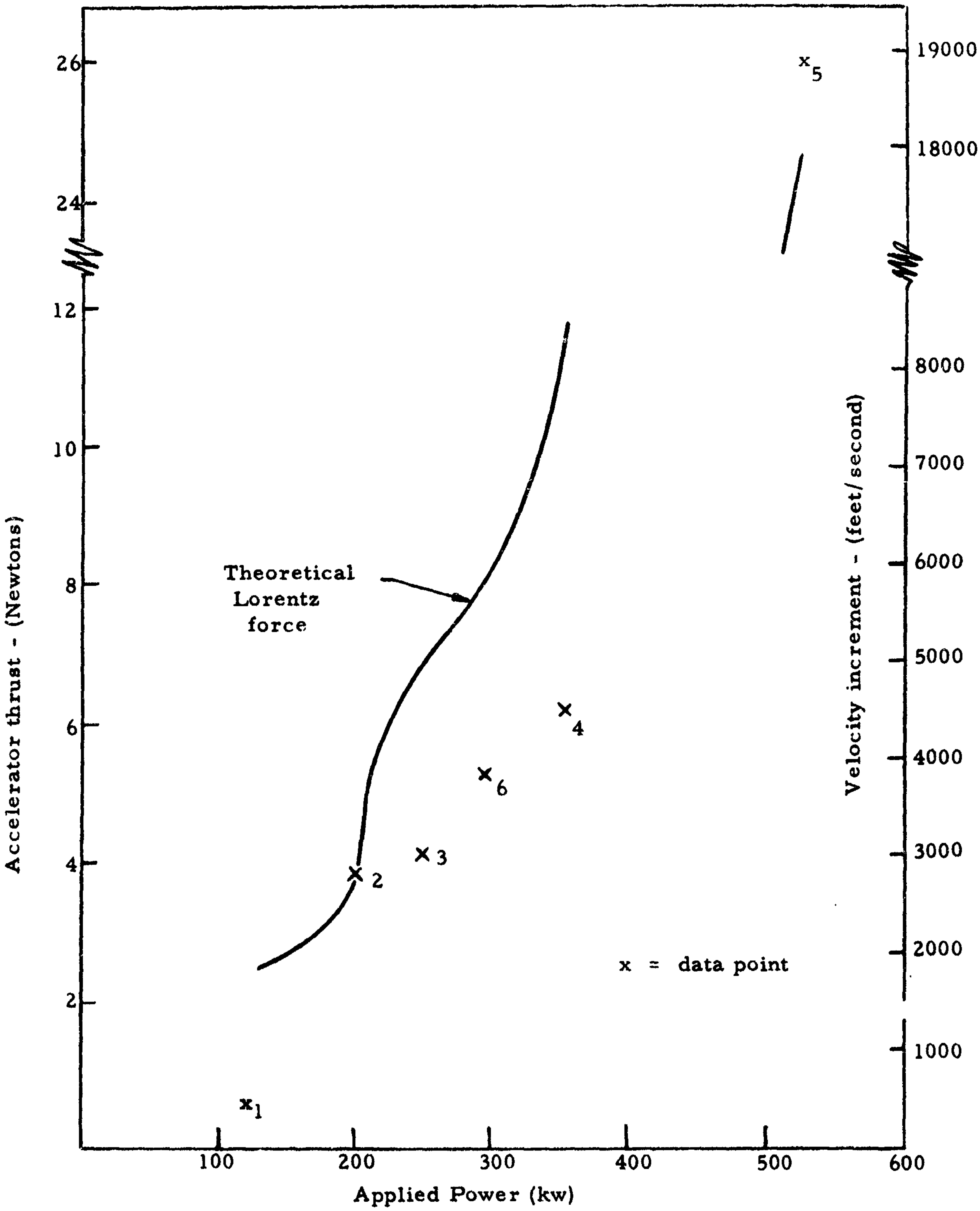

Figure 2.6, Experimental results for velocity increment obtained with a confined channel Lorentz accelerator. Mass flow rate of air = 4.5 gr/sec. No pressure correction.

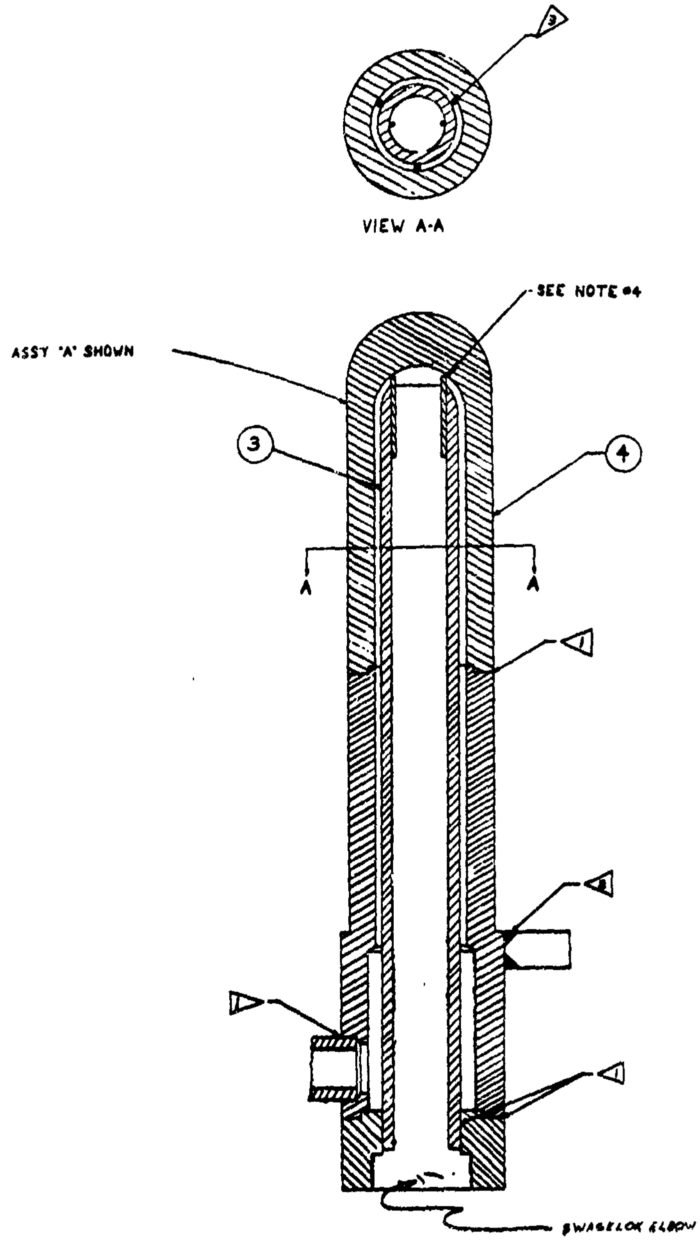

1 MATING SURFACES JOINED WITH SILVER SOLDER

2 DOUBLE-BEVEL BRAZE

3 B&S GAUGE NO. 18 (.0400) - TYP -- 3 WIRES SILVER SOLDERED TO TUBE (CAI-2-G) FOR POSITIONING INSIDE CAI-2-B. FIGURE.

4 SPACER RODS ARE TO TOUCH CAP END ON ASSEMBLY, AS SHOWN.

Figure 2.7. Assembly drawing of the water cooled anode design

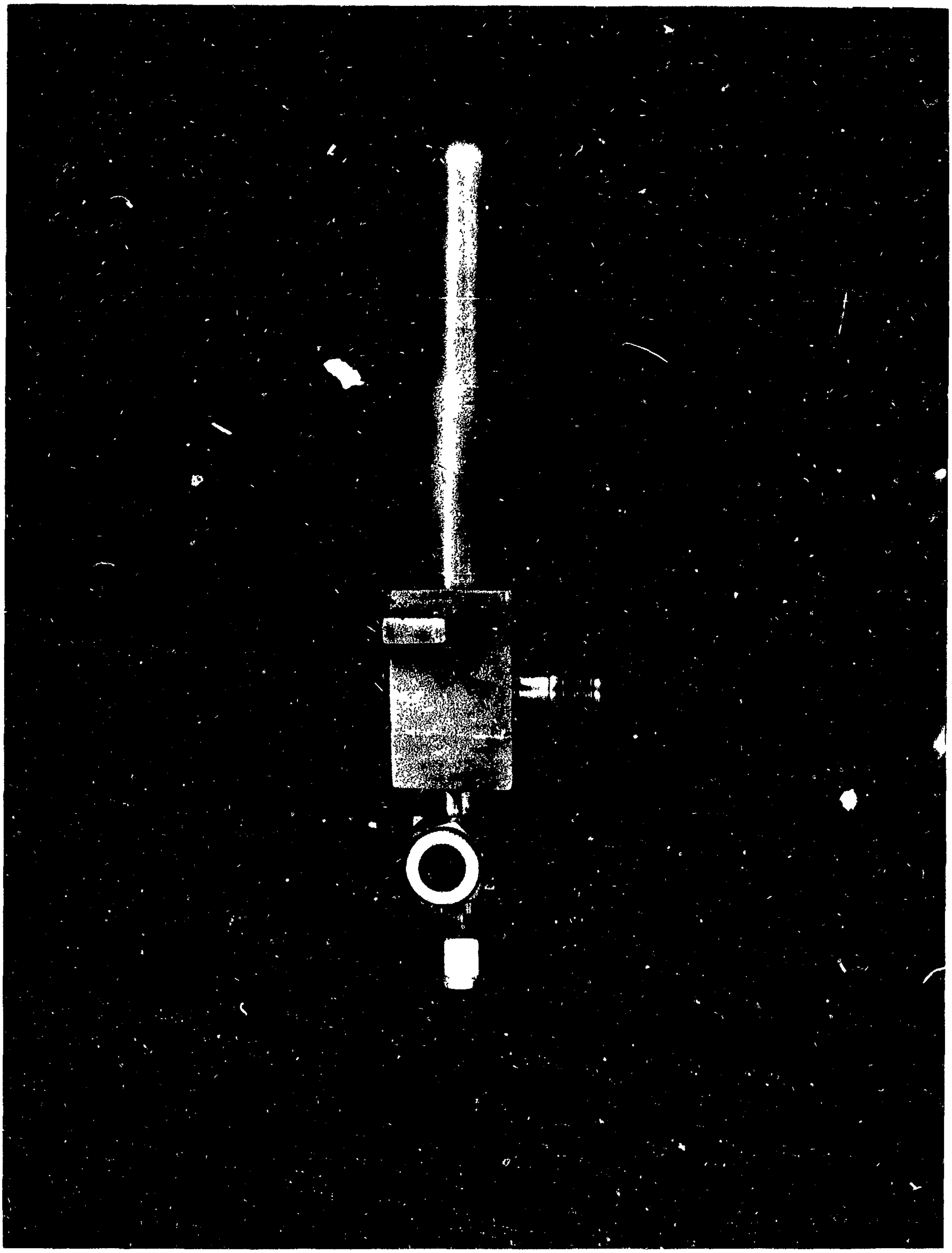

Figure 2.8 View of an accelerator anode with 10 W3 copper elkonite cap

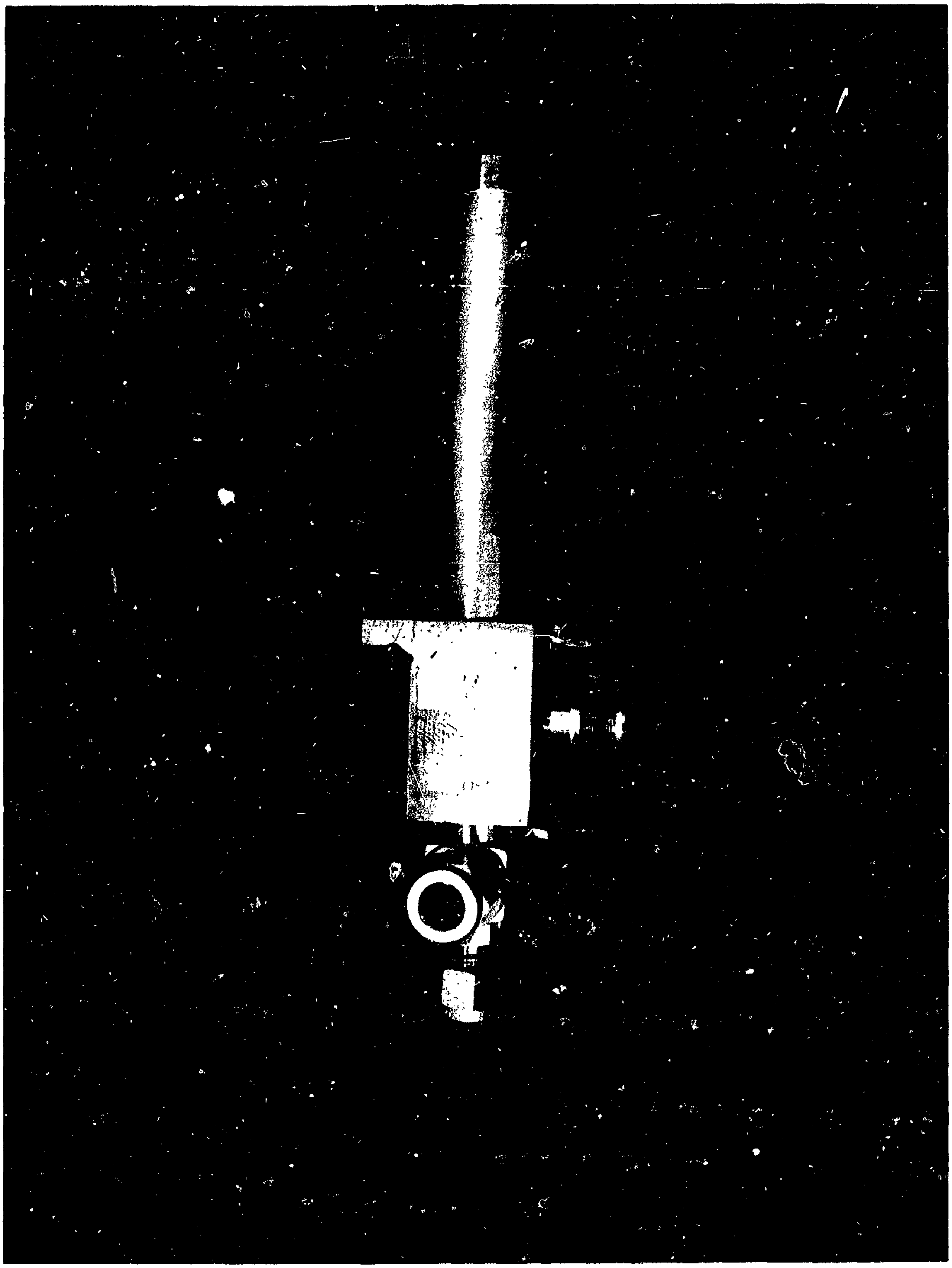

Figure 2.9 View of CA-1 accelerator cathode with tungsten cap

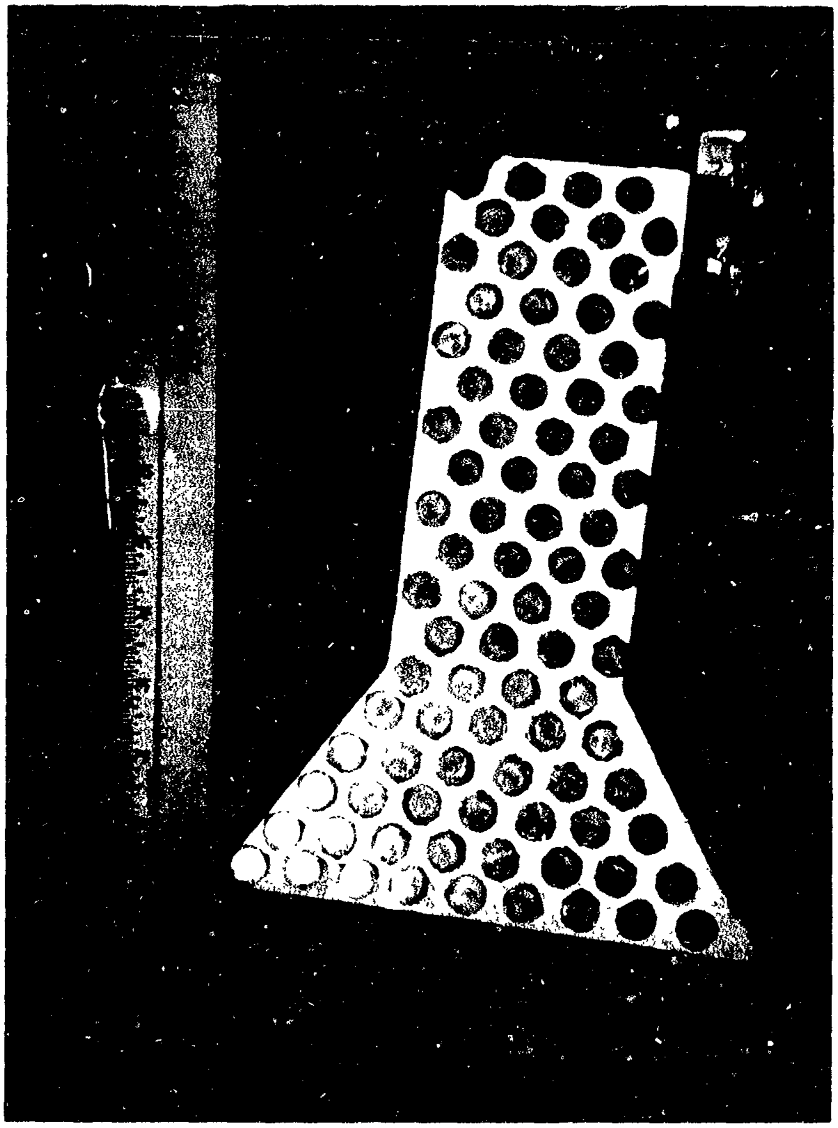

Figure 2.10 Segmented sidewall composed of brass studs and zirconia insulator

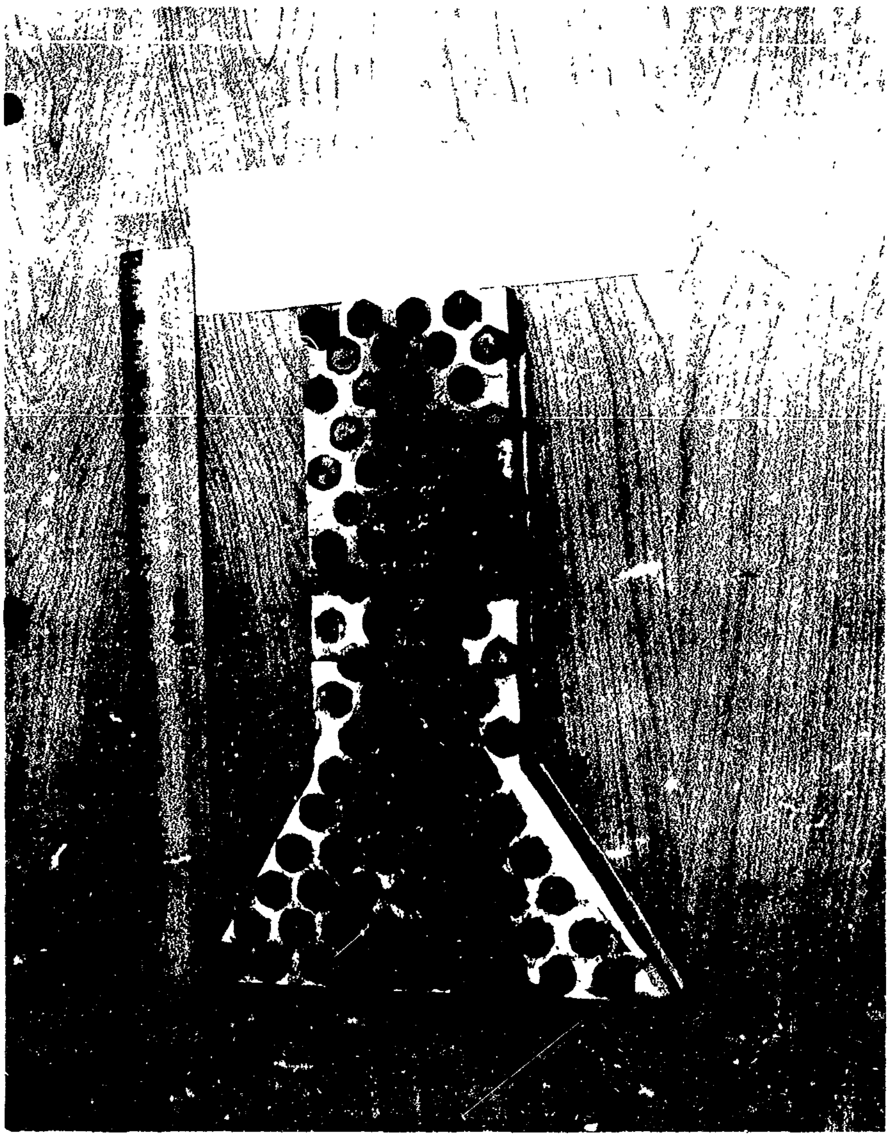

Figure 2.11 Uncooled segmented sidewall after the tests

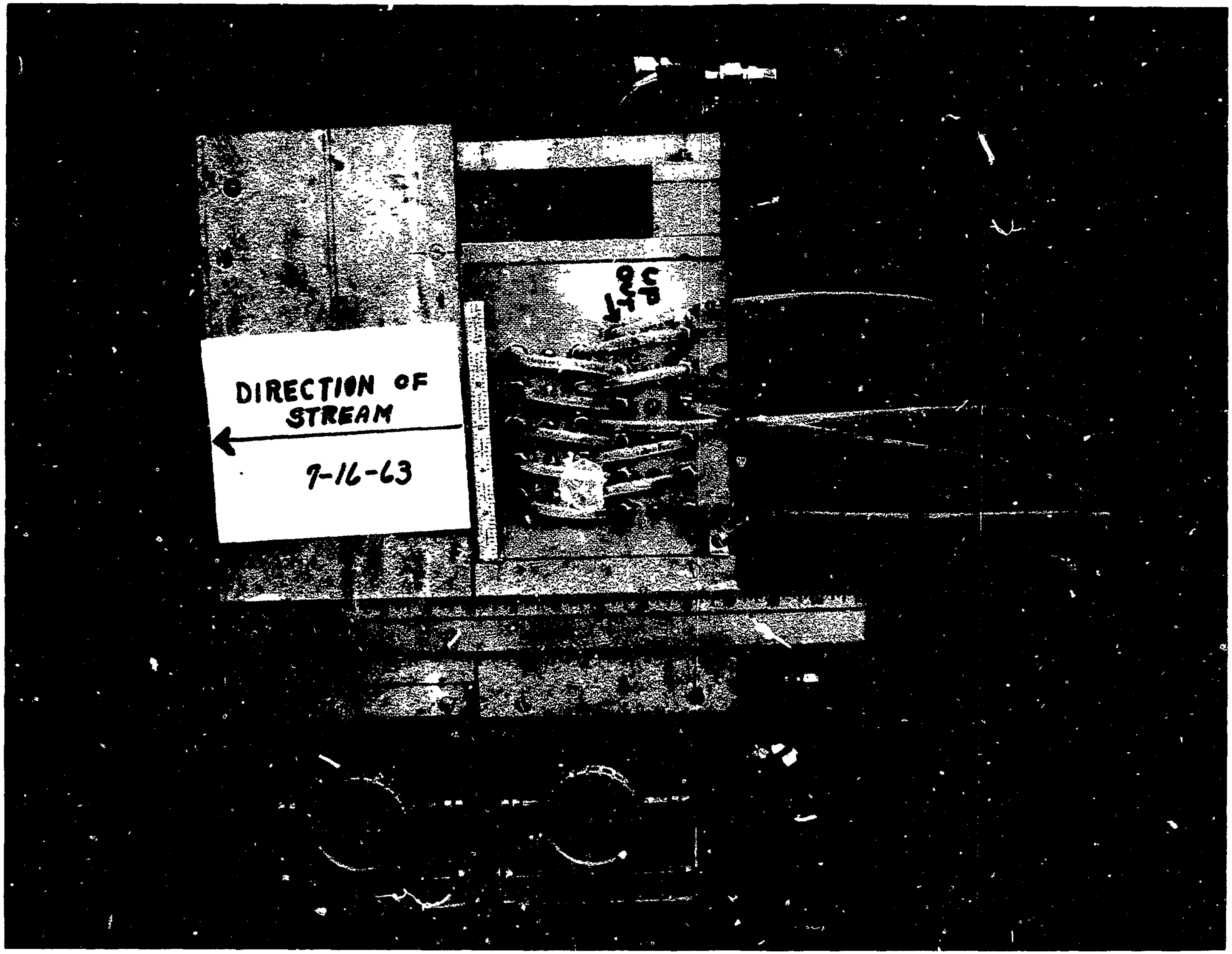

Figure 2.12 View of the preliminary single electrode-pair accelerator with the cooled portion of the sidewall in position

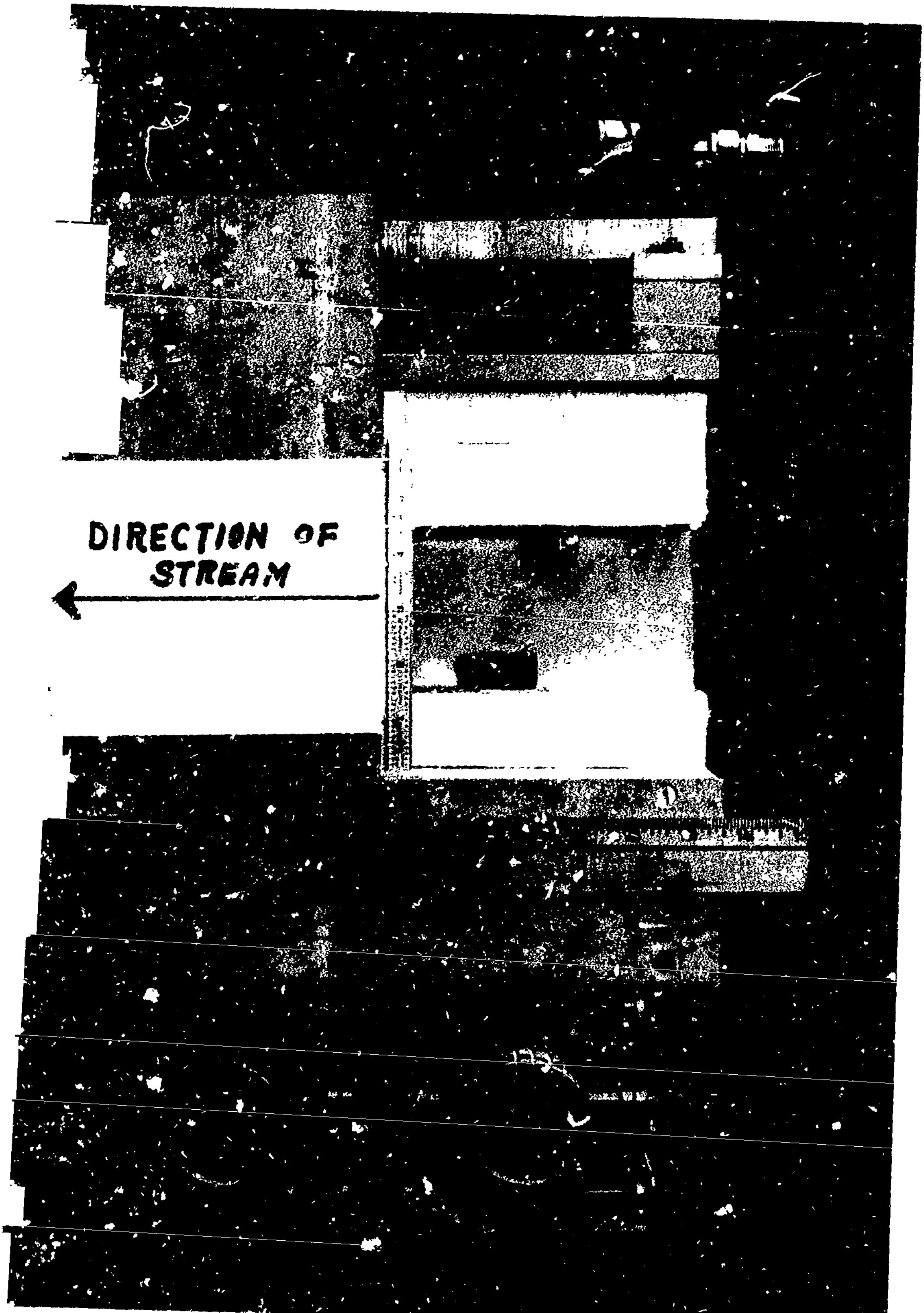

Figure 2.13 View of the preliminary accelerator with the cooled portion of the sidewall removed

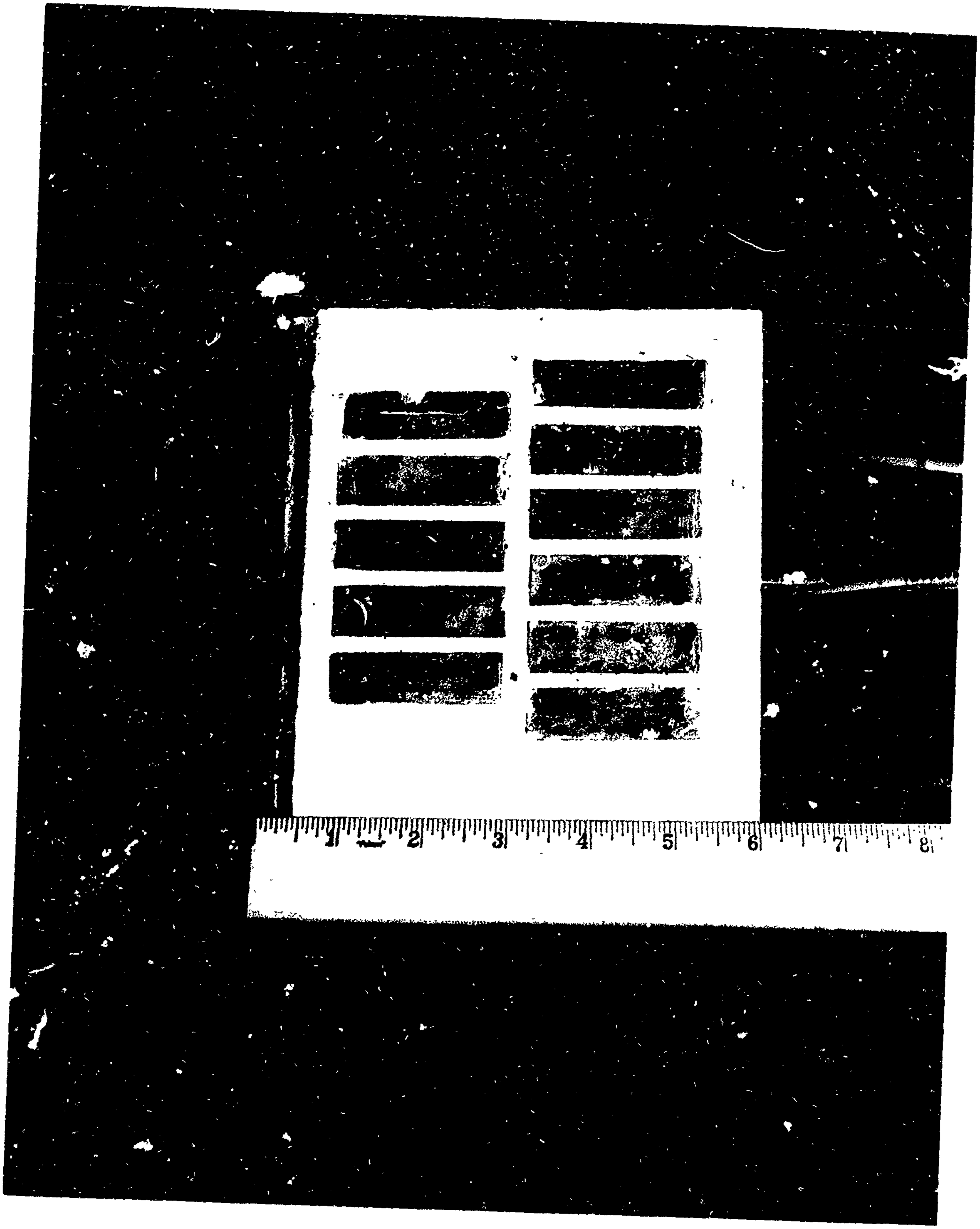

Figure 2.14 Sidewall cooling bars embedded in zirconia for preliminary accelerator.

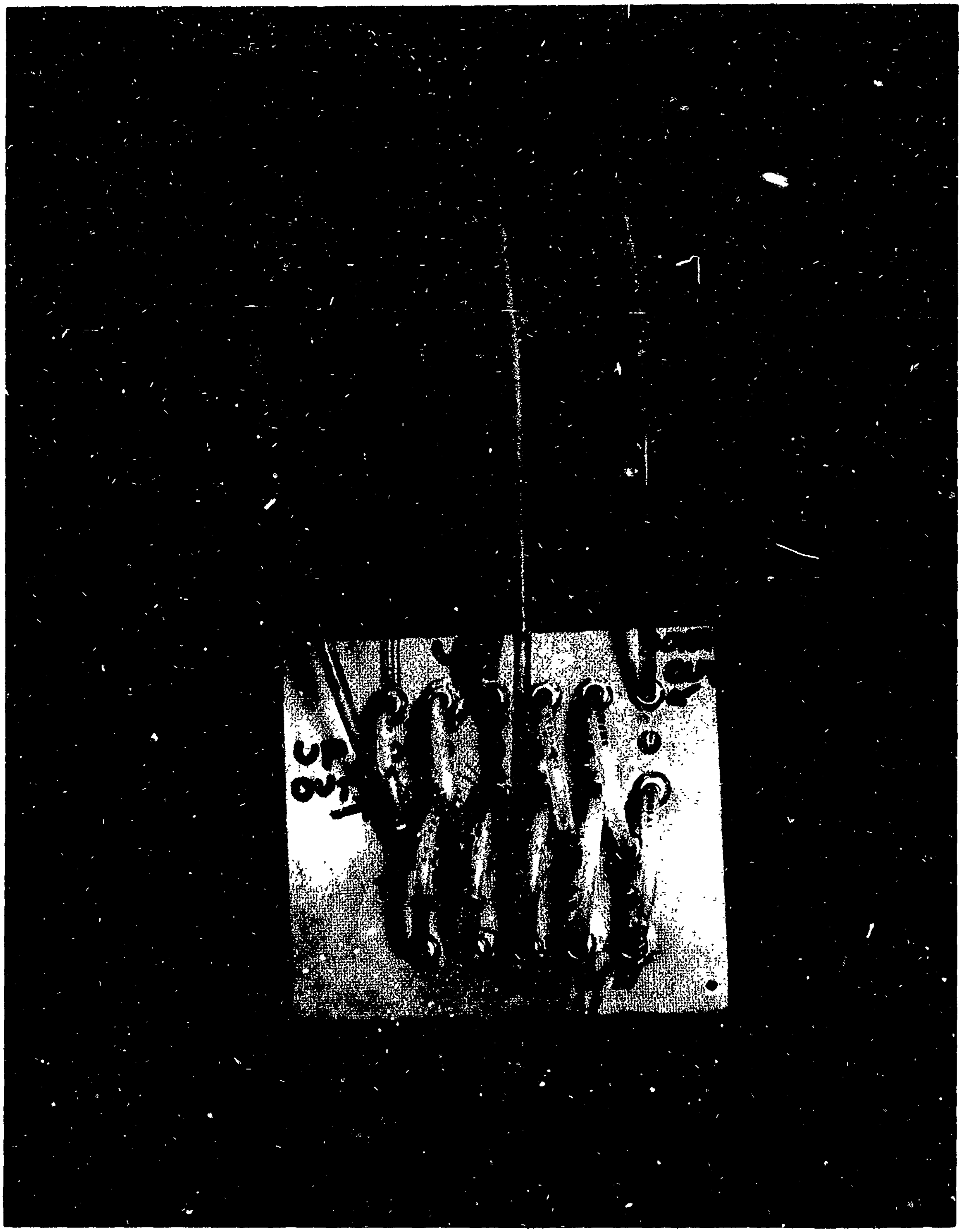

Figure 2.15 Rear view of cooled sidewall showing water manifolds

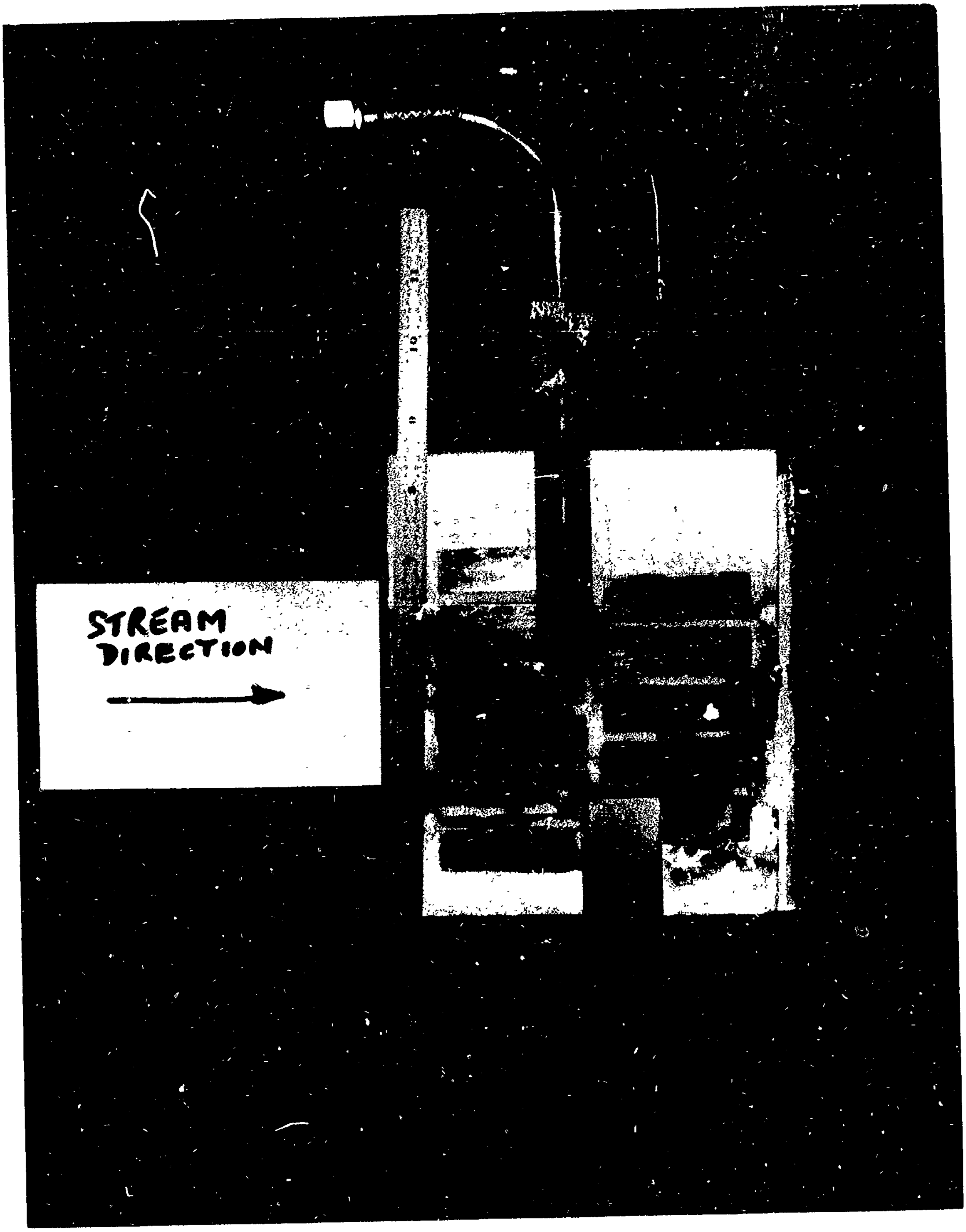

Figure 2.16 View of the cooled sidewall after testing. The electrodes are shown to indicate their positions during the tests

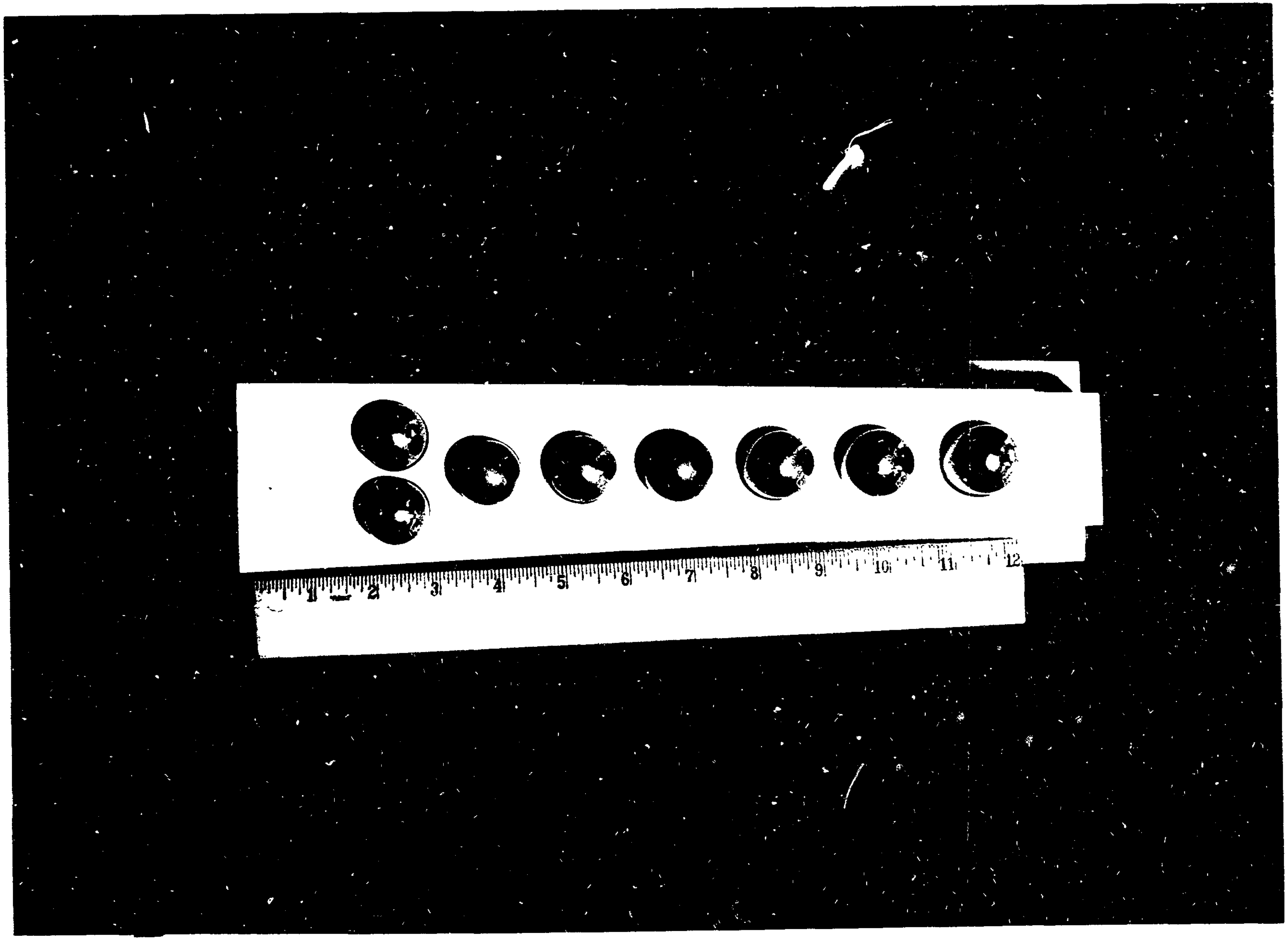

Figure 2.17 View of the anode holder block of accelerator CA-1 with the electrodes in position

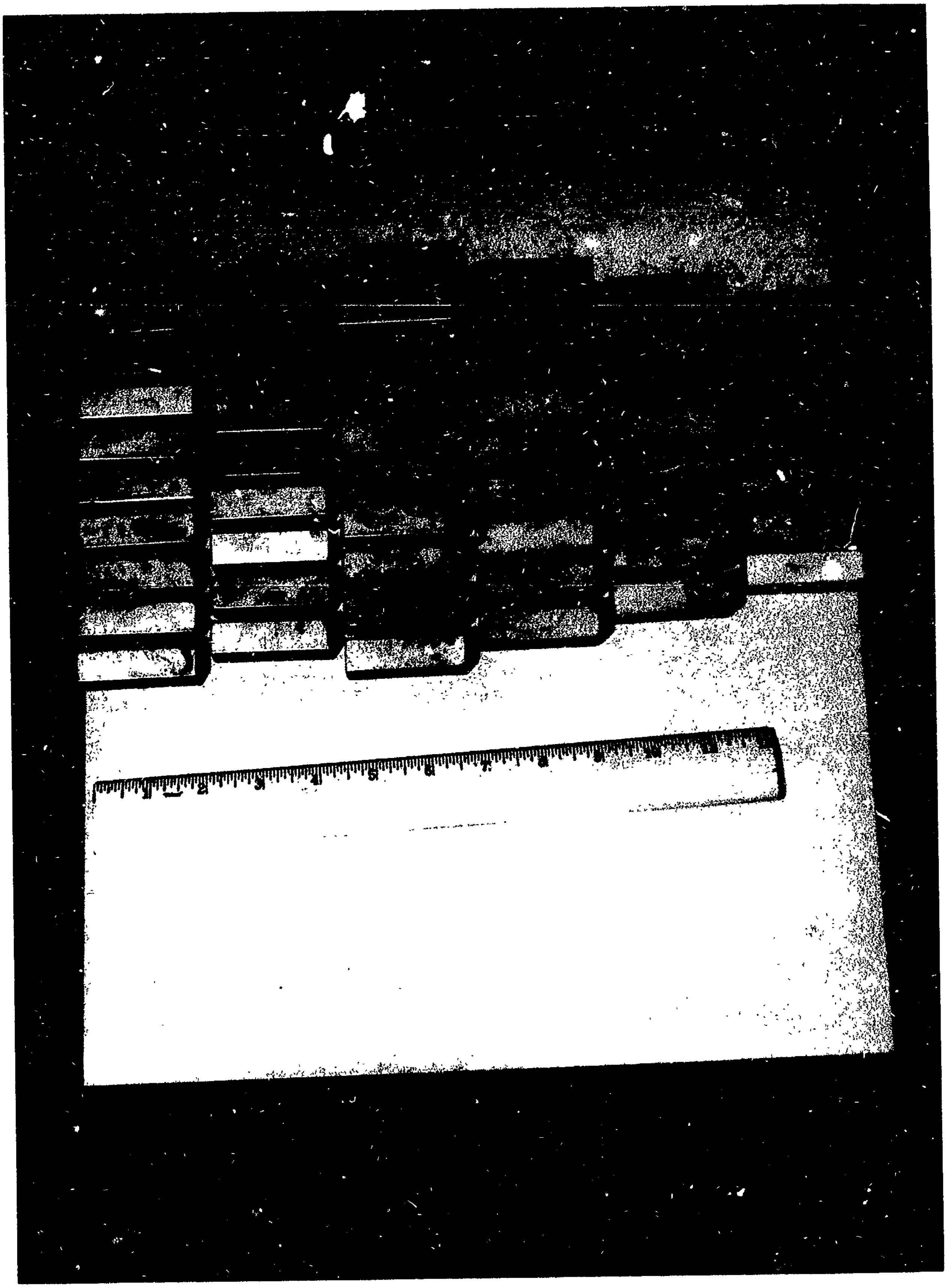

Figure 2.18 View of the left sidewall of accelerator CA-1 prior to application of the zirconia ceramic in the interstices between the cooling bars

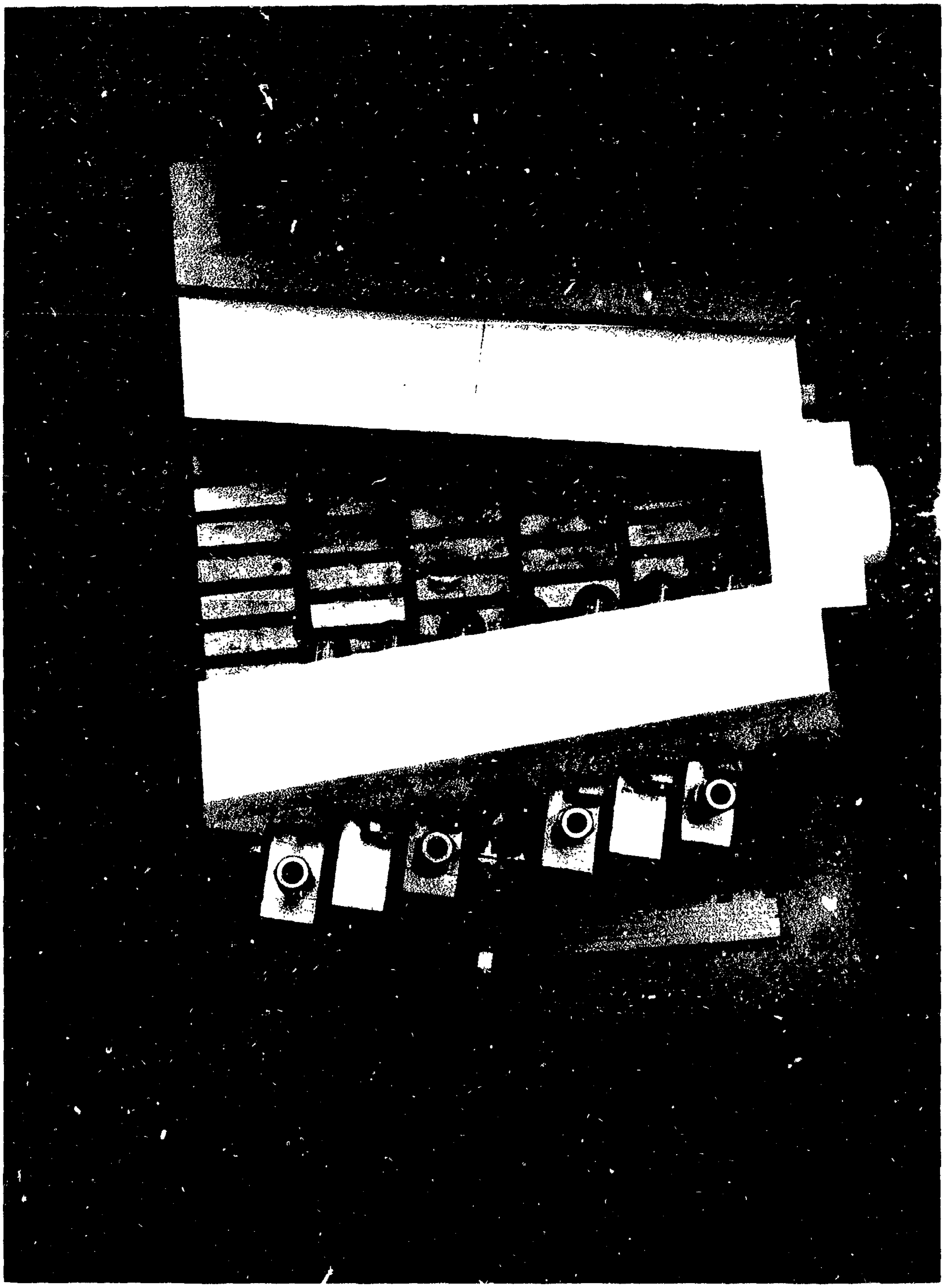

Figure 2.19 View of the CA-1 accelerator, partially assembled

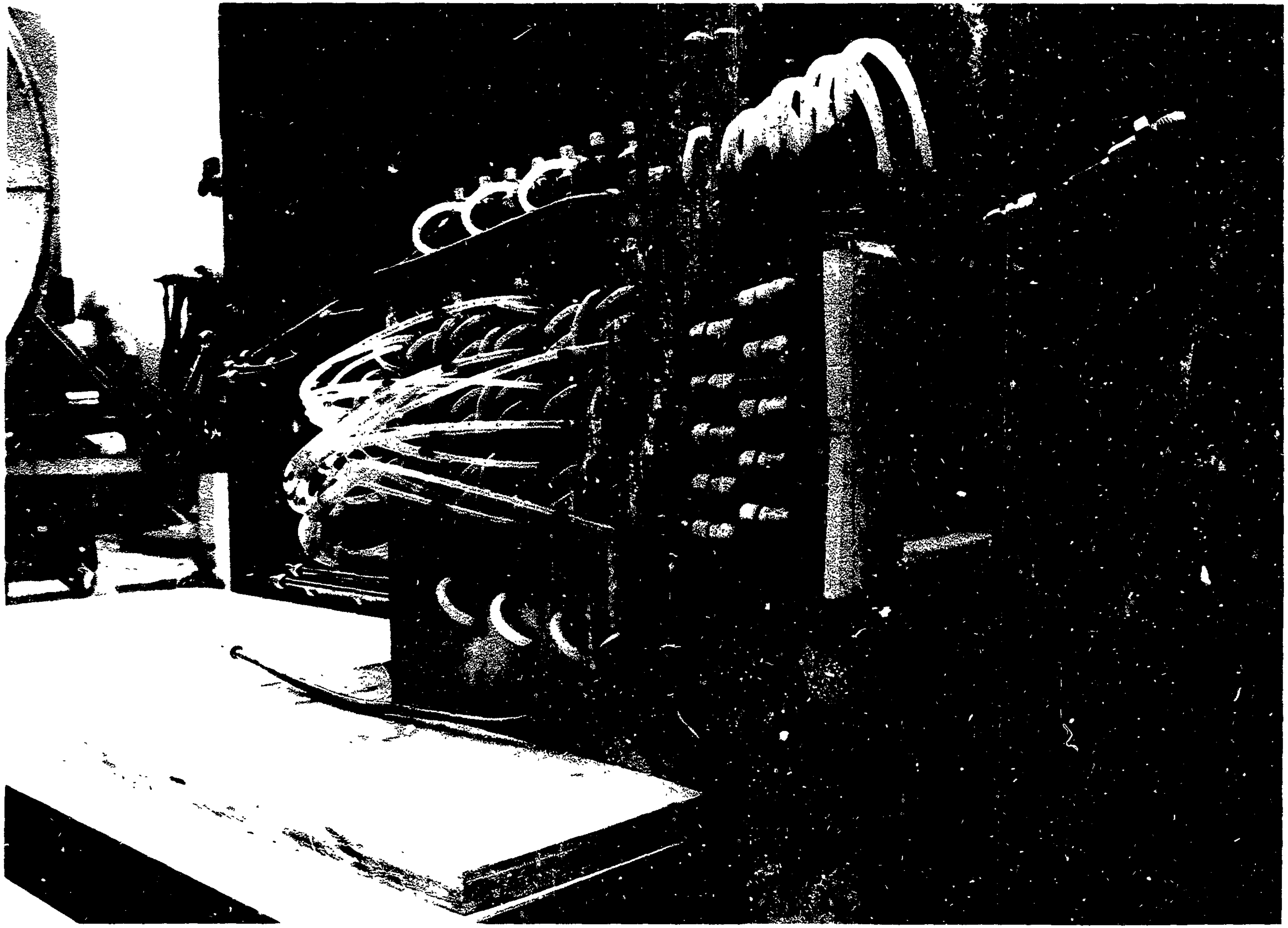

Figure 2.20 View of right side (looking upstream) of CA-1 accelerator

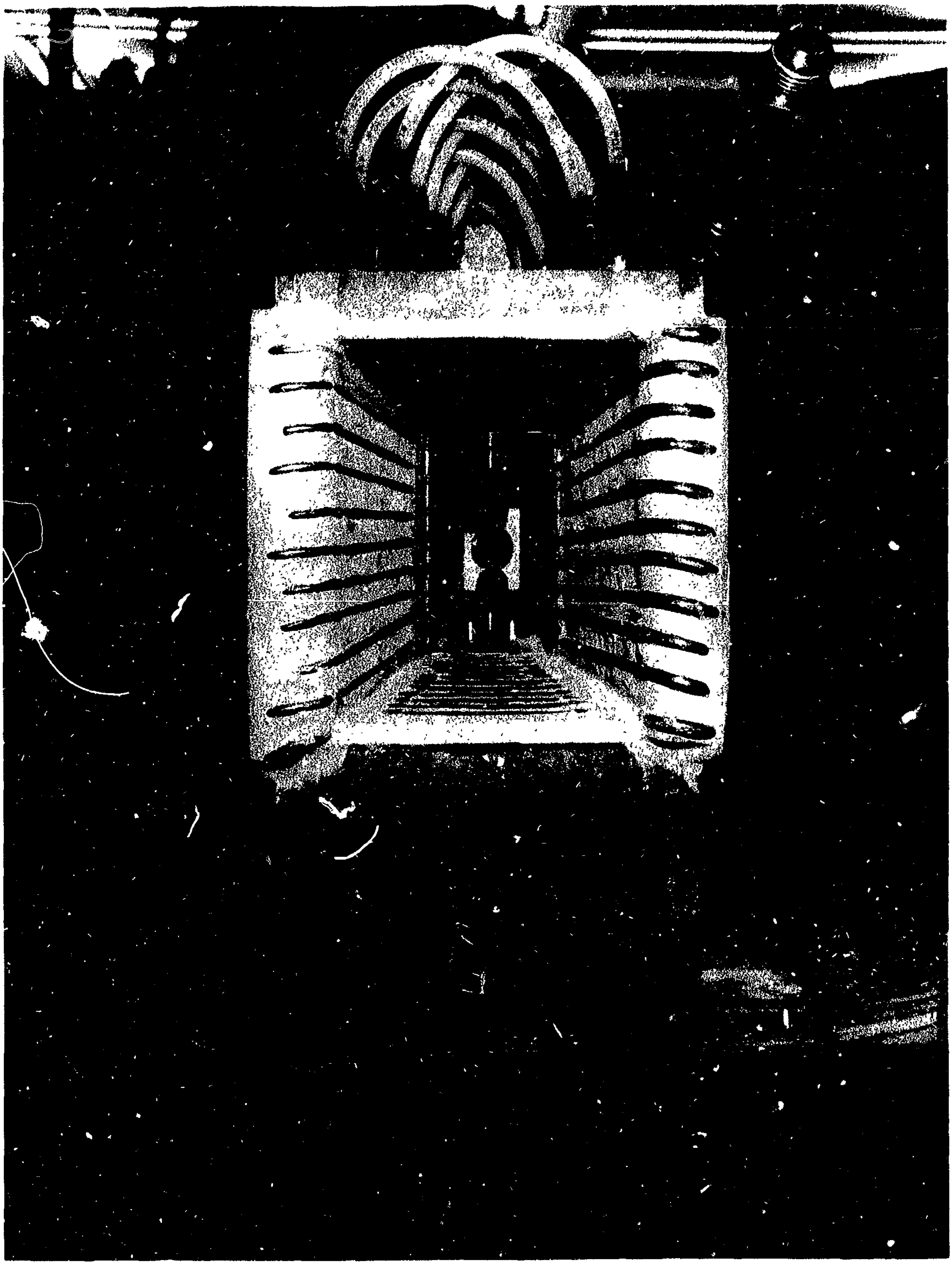

Figure 2.21 View looking upstream of CA-1 accelerator with nozzle in place

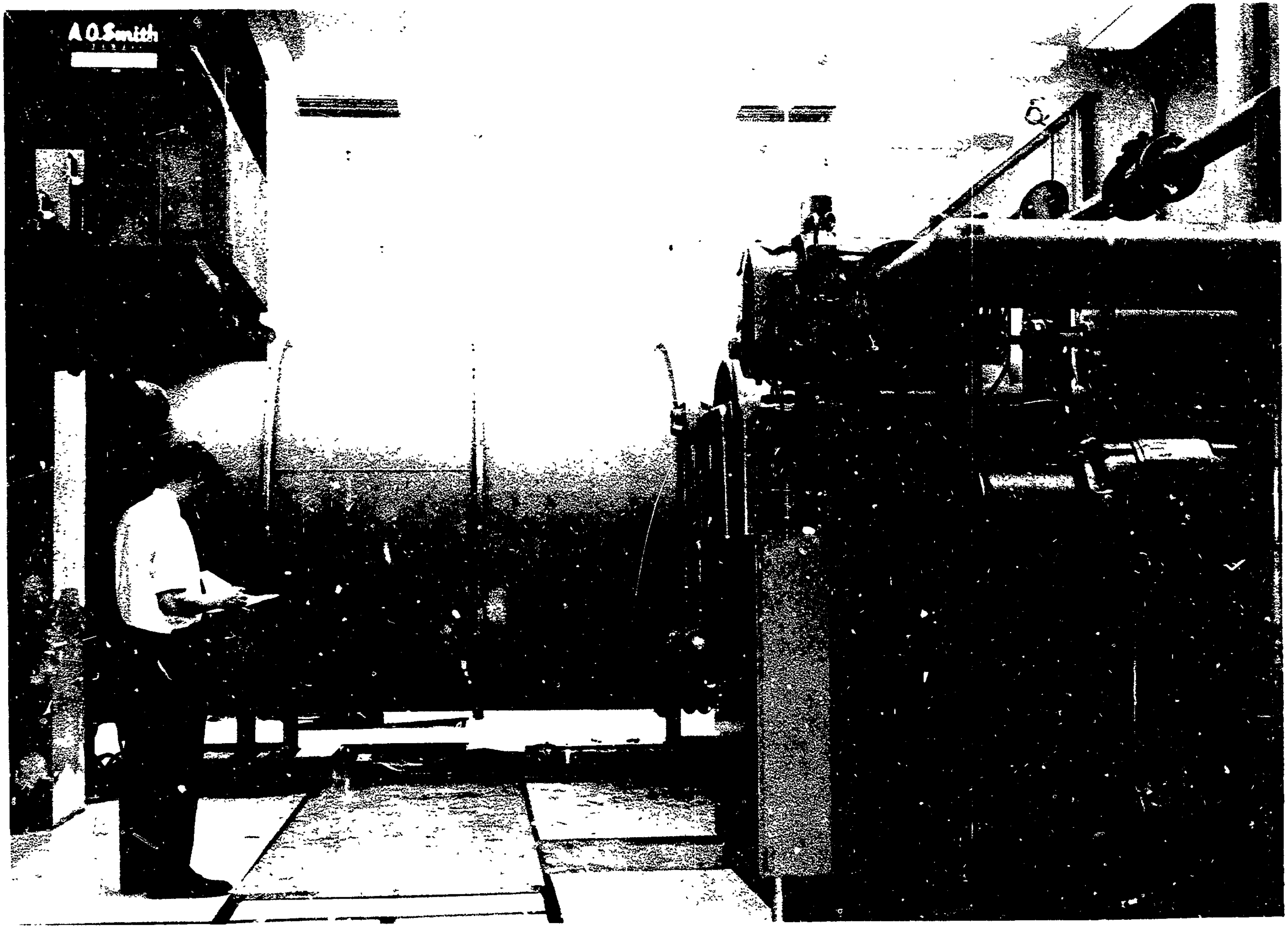

Figure 2.22 View of the vacuum tank test facility

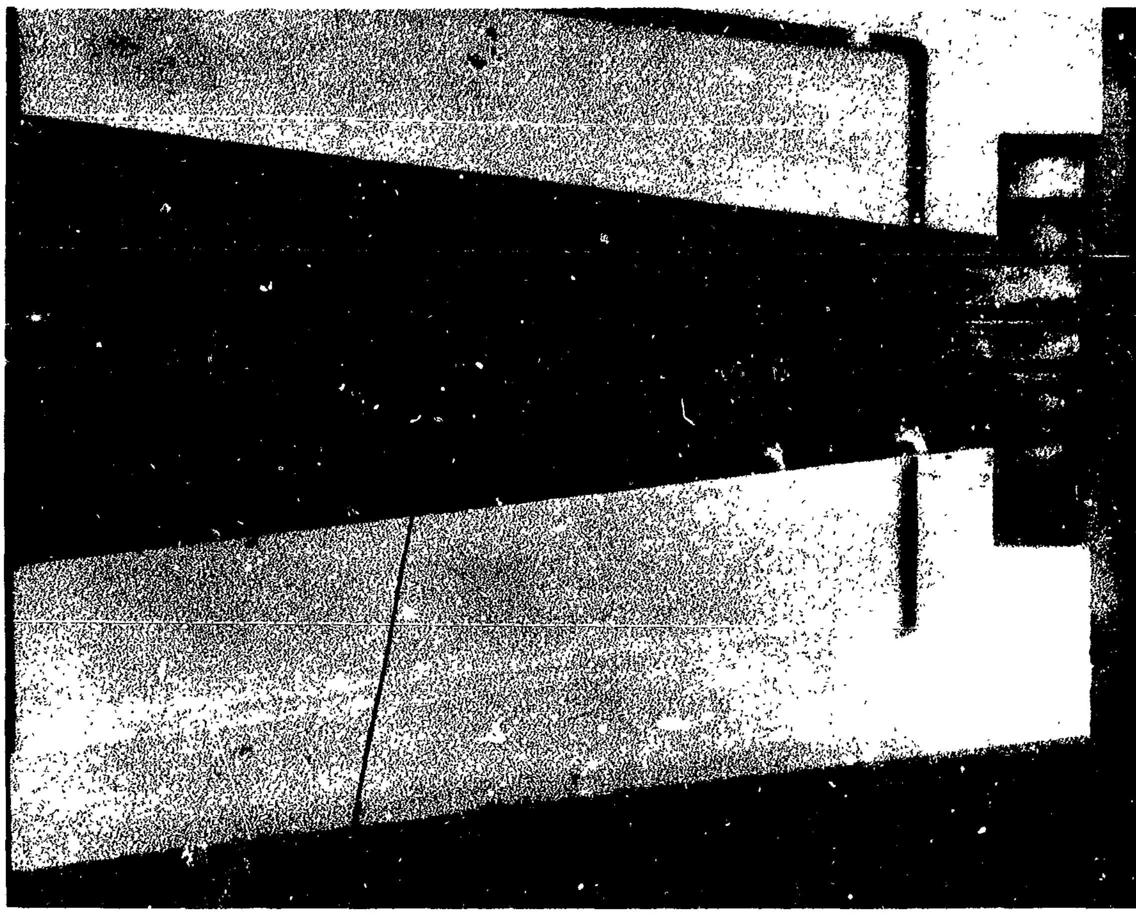

Figure 2.23 View of left sidewall of CA-2 before the fifth test

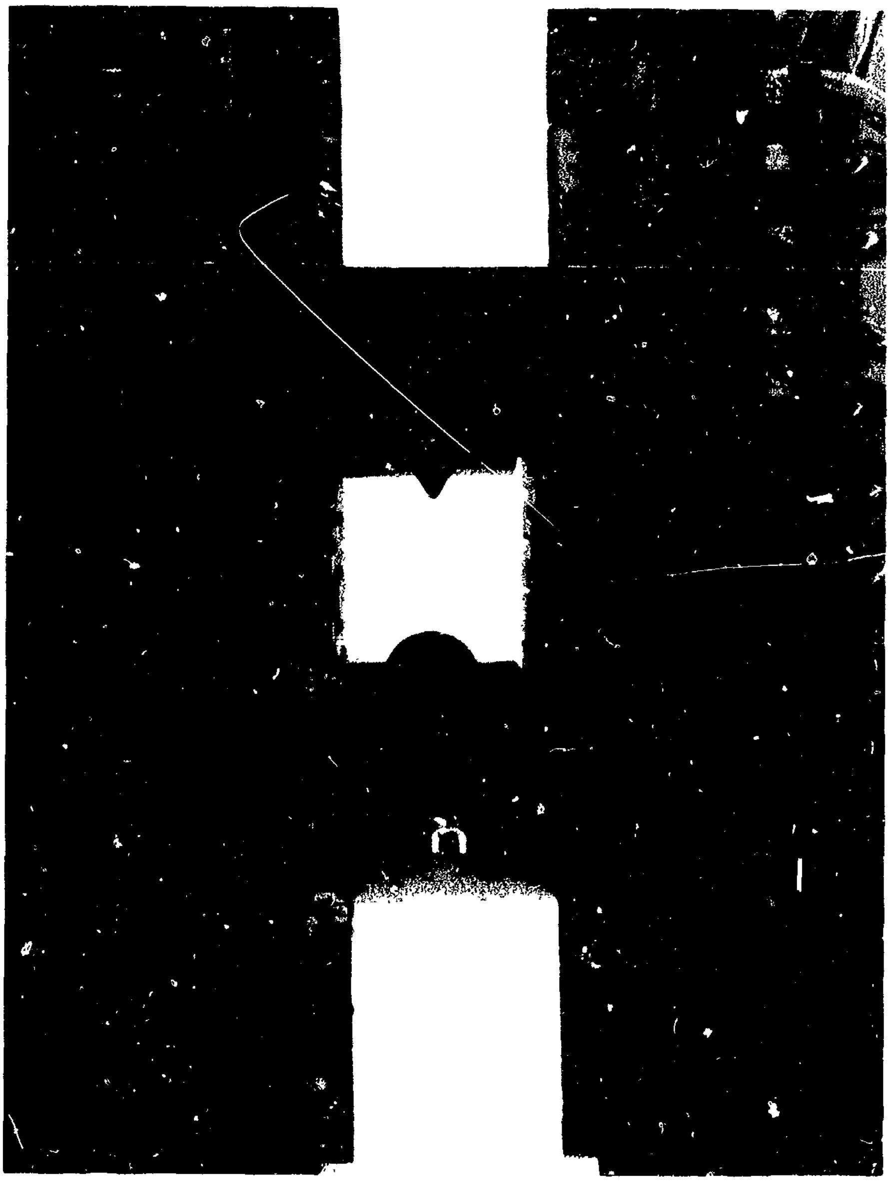
Figure 2.24 View looking upstream at CA-2 before the fifth test

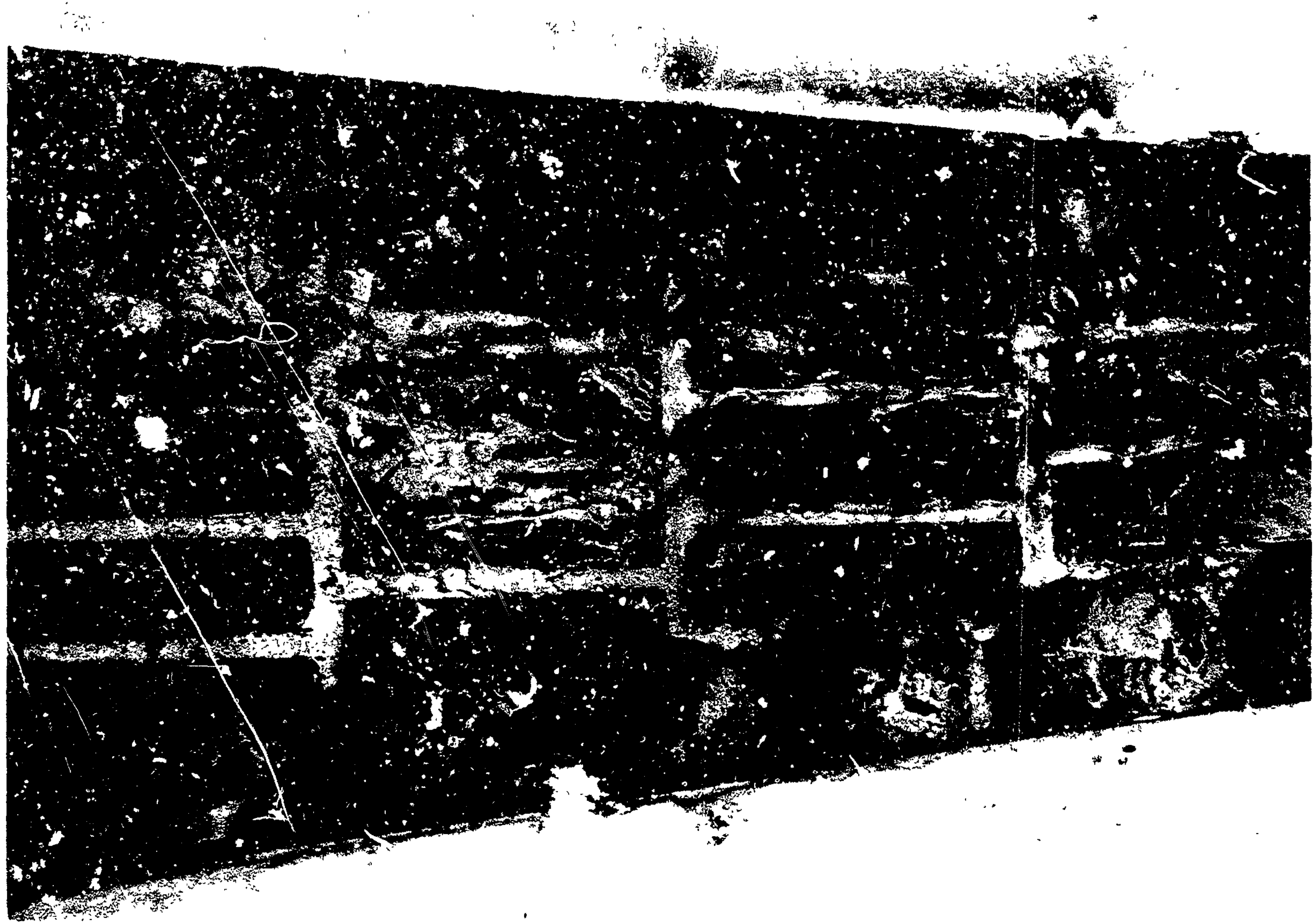

Figure 2.25 View of CA-1 left sidewall after third test

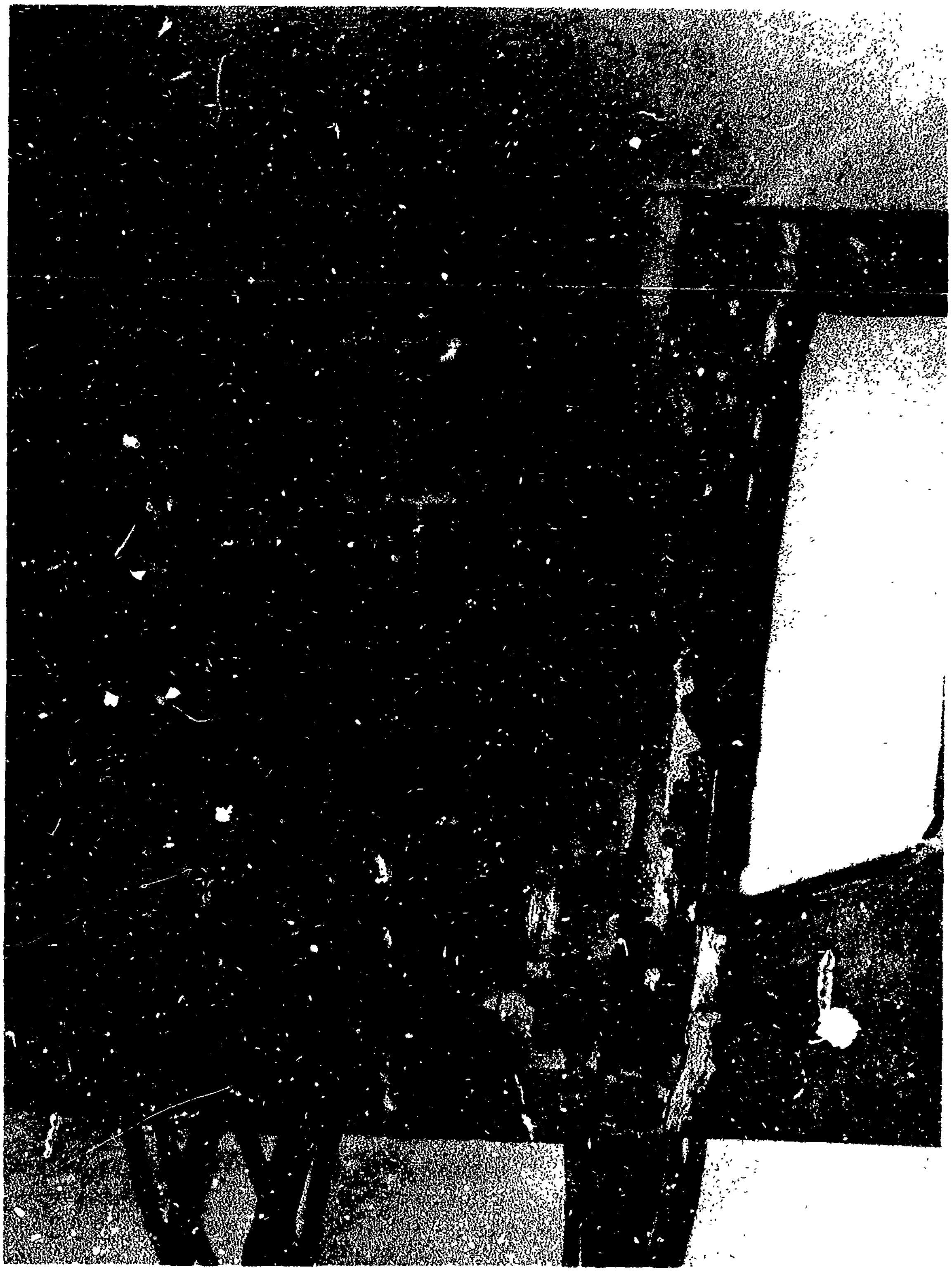

Figure 2.26   Right sidewall of CA-1 after the fourth test

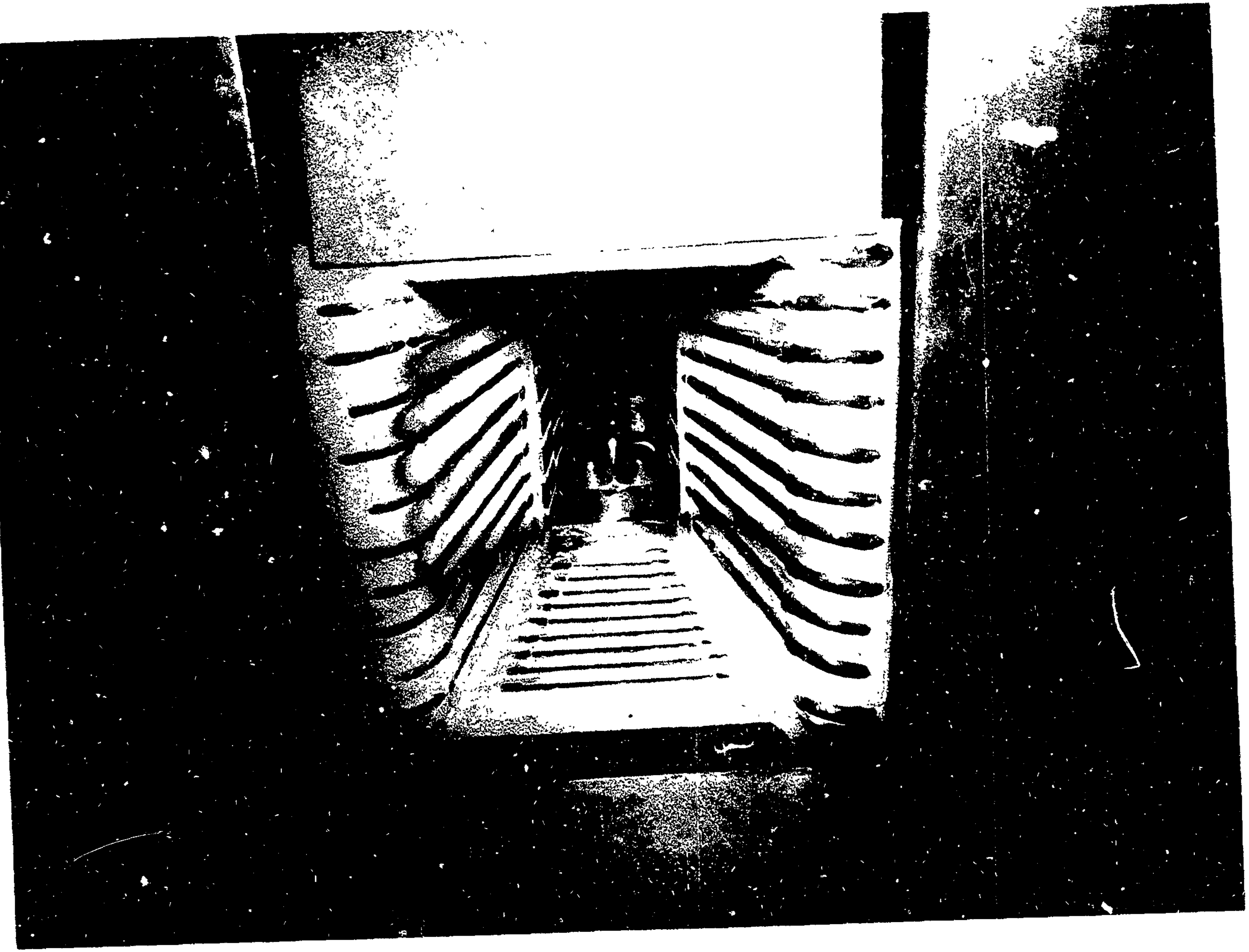

Figure 2.27 Upstream view of accelerator CA-1 after Test 1

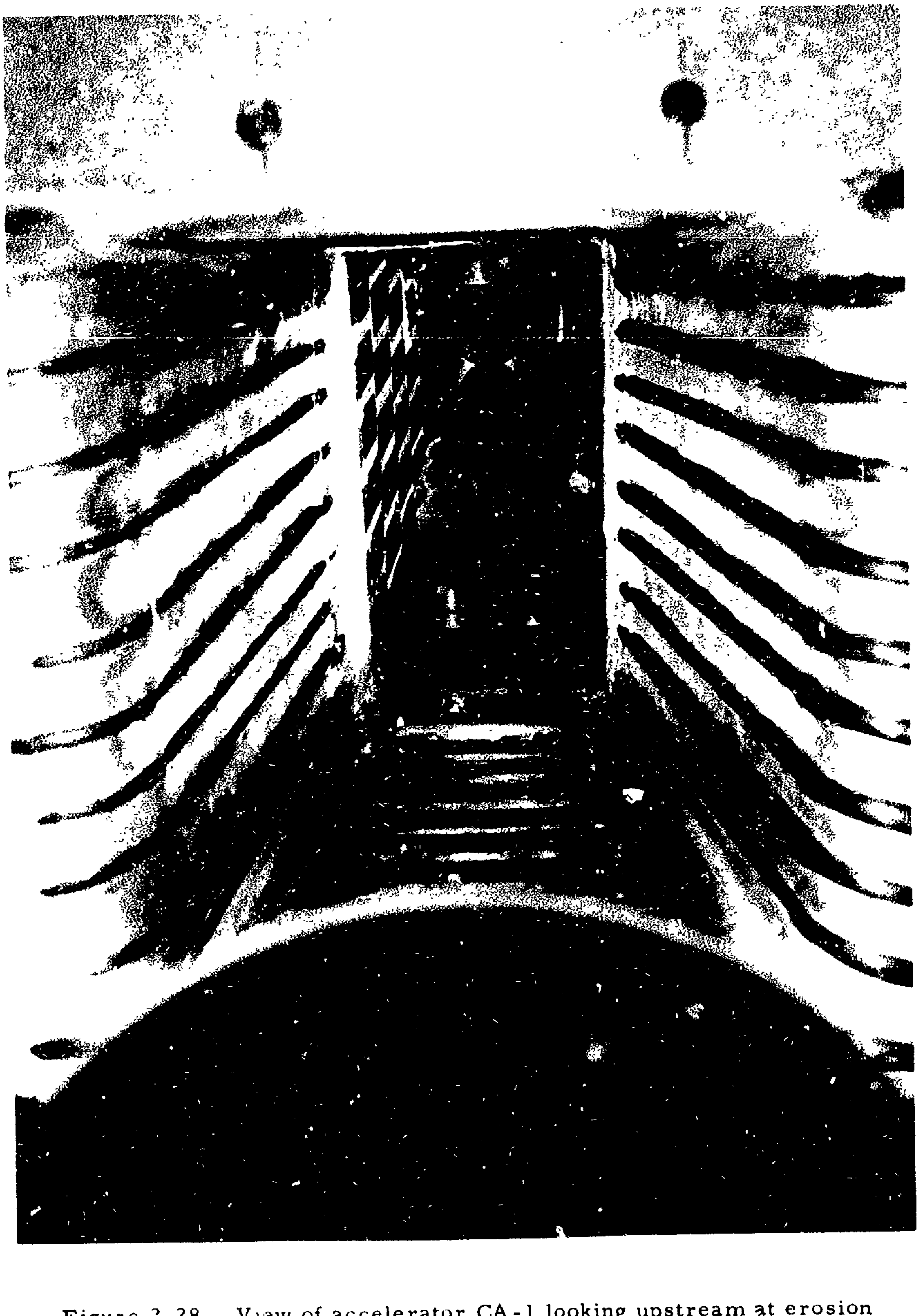

Figure 2.28 View of accelerator CA-1 looking upstream at erosion of boron nitride anode holder after Test 2

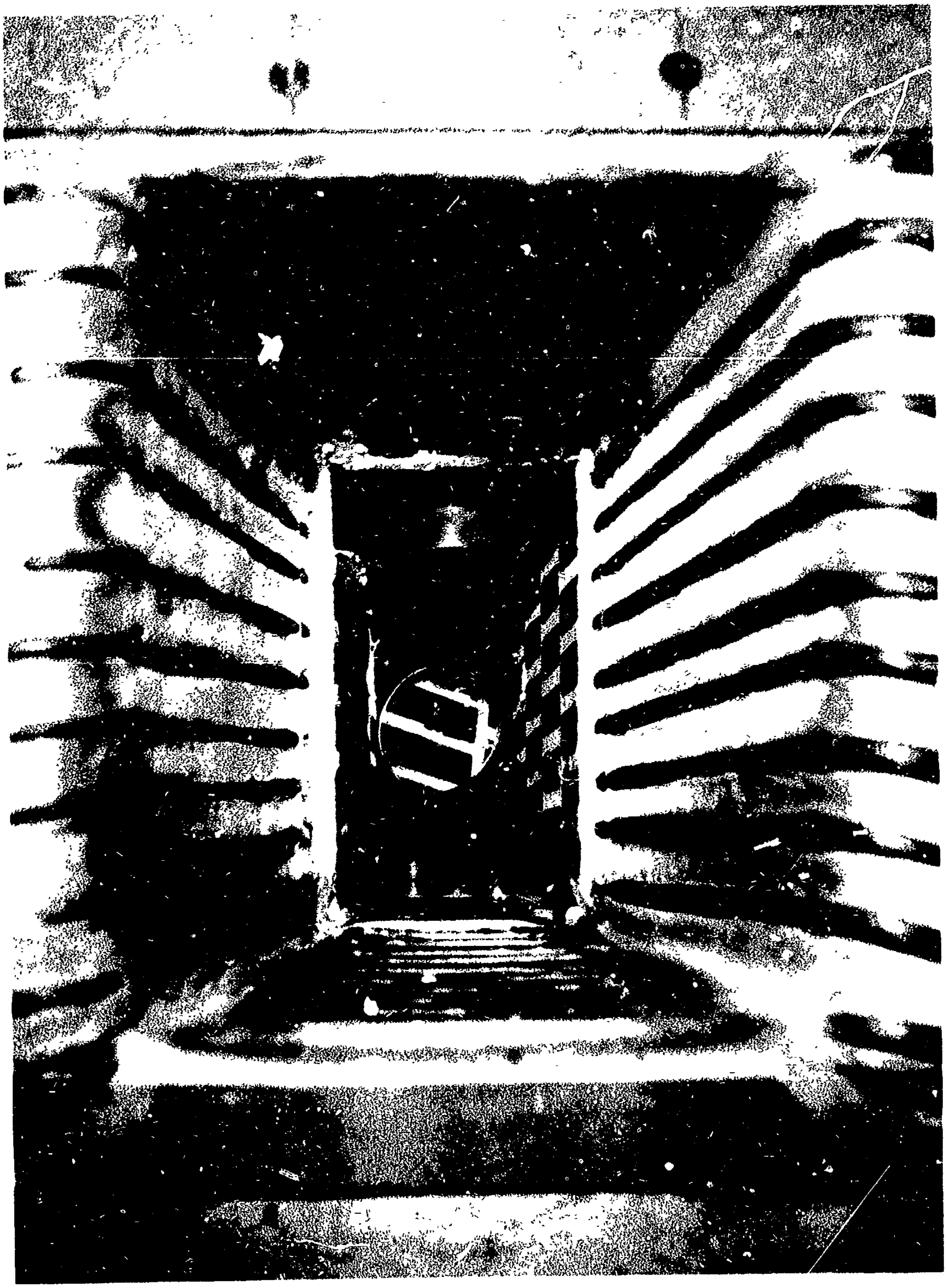

Figure 2.29 Upstream view of accelerator CA-1 after Test 2

TABLE 2.1

PERFORMANCE GOALS FOR FEASIBILITY STUDY

Working fluid	air (N_2 - O_2 mixture + argon)
Mass flow rate	0.01 lb/sec
System	arc jet + crossed-field accelerator
Exit velocity	25,000 ft/sec
Velocity ratio across the accelerator	> 2
Exit density	> 10^{-7} lb/ft^3 (approximately)
Exit area	> 0.2 ft^2
Contamination of stream	< 1% by weight
Core velocity variation at exit	< $\pm$ 5%
Run duration	5 minutes

TABLE 2.2

CONDITIONS FOR THEORETICAL COMPUTATION OF OHMIC DROP ACROSS THE FIRST ELECTRODE-PAIR

Mass flow rate of air	$\dot{m} = 4.54 \times 10^{-3}$ kg/sec
Arc jet exit velocity	$U_{o1} = 3810$ meter/sec
Electrode gap	$h_1 = 0.038$ meters
Electrode width	$w_1 = 0.0254$ meters
Electrode length	$L_1 = 0.0254$ meters
Electrode current	$I_1 = 450$ amperes
Stream cross-sectional area	$A_s = 3.5\ in^2 = 2.26 \times 10^{-3}\ m^2$
Inlet enthalpy	$H_1 = 1.57 \times 10^7$ joules/kg

TABLE 2.3

THEORETICAL CALCULATIONS OF OHMIC DROP AND OHMIC DISSIPATION FOR FIRST ELECTRODE-PAIR FOR CONDITIONS GIVEN IN TABLE 2.1

(Some of These Results are Plotted in Figure 2.5)

B_1 (gauss)	h_1 (meters)	Pressure (mm Hg)	I_1 (amps)	$\hat{\overline{V}}_1$ (volts)	$I_1\overline{V}_1$ (kilowatts)
0	.038	15.2	100	40	4
0	.038	15.2	250	68	17
0	.038	15.2	400	93.5	37.4
0	.051	15.2	500	135	67.6
0	.051	4.5	500	144	72.1
500	.038	≈11	150	131	19.6
500	.038	≈11	300	179	53.7
500	.038	≈11	450	186	83.6
2000	.038	≈11	150	580	87.1
2000	.038	≈11	300	465	139.5
2000	.038	≈11	450	408	184.0
2000	.076	≈ 9	75	806	60.5
2000	.076	≈ 9	150	700	105.8

TABLE 2.4

CONDITIONS ASSUMED FOR ANALYSIS OF ACCELERATOR CA-1 PREDICTIONS GIVEN IN TABLE 2.5

Inlet velocity	
(Supplied by arc jet. Calculations based on low value to assure achievement of final exit velocity ratio requirement.)	U_o = 8720 ft/sec = 2660 m/sec
Exit velocity	U_e = 25,000 ft/sec = 7620 m/sec
Applied magnetic field	B = 2000 gauss = 0.2 webers/m^2
Electrode gaps	h_1 = 0.038 m h_2 = 0.047 m h_3 = 0.055 m h_4 = 0.064 m h_5 = 0.071 m
Average channel width	$\bar{w}$ = 0.057 m
Total channel length	L = 0.18 m

TABLE 2.5

PREDICTED OPERATING CHARACTERISTICS FOR ACCELERATOR CA-1 FOR CONDITIONS GIVEN IN TABLE 2.4

	Electrode-pair					Total
	1	2	3	4	5	
Voltage (volts)						
V_d	30	30	30	30	30	
$\overline{V}$	400	100	75	50	25	
$h\overline{U}B$	27	41	58	74	93	
V_o	457	171	163	154	148	
Current (amperes)	450	450	450	450	450	2250
Power (kw)						
P_{acc}	12.0	18.3	25.2	33.2	41.5	130.2
iV_d	13.5	13.5	13.5	13.5	13.5	67.5
$i\overline{V}$	180.0	45.0	33.5	22.5	11.2	292.2
Total	205.5	76.8	72.2	69.2	66.2	489.9
Thrust (newtons)	3.9	4.6	5.0	5.4	5.6	24.5

TABLE 2.6

CONDITIONS ASSUMED FOR ANALYSIS OF ACCELERATOR CA-2. PREDICTIONS GIVEN IN TABLE 2.7

Gas	Air
Mass flow rate	$\dot{m} = 4.54 \times 10^{-3}$ kg/sec
Arc jet power (net power to Plasma stream)	65 kw
Arc jet exit velocity	$U_o = 3300$ m/sec
Electrode gaps	$h_1 = 0.038$ m
	$h_2 = 0.047$ m
	$h_3 = 0.055$ m
	$h_4 = 0.064$ m
	$h_5 = 0.071$ m
	$h_6 = 0.081$ m
Channel width (constant)	$w = 0.047$ m
Channel exit area	$A_c = 0.005$ m^2

TABLE 2.7

PREDICTED OPERATING CHARACTERISTICS FOR ACCELERATOR SUBSYSTEM CA-2 FOR CONDITIONS GIVEN IN TABLE 2.6

	Electrode-pair						Total
	1	2	3	4	5	6	
Voltage (volts)							
V_d	30	30	30	30	30	30	
$\bar{V}$	200	110	75	60	40	20	
$h\bar{U}B$	18	26	35	46	58	78	
V_o	248	166	140	136	128	128	
Current (amperes)	500	500	500	250	500	500	2750
Power (kw)							
P_{acc}	8.8	12.8	17.6	11.5	29.0	38.9	118.5
iV_d	15.0	15.0	15.0	7.5	15.0	15.0	82.5
$i\bar{V}$	100.0	55.0	37.5	15.0	20.0	10.0	237.5
Total	123.8	82.8	70.1	34.0	64.0	63.9	438.6
Power available (kw)	160	80	80	40	120	80	560
Thrust (newtons)	2.5	3.1	3.6	2.1	4.7	5.3	21.2
Acc. Efficiency (%)	7.1	15.5	25.1	33.8	44.3	60.8	

TABLE 2.8

OPERATING CHARACTERISTICS OF PRELIMINARY ACCELERATOR AT B = 500 Gauss

Arc jet conditions:

$\dot{m}$ = 0.01 lb/sec, air
I = 600 amps, V = 255 volts, P - 153 kw (arc jet only)
I = 525 amps, V = 252 volts, P - 132 kw (accelerator on)

I amps	V volts	P kw	B gauss	θ_{acc} newtons	θ_{total} newtons	hIB newtons	θ_{acc}/hIB
0	0	0	0	-	-	-	-
100	118	11.8	0	-	-	-	-
200	100	20.0	0	-	-	-	-
300	90	27.0	0	-	-	-	-
400	75	30.0	0	-	-	-	-
500	60	30.0	0	-	-	-	-
100	278	27.8	500	0.44	11.56	0.191	2.3
200	260	52.0	500	1.34	12.46	0.382	3.46
300	240	72.0	500	2.68	13.80	0.572	4.61
400	235	94.0	500	3.11	14.23	0.763	4.08
500	232	116.0	500	3.58	14.70	0.954	3.76

TABLE 2.9

TEST OF SEGMENTED ACCELERATOR SIDEWALL WITHOUT WATER COOLING SHOWN IN FIGURES 2.10 and 2.11

Test Time (seconds)	Arc Jet Power (kw)	Accelerator Current (amperes)	Accelerator Power (kw)	Magnetic Field (webers/m^2)	Expellant and Flow Rate (kg/sec)
10	32	400	20	0.052	argon 1.36×10^{-3}
35	32	500	25	0.052	argon 1.36×10^{-3}
34	32	500	25	0.052	argon 1.36×10^{-3}
23	32	400	20	0.052	argon 1.36×10^{-3}
31*	32	400	20	0.052	argon 1.36×10^{-3}
38**	32	300	14.1	0.043	argon 1.36×10^{-3}
33	32	300	14.1	0.043	argon 1.36×10^{-3}
42	39	300	40.5	0.043	nitrogen 0.54×10^{-3}
52	32	300	15.6	0.043	argon 1.36×10^{-3}
30	39	300	40.5	0.043	nitrogen 0.54×10^{-3}

* Total of five tests

** Total of four tests

TABLE 2.10

OPERATING CONDITIONS FOR 1, 2 and 3 of CA-1 TESTS

Expellant	Air
Mass flow rate	$\dot{m} = 4.54 \times 10^{-3}$ kg/sec
Arc jet power (net power to plasma stream)	24 kw
Arc jet exit velocity	$U_o = 2190$ m/sec
Electrode gaps	$h_1 = 0.038$ m
	$h_2 = 0.047$ m
	$h_3 = 0.055$ m
	$h_4 = 0.064$ m
	$h_5 = 0.071$ m
Channel width at successive electrode pairs	$W_1 = 0.053$ m
	$W_2 = 0.056$ m
	$W_3 = 0.059$ m
	$W_4 = 0.062$ m
	$W_5 = 0.065$ m
	$W_{exit} = 0.076$ m
Channel exit area	$A_c = 0.011$ m^2
CA-1 nozzle exit area	$A_n = 0.029$ m^2

TABLE 2.11

PERFORMANCE DATA FOR TESTS 1, 2 and 3 of CA-1.

Test Conditions are Described in Table 2.10

Test No.	Electrode Pair	I_o (amp)	V_o (volts)	P_{acc} (kw)	B (webers/m^2)	θ_{acc} (newtons)	$\frac{\theta_{acc}}{hI_oB}$	U_f-U_o (m/sec)	η_{acc} (%)	Tank Pressure (mm/Hg)	Duration of Acc. Test (sec)
1	1	200	190	38	0.05					7.0	165
	2	200	150	30	0.05	o(0.5)*	o(0.2)	(100)	o(0.1)		
	3	200	120	24	0.05						
	4	200	100	20	0.05						
	5	200	100	20	0.05						
	(Total)	1000		132							
2	1	200	280	56	0.10	3.78	1.03	833	5.0	0.7	181
	2	200	210	42	0.10						
	3	200	185	37	0.10						
	4	200	170	34	0.10						
	(Total)	800		199							
3	1	300	300	90	0.10	4.17	0.65	918	4.3	1.3	92
	2	300	220	66	0.10						
	3	300	170	51	0.10						
	4	230	155	35	0.10						
	5	100	150	15	0.10						
	(Total)	1230		257							

*o(x) = of the order of

TABLE 2.12

ENERGY BALANCE FOR TESTS 1, 2, 3 and 4 of CA-1

Test Conditions are Described in Table 2.10

	Power (kw)			
	Test 1	Test 2	Test 3	Test 4
Total power applied in accelerator	132.0	199.0	257.0	360.0
Power absorbed by coolant:				
First anode	0.8	2.7	2.3	14.6*
First cathode	0.2	3.4	1.2	11.9**
Second anode	8.6	8.9	9.5	
Second cathode	5.6	4.9	2.8	
Third anode	4.8	9.7	9.1	-
Third cathode	5.3	4.3	4.9	-
Fourth anode	7.7	7.8	17.5	-
Fourth cathode	3.5	6.9	6.6	-
Fifth anode	3.5	4.4	-	-
Fifth cathode	5.0	3.3	3.2	-
Sixth anode	3.0	1.8	-	-
Sixth cathode	1.7	3.3	0.8	-
Seventh anode	3.1	2.7	0.8	3.9
Seventh cathode	7.8	8.7	1.5	8.5
Arc nozzle	11.9	13.9	5.3	18.1
Left sidewall	35.9	22.7	57.2	29.0
Right sidewall	12.5	6.5	17.2	50.1
TOTAL	120.9	115.9	139.0	
Net power input to stream:				
Arc jet	24.0	24.0	24.0	55.5
Accelerator	11.1	83.1	116.0	
TOTAL	35.1	107.1	140.0	
Average stagnation enthalpy at accelerator exit (joules/kg)	7.7×10^6	2.4×10^7	3.1×10^7	

- Instrumentation malfunction; * Total power absorbed by 1st and 2nd anodes; ** Total power absorbed by 1st and 2nd cathodes.

3. ELECTROMAGNETIC DESIGN OF THE CROSSED-FIELD ACCELERATOR

The following analysis of a linear crossed-field accelerator having multiple, separately powered electrode pairs is based upon the assumption of one-dimensionality and of constant pressure in a friction-free flow channel.* It has been found in previous work (References 1 to 3) that these assumptions are satisfied to a reasonable degree of accuracy in an accelerator operating in the pressure range of 1 to 10 mm Hg and with currents per electrode pair of the order of several hundred amperes. All equations are given in MKS units.

The total Lorentz force in an idealized accelerator is related to the velocity increment of the stream by the relation:

$$\Theta = \dot{m}\,(u_e - u_o) \tag{3.1}$$

where

Θ = total Lorentz force

$\dot{m}$ = mass flow rate of working fluid

u_e, u_o = exit and inlet mass average gas velocities, respectively

The total Lorentz force is related to the electric currents and magnetic field by

$$\Theta = \sum_{k=1}^{n} \theta_k = \sum_{k=1} h_k B_k I_k \tag{3.2}$$

where

θ_k is the Lorentz force for the k^{th} electrode

* without heat transfer

where the values of k indicate the successive electrode-pairs: h_k is the electrode gap, B_k is the magnetic field strength, and I_k the applied current at the k^{th} electrode-pair. The total current applied is

$$I_o = \sum_{k=1}^{n} I_k \tag{3.3}$$

The cross current has an associated magnetic field which is given by the Maxwell equation:

$$\vec{\nabla} \times \vec{B}' = \mu \vec{J} \tag{3.4}$$

where

μ = permeability = $4\pi \times 10^{-7}$ henries/m

J = current density $\approx I_o/wL$ amperes/m^2 (assuming uniform current distribution)

w and L are respectively the width and length of the arc column

B' = magnetic induction webers/m^2

This equation can be written in the following approximate form:

$$\frac{dB'}{dx} = -\mu J \tag{3.5a}$$

with the boundary condition:

$$\int B' dx = 0 \tag{3.5b}$$

integrated over the discharge.

For "n" electrodes spaced closely and giving a fairly uniform current sheet, β varies linearly over the length of the accelerator from:

$$B' = \frac{\mu I}{2w} \quad \text{to} \quad B = -\frac{\mu I}{2w}$$

where I is the total current. Utilizing the same current per electrode as before, B' can reach a maximum absolute value of 63 n gauss. The total field is:

$$B = B_a + B' \tag{3.6}$$

where B_a is the applied field.

For a friction-free, constant pressure accelerator the directed kinetic power input to the flow stream by the k^{th} electrode pair is the change in directed kinetic energy:

$$\left(P_{acc}\right)_k = \frac{\dot{m}}{2}\left(u_{ek}^{\ 2} - u_{ok}^{\ 2}\right) \tag{3.7}$$

Using equation (3.1) this can be written as

$$\left(P_{acc}\right)_k = \theta_m^{\ 2}/2\dot{m} + \theta_k u_{ok} \tag{3.8}$$

$$= I_k h_k B_k \left(u_{ok} + \frac{\theta_k}{2\dot{m}}\right) \tag{3.9}$$

Equation (3.7) can also be factored:

$$\left(P_{acc}\right)_k = \dot{m}\left(u_{ek} - u_{ok}\right)\left(\frac{u_{ek} + u_{ok}}{2}\right)$$

Noting that the average back emf at the electrode is

$$V_{bk} = h_k B_k \left(\frac{u_{ok} + u_{ek}}{2}\right) = h_k B_k u_k \tag{3.10}$$

We can write:

$$p_{acc_k} = \theta_k \cdot \frac{V_{bk}}{h_k B_k}$$

noting $\theta_k = h_k B_k I_k$

$$p_{acc_k} = I_k V_{bk}$$

The total electric power required for each electrode-pair is the product of the applied current (I_k) and the applied voltage (V_o). The applied voltage must equal the sum of the electrode drop potential (V_d), which is known from previous experiments (References 1, 2 and 3) to be about 30 volts, the back emf (Equation 3.10) and the resistive voltage drop across the plasma $(\bar{V}_k)$. Thus the total electric power input to the kth electrode is:

$$p_k = I_k V_{ok} = I_k \ (V_d + V_{bk} + \bar{V}_k) \tag{3.11}$$

Applying Ohm's Law to a simplified rectilinear model:

$$\bar{V}_k = I_k R_k = I_k \cdot \frac{h_k}{w_k L_k} \cdot \left(\frac{1 + \sigma_o \psi B_k^2}{\sigma_o} \right) \tag{3.12}$$

where:

σ_o = scalar conductivity of the plasma

ψ = ion slip coefficient

Equation (3.12) is based upon the following assumptions:

(a) The electric field and the magnetic field intensities are uniform over the gap region of each electrode-pair.

(b) The anode is placed upstream of the cathode so that the current density vector is transverse to the flow. In the presence of a magnetic field the conductivity of a plasma is a tensor and the current density and electric field vectors are not parallel.

(c) The discharge cross-sectional area is equal to the projected area of the electrodes.

Using the analysis given in Reference 3, under the assumption that the degree of ionization is in equilibrium at the electron temperature, the average value of the conductivity expression $\sigma_o / (1 + \sigma_o \psi B^2)$ of Equation (3.12) can be computed. The computation involves an iterative procedure in which the conductivity is related to the enthalpy of the plasma, the enthalpy is computed from the addition of energy by Ohmic heating and a knowledge of the inlet conditions, and the Ohmic heating is evaluated with the aid of the Ohm's law (Equation 3.12).

The plasma properties of σ_o, ψ, and the enthalpy, H, are given as a function of temperature for equilibrium air at the pressures of 4.55 and 15.2 mm Hg in Figures 2.1, 2.2, 2.3, 2.4. The data for enthalpy and species number densities were taken from Reference 4. Using these curves as the required equations of state, the calculations described above were performed to determine the Ohmic drop across the first electrode-pair of the accelerator for the conditions expected in the experimental program. The numerical results are given in Tables 2.2 and 2.3 and in Figure 2.5.

The analysis of the Ohmic drop indicated that the following effects tend to reduce $\bar{V}_k$:

(a) Increased temperature and enthalpy of the plasma.

(b) Increased degree of ionization.

(c) Higher static pressure (slight effect).

(d) Lower magnetic field.

Using the values for $\bar{V}_k$ given in Table 2.3 as a guide, the performance of an idealized (friction-free, constant pressure) accelerator was calculated for several sets of operating conditions. The conditions chosen and the corresponding predictions of the performance of the accelerator are given in Tables 2.4, 2.5, 2.6 and 2.7.

The accelerator efficiency of the k^{th} electrode can be written

$$\left(\eta_{acc}\right)_k = \frac{V_{bk}}{V_d + V_{bk} + \bar{V}_k} = \frac{1}{1 + \dfrac{V_d + \bar{V}_k}{V_{bk}}}$$

Values for the two idealized accelerator configurations studied are shown in Tables 2.5 and 2.7 and vary from 7.1 to 60.8 percent for the idealized CA-2 configuration.

A striking factor in the calculations for both idealized accelerators is the high Ohmic voltage drop at the first electrode pair (400 and 200 volts respectively for CA-1 and CA-2). These values drop to about 100 volts at the second electrode pair. The relatively high voltage requirements of the first electrode pair is an important factor in causing sidewall breakdown and indicates the need for additional preheating of the incoming gas and/or reduction of the B field at the entrance.

4. ELECTRICAL AND MECHANICAL DESIGN

4.1 ELECTRODES

It had been found in previous experiments with high current, low pressure, crossed-field accelerators (References 1, 2, 3) that the discharges spread only partially over the surfaces of the electrodes. To reduce the heat flux per unit area to an electrode it is necessary to limit the current applied to each electrode pair. It was found that water-cooled electrodes could be designed to operate with little or no ablation at about 500 amperes per electrode-pair. At about 1000 amperes per electrode-pair, the mode of heat transfer from the electrode material to the cooling water would on occasion change from nucleate to vapor film boiling in the vicinity of the arc attachment, allowing rapid erosion of the electrode. Thus it was decided that the accelerators for the present program would be designed on the basis of approximately 500 amperes per electrode-pair.

Anodes tips were made of Elkonite 10W3 which is sintered tungsten in a matrix of copper. The anode tips were made spherical in form, as shown in Figures 1.1, 2.7, 2.8, 2.17, 2.19 and 4.1. Anode diameters were 0.75 inches in the preliminary accelerator and increased to 1.00 inches in CA-1 and CA-2.

The preliminary accelerator tests (one electrode pair) were run utilizing an uncooled block of tungsten (1 inch x 1 inch x 5 inches) for a cathode. Cathodes for CA-1 and CA-2 were made of thoriated tungsten. The shape utilized on CA-1 was cylindrical with a large radius tip. The CA-2 design was converted to use a 60° conical tip to concentrate the cathode discharge. Cathode configurations are shown in Figures 2.9, 2.16, 2.21, 2.23, 2.24 and 4.2.

4.2 ELECTRODE HOLDERS

Electrode holders were fabricated of boron nitride (see Figures 2.17, 2.19, 2.21, 2.23, 2.24, 2.25, 2.29, 4.3 - 4.8) without special cooling passages. A certain amount of cooling was obtained through the water-cooled electrodes and sidewall studs. The thickness of boron nitride between the electrodes and sidewalls in the electrode holders of accelerator CA-2 was reduced when a constant channel width design was adopted by making the rows of studs (water-cooled segments) next to the holders wider than for CA-1 (Figure 2.24). This design did not appreciably reduce electrode holder erosion (compare Figures 4.5 and 4.7). The electrode holder performance was considered adequate and probably would operate satisfactorily for five minutes as specified, although full-power, full-duration runs at elevated B fields were not run.

4.3 MAGNET

The externally applied magnetic field was arbitrarily made uniform. The entire arc discharge portion of the accelerator was submerged in the gap between trapezoidal pole faces. The magnet used is able to produce a field of 4000 gauss in the 10 inch gap utilized. The trapezoidal face is isosceles with bases of 4 and 6 inches and a 12 inch altitude. The distance between coils is about 10 inches.

The design value of the applied magnetic field is 2000 gauss, based on experience with free-jet accelerators. This value proved too high at the entrance to the accelerator for practical operations due to wall breakdown. It is obvious in retrospect that the B field at the entrance to the accelerator should have been reduced, but this factor was not fully appreciated until after termination of experimental work.

4.4 ACCELERATOR CHANNEL

It is reasonable to utilize an arc heater and de Laval nozzle to preheat and pre-accelerate the gas entering a crossed-field accelerator. In the present case an entering velocity of 10,000 to 12,000 feet per second was indicated as attainable with a low pressure arc heater and nozzle. The flow entering the channel is therefore supersonic. A fully-confined channel geometry was initially chosen because of the requirement for flow and pressure control in the final application.

It was decided to use a rectangular channel with expanding cross section, i.e. with a channel width w linearly increasing in the downstream direction x (at a small expansion half-angle) and with channel height h also linearly increasing with x (at a larger expansion half-angle) as shown in Figures 2.17, 2.19, 2.20 and 2.21.

It was decided to have the electrodes protrude approximately three-fourth inch into the stream to keep the hottest part of the discharge column away from the boron nitride electrode holders. Although this geometry was bound to give a series of weak shock waves down the channel it was felt that the degradation of momentum in the core due to these shock waves would be small compared to the momentum increment due to Lorentz forces, and the advantages of this arrangement outweighed the disadvantages in this early accelerator.

Crossed-field accelerators with free-jet (unconfined) plasma flow streams have been developed to produce high gas velocities at reasonable efficiencies. Confined channels of uniform cross section have been much less successful due to wall-friction (boundary-layer growth), shock induction (particularly from electrodes), heat losses to walls and wall deterioration. Wind tunnel (and space propulsion) applications in general require test section and jet static pressures different from those optimum for arc operation. Some form of flow confinement (by magnetic field or wall structure) is required, at least downstream from the crossed-field accelerator. Since boundary flows are much better behaved in favorable (negative) pressure gradients, the test section (or final jet) static pressure should be below that in the arc section. Since the main flow field is supersonic, a favorable pressure gradient requires an expanding cross section. This type configuration was chosen for the 500 kw accelerator. Another important factor determining channel shape is the general suitability of rectangular geometry for perpendicular (B and E) crossed fields. To reduce the magnetomotive force necessary to produce the desired magnetic field and reduce the electrode current required for a given power input the channel has been made relatively narrow in the B direction. This tends to increase the sidewall heating and the voltage impressed on the sidewall, and these are the very factors that have caused difficulty on the present program. In retrospect it is apparent that the main problem was in the use of an excessive B field at the channel entrance. This factor is discussed further in Section 9 and Reference 5.

4.5 ACCELERATOR CHANNEL PRESSURE

The channel pressure selected (1 - 10 torr) is in the range where free-jet accelerator had been operated most successfully. In this range, the electrical conductivity is not very sensitive to pressure variations, as indicated by the ion-slip coefficients at two pressures (Figures 2.2 and 2.3).

The channel pressure influences the heat transfer rate to the channel walls by changing convective heat transfer (in almost direct proportion to pressure) and changing electron-ion recombination rates at the wall.

In order to avoid flow separation and pressure drag in the channel, it is advisable to design for a favorable (negative) pressure gradient. Since the flow is supersonic, this requires an expanding flow area.

For a given mass flow and velocity requirement the channel pressure is set by the physical size of the accelerator as the channel size is decreased, frictional losses and the difficulty of fabricating the accelerator increase. The maximum size of the accelerator is restricted somewhat by the practical size of the magnet. In the present application the requirement of maintaining the pressure so that density would be greater than that corresponding to an altitude of 300,000 feet sets a lower limit on the pressure. The above considerations led to the requirement that the channel pressure be in the range of one to 10 mm Hg. This is the region where electrical breakdown voltages minimize and where most accelerator operating data has been collected.

4.6 AERODYNAMIC CHOKING

One of the important problems in accelerator design lies in avoiding choking induced by joule heating of the flow stream. One condition for avoiding choking in a simple accelerator model is a limitation on the ratio of the rate of change of directed kinetic energy and heating:

$$\frac{\sigma\ Bu}{j} > \left(\frac{\gamma - 1}{\gamma + 1}\right) (1 + \gamma\ M^2)$$

This equation, for a uniform arc discharge, limits the current density. The maximum value is smallest at the entrance where σ and u are small and where B should be small to avoid sidewall breakdown. Thus, for $\gamma = 1.15$ (5000°K and 4.5 torr) and M = 4470/1505 = 3 for 37.5% conversion of total enthalpy to directed kinetic energy

$$\frac{\sigma B u}{j} > 0.792$$

At $B = 0.1$ and $\sigma = 388/(1 + 2900 \times .01) = 12.9$, $j < 7280$ amps/m^2 to avoid choking. At the channel entrance on CA-1 and CA-2, the maximum arc area per electrode is 1.77×10^{-3} in^2 so that even at 100 amperes $j = 100/1.77 \times 10^{-3} = 56,500$ amps/m^2, or eight times the choke value.

If the arc were concentrated in a narrow filament, the effective value of σ would be much larger, allowing a larger j. The sidewall would probably also be less effected by a concentrated arc on centerline. The arc will be less diffuse and σ higher at low B field. Here again a low B field is indicated for the entrance.

For $B = .0183$, $\sigma = 194$ for a 5000°K inlet temperature. This would allow:

$$j_{max} < \frac{194 \times .0183 \times 4470}{0.792} = 20,000 \text{ amps/m}^2$$

a more reasonable limit.

The question of choking was not investigated experimentally due to problems with sidewall failure. The machines were, however, observed to be in supersonic flow at the exit as indicated by shock patterns.

4.7 ACCELERATOR SIDEWALLS

Confinement of the flow in a crossed-field accelerator is necessary in almost any practical application of the device to control the channel pressure independent of downstream and ambient conditions and under some conditions to prevent degradation of the stream velocity through mixing with the surrounding atmosphere.

The use of channel walls made of thick ceramic materials, even with water cooling, has been found inadequate because of their high rate of ablation at power levels of interest for practical devices. In order to handle the high heat fluxes to the walls, a wall formed of water-cooled metallic elements appears desirable.

The use of a highly cooled wall does not affect appreciably the efficiency of the device. This is because the enthalpy of the gas is so great that the driving potential for heat transfer, which is equal to the difference between the wall surface temperature and the adiabatic wall temperature of the stream, is practically independent of the wall temperature for ranges of temperatures which materials will withstand. The wall material and temperature can have an effect upon the recombination reactions which will occur there and will also, therefore, have some effect on the heat transfer rate.

The metallic elements must be segmented to avoid short circuits so that the accelerating discharge will pass through the plasma rather than through the side wall. Designs of that sort are shown in Figures 2.11 and 2.14. The gaps between the sidewall elements must be filled with some insulating material to maintain a gas-tight confined channel. As insulators become electrically conducting at high temperatures, it is necessary to design the sidewall so that heat transfer from the insulating material to the water-cooled metallic elements is sufficient to keep the temperature of the insulator within tolerable bounds. Cooling of the insulator is improved by making the gaps between elements small.

Five separate current paths between the cooled metal sidewall elements are possible, namely (1) through the insulation, (2) along the insulation surface, (3) through the gas between elements (if the insulation is cut back), (4) through the general boundary layer and (5) a loop through the main plasma stream. It is not possible, on the basis of information available, to determine which current path initiated breakdown in any of the experiments. It is important that hot spots do not develop on the metal elements and that the boundary layer and insulation be kept cool. The boundary layer flow tends to be vulnerable to breakdown because velocities and the associated back emf are low. Normal current paths through the boundary layer are also parallel to the B field, the low resistance direction.

If the sheath voltage drops on the metal wall elements occur across a length of the order of the Debye length, this protective factor should be relatively independent of element spacing.

An initial test of the segmented sidewall design was performed with the uncooled sidewall shown in Figures 2.10 and 2.11. The tests were performed in an unconfined accelerator using argon.

The sidewall shown in Figure 2.14 was tested in the accelerator shown in Figure 2.13, using air as the working fluid. The test conditions are described in Table 9. This test indicated that more than fifty volts per gap could be sustained without arc attachment through the sidewall. Note that the maximum B field was only 520 gauss.

Sidewalls of CA-1 were of the same configuration as the model shown in Figure 2.14. The sidewall elements were 5/8 inches by 5/8 inches in cross sections and 2-1/4 inches long. The gaps were filled with zirconium oxide cement. CA-1 is shown in Figures 2.17 through 2.21. Four tests were performed with CA-1. The test conditions and results are described in Tables 2.6, 2.10, 2.11, 2.12., 4.1 and 4.2. In the third and fourth tests, arc attachment to the sidewall occurred after steady-state operation of about 180 and 45 seconds respectively. The condition of the accelerator after the tests is shown in Figures 2.25 and 2.26.

Because of the length of time which elapsed before arcing occurred in the third and fourth tests, it was thought that heat transfer to the zirconia insulator raised it above the temperature at which it became appreciably conducting and that the enhanced conductance of the whole wall permitted attachment of the arc.

The sidewalls of the accelerator CA-2 were designed on the basis of the experience gained from testing of accelerator CA-1. The elements of the sidewall were reduced in height from 5/8 inches to 1/2 inches, the gaps between elements were reduced from 1/8 inches to 1/16 inches and the insulating material used was recessed from the streamside surface of the wall by 1/4 inches. The available data on the properties of insulating materials indicated that the use of thoria rather than zirconia would tend to prevent the sidewall from becoming conducting because the thoria is many orders of magnitude less conducting at a given temperature level. Arc attachment also occurred in the fifth and sixth tests which were performed with CA-2.

In an attempt to reduce the voltage required to pass the desired current through each electrode pair, modifications of the arc jet were made during the program. By removing the stilling chamber upstream of the de Laval nozzle and by redesigning the nozzle, the efficiency of the arc jet was increased slightly. It was hoped to increase the total enthalpy of the gas at the accelerator inlet and to lower the voltage drops across the electrodes.

Test conditions and results relevant to the problem of arc attachment are summarized in Table 4.2. Two possible causes for arc attachment, namely excessive heat transfer and excessive voltage (due to excessive B field at low temperatures) can be examined on the basis of the experimental results presented in Table 4.3. A plausible explanation of the behavior observed would be:

(a) Arc attachment occurred in CA-1 when the zirconia insulator became conducting.

(b) Arc attachment occurred in CA-2 because the presence of thoria reduced the breakdown potential required to start the attached arcs.

The second test on the CA-1 accelerator in which the power input to the accelerator was 199 kw and the total enthalpy of the inlet stream was 25 kw, was relatively successful.

In retrospect, it is believed that the sidewalls performed very well. They were simply overloaded by the high arc voltage required to drive a reasonable current through the cold gas in the strong magnetic field at the accelerator entrance. (Note that breakdown occurred near the entrance in every case.)

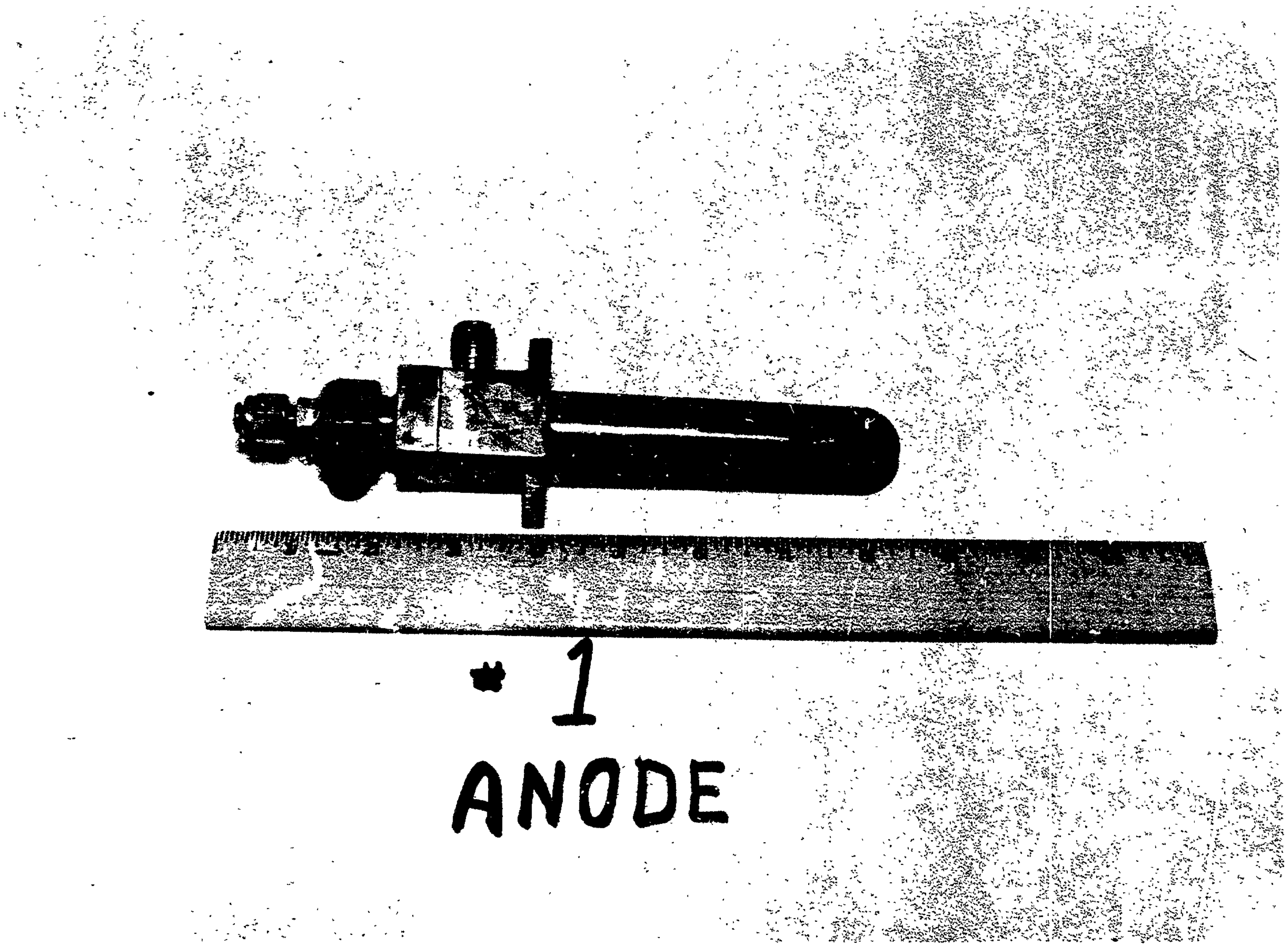

Figure 4.1 View of CA-1 first anode after third test

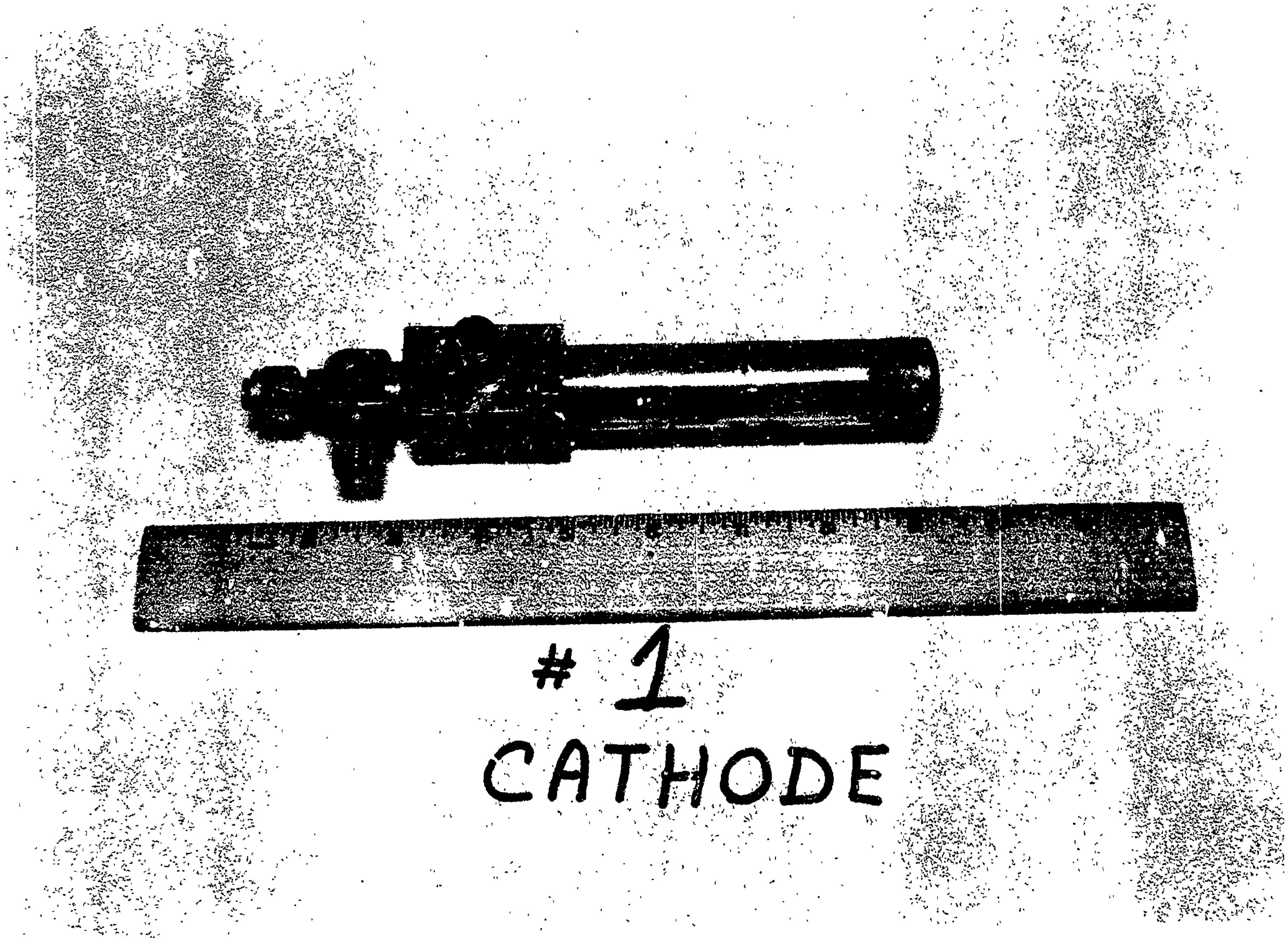

Figure 4.2 View of CA-1 first cathode after third test

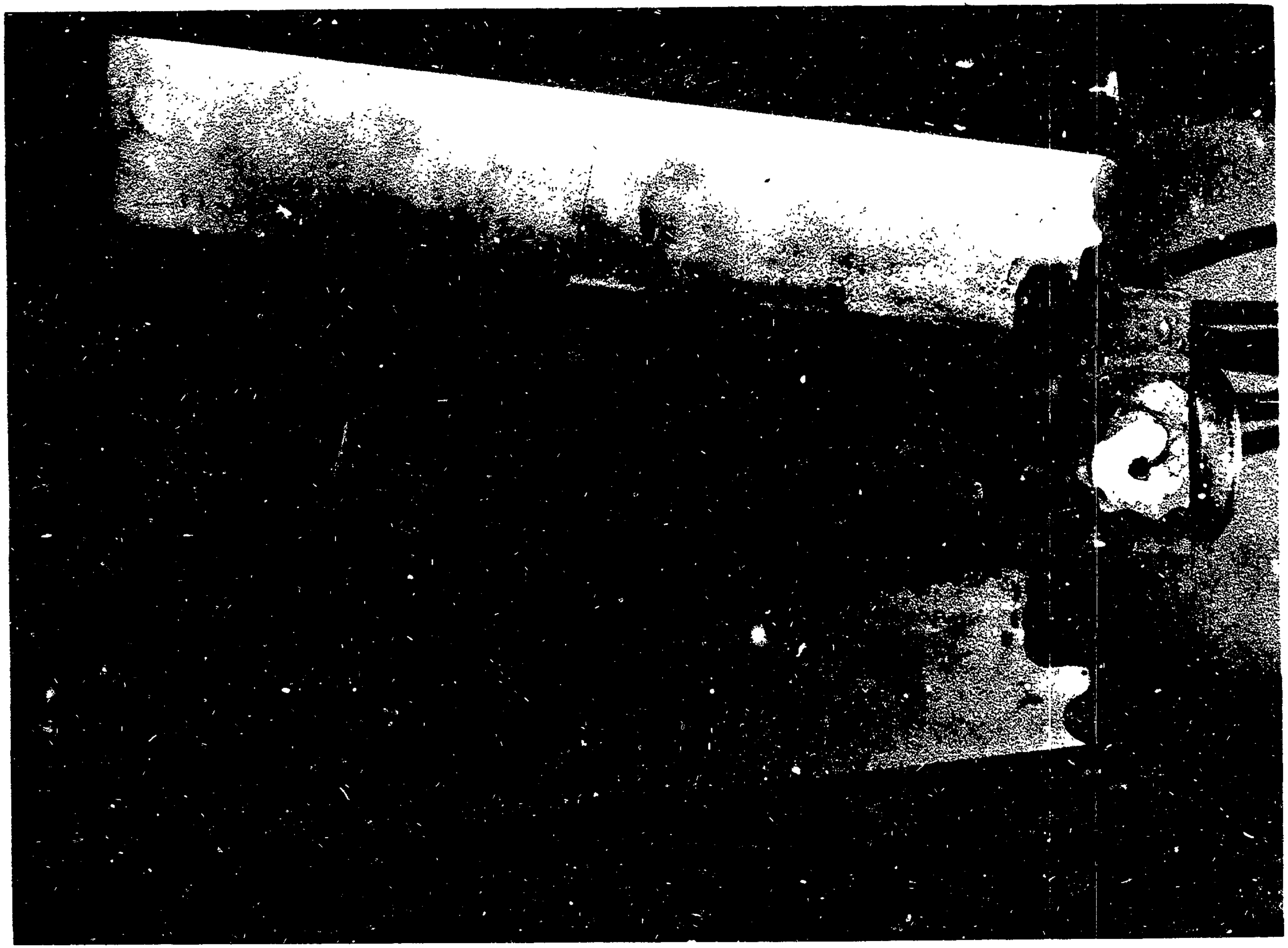

Figure 4.3 Sideview of CA-1 after the fourth test

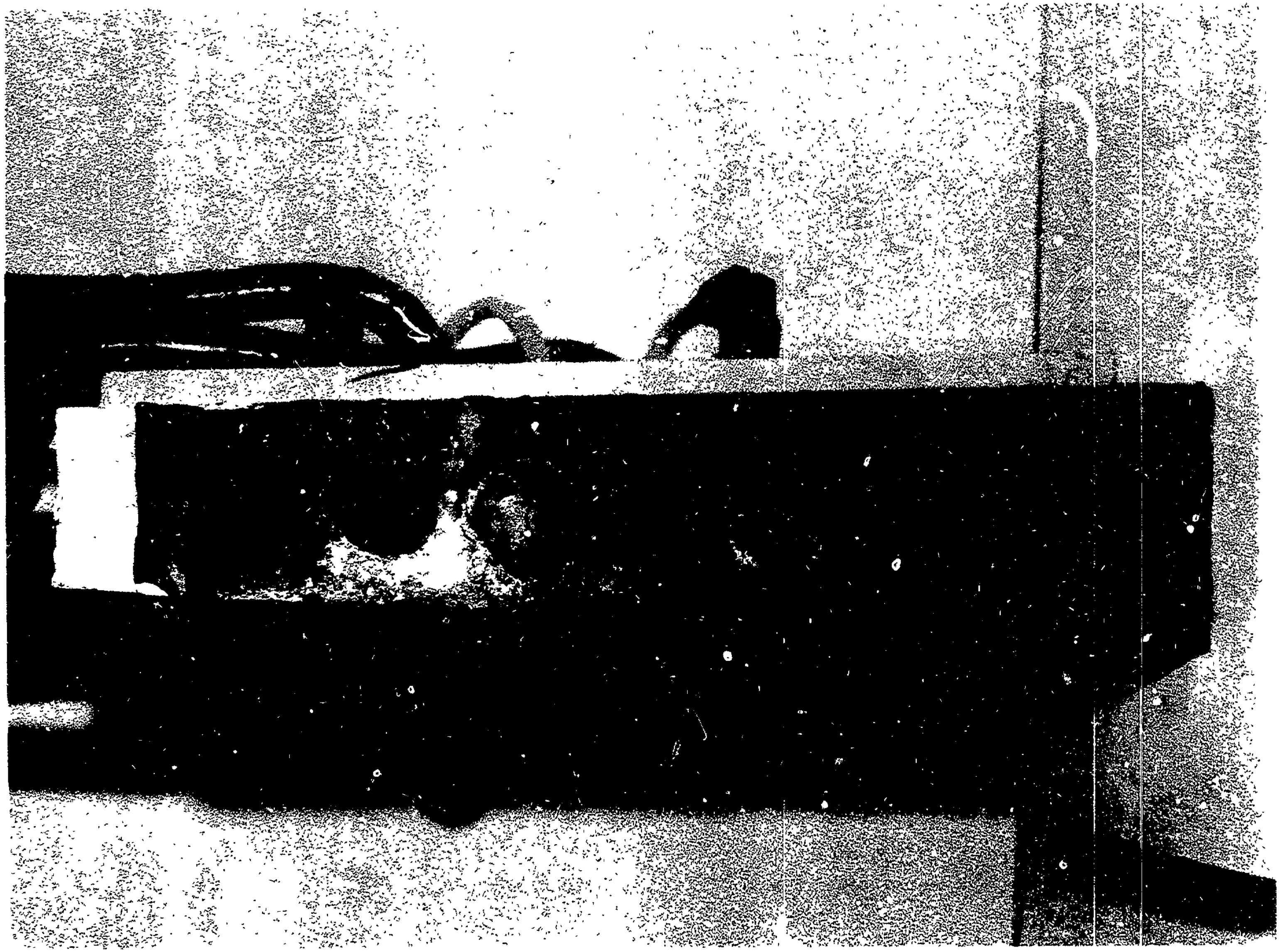

Figure 4.4 The cathodes of CA-1 after the fourth test

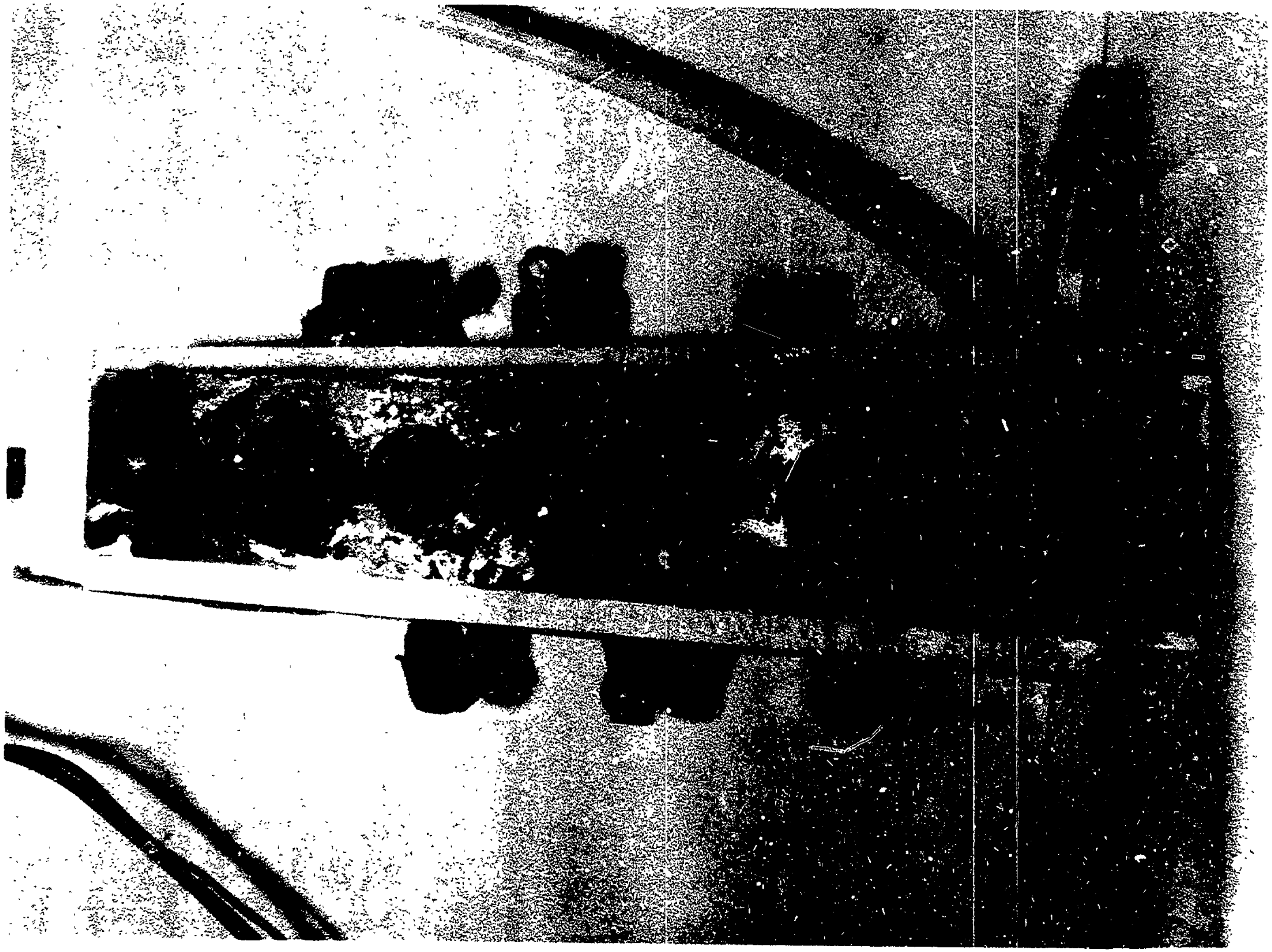

Figure 4.5 The anodes of CA-1 after the fourth test

Figure 4.6 View of left sidewall of CA-2 after the sixth test

Figure 4.7 View of CA-2 anode holder after the sixth test

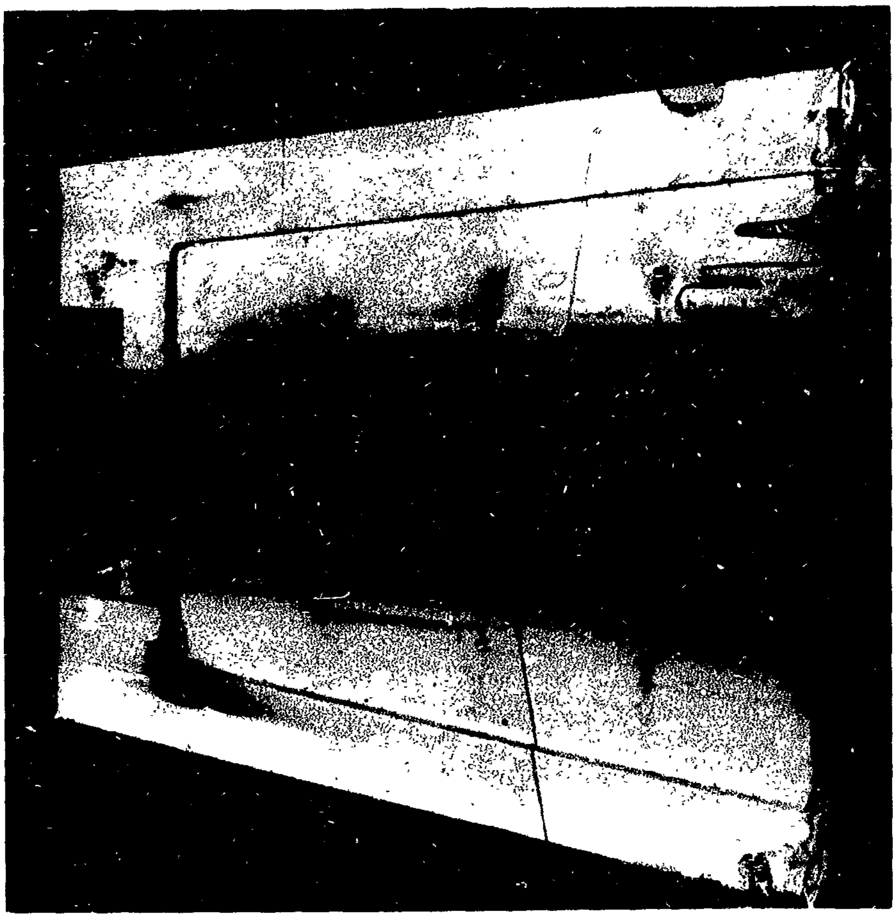

Figure 4. 8 View of right sidewall of CA-2 after the fifth test

TABLE 4.1

PERFORMANCE DATA FOR TESTS 4, 5 and 6

Test No.	Electrode Pair	I_o (amp)	V_o (volts)	p_{acc} (kw)	B (webers/m^2)	θ_{acc} (newtons)	$\frac{\theta_{acc}}{hI_oB}$	U_f-U_o (m/sec)	η_{acc} (%)	Tank Pressure (mm/Hg)	Duration of Acc. Test (sec)
4	1	450	240	108	0.10	6.2	0.53	1390	5.5	0.7	46
	2	450	160	72	0.10						
	3	450	140	63	0.10						
	4	240	135	32	0.10						
	5	545	155	85	0.10						
	(Total)	2135		360							
5	1	≈450	≈300	135	0.20	28.0	1.06	6900	37.2	0.7	≈ 2
	2	430	139	68	0.20						
	3	158	340	53	0.20						
	4	75	370	27	0.20						
	5	450	≈160	72	0.20						
	6	≈400	330	132	0.20						
	(Total)	1963		487							
6	1	485	155	75	0.05	5.3	0.67	1265	7.0	0.7	27
	2	508	120	61	0.05						
	3	384	105	40	0.05						
	4	254	91	23	0.05						
	5	490	103	51	0.05						
	6	450	86	39	0.05						
	(Total)	2671		289							

TABLE 4.2

OPERATING CONDITIONS FOR CONFINED CHANNEL, CROSSED-FIELD ACCELERATOR EXPERIMENTS USING THE ACCELERATOR SHOWN IN FIGURES 2.17 - 4.8

Test	1	2	3	4	5	6	6A
Plasma enthalpy* (10^7 joules/kg)	1.38	1.72	2.53	3.60	4.42	3.01	3.01
Magnetic field (gauss)	500	1000	1000	1000	2000	500	700
Voltage (volts)							
First electrode pair	240	280	300	240		155	161
Second electrode pair	150	210	220	160	140	120	183
Current (amperes)							
First electrode pair	200	200	300	450	450	480	480
Second electrode pair	200	200	300	450	450	500	500
Test time to failure (sec)	none	none	92	45	1	15	0
Sidewall							
Insulation		zirconia				thoria	
Gap between elements (inches)	1/8	1/8	1/8	1/8	1/16	1/16	1/16
Recess depth** (inches)	0	0	0	0	1/4	1/4	1/4
Element height (inches)	5/8	5/8	5/8	5/8	1/2	1/2	1/2
Voltage between centrally located elements							
Maximum sustained	-	-	-	-	30	50	50
At breakdown	-	-	-	-	35		50

*Plasma enthalpy based upon net energy input in arc jet plus total power applied to first electrode pair.

** Recess depth refers to depth of insulator below streamside surface of sidewall elements.

Centrally located elements were those indicated in Figure 2.20.

Test 6A is listed separately as failure occurred while magnetic field was being increased after 15 seconds of operation at 500 gauss.

Instruments read off scale above 50 volts.

TABLE 4.3

SUMMARY OF EXPERIMENTAL EVIDENCE ABOUT CAUSES OF DOUBLE ARCING ON A CONFINED, CROSS-FIELD ACCELERATOR

Test	Occurrence	Possible Cause	Reason	Contradictory Evidence
1	No failure	Low voltage and power		Voltage higher than in Test 6
2	No failure	Low voltage and power		Voltage higher than in Test 6
3	Failure after steady operation for 92 seconds	High voltage		Did not occur immediately
		Melting of zirconia	Zirconia becomes appreciably conducting near its melting point	
4	Failure after steady operation for 46 seconds	High voltage		Did not occur immediately. Voltage lower than in Test 3.
		Melting of zirconia	Occurred sooner than in Test 3 because of increased power level	
5	Rapid failure	High voltage	Almost immediate breakdown. Voltage higher than in previous tests	
		Melting of thoria	Higher power level than previous tests	Narrower gaps and thoria recessed. Resistivity of thoria high at melting point of copper
6	Rapid failure for B 500 gauss	High voltage	Voltage between centrally located elements higher than that observed in Test 5. Thoria could improve emission from copper elements	Total voltage lower than in previous test
		Melting of thoria		Lower power and higher resistance insulator than in Tests 3 and 4

5. DESCRIPTION OF ACCELERATORS CA-1 and CA-2

Photographs illustrating the construction of Accelerator Model CA-1 are shown as Figures 2.17, 2.18, 2.19, 2.20 and 2.21. Major elements, dimensions and materials are indicated in Figure 5.1.

Accelerator Model CA-2 is shown in some detail in Figures 1.1, 2.23, and 2.24. A drawing indicating the construction is shown in Figure 5.2.

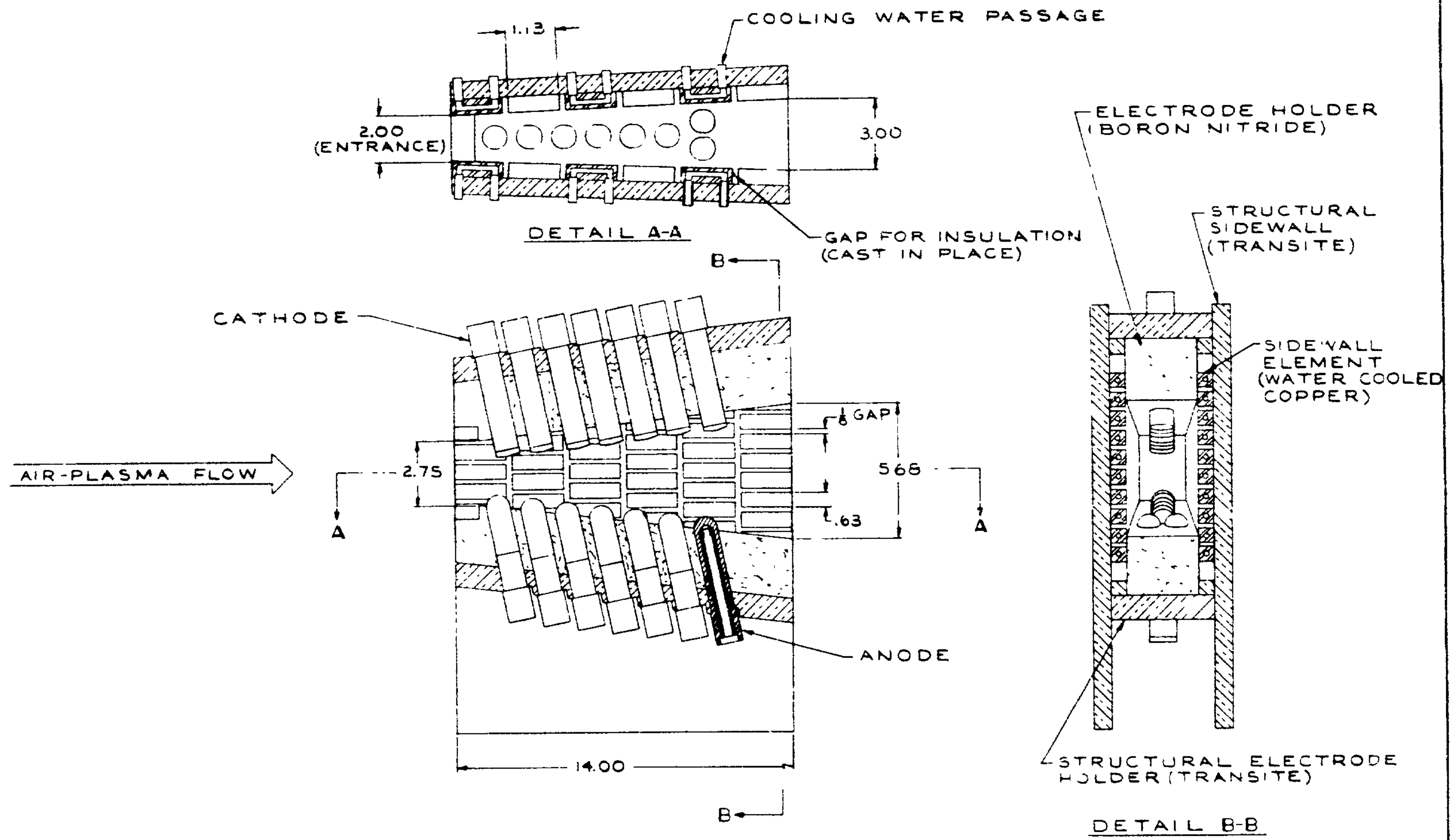

CROSSED FIELD ACCELERATOR
MODEL NO. CA-1

FIGURE NO. 5.1

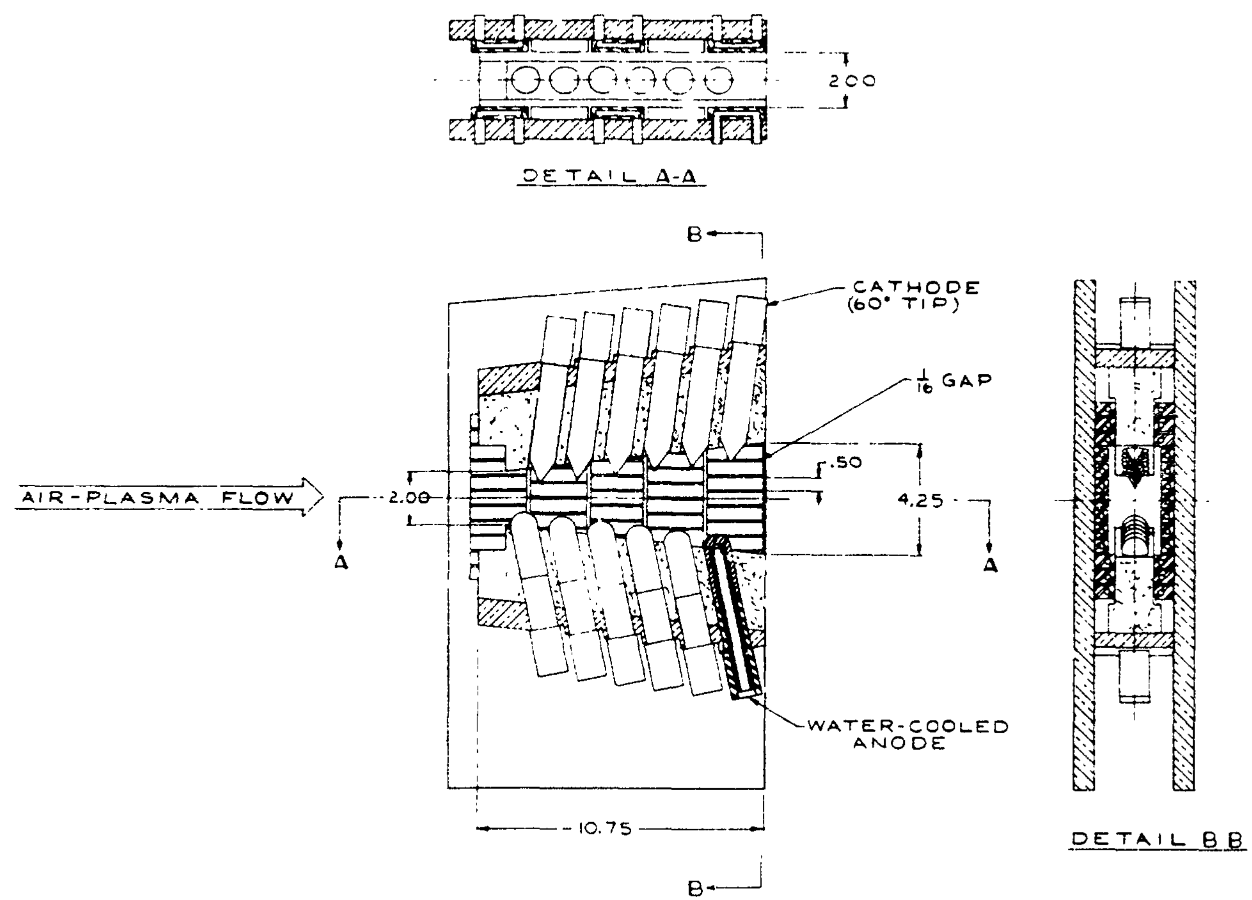

CROSSED FIELD ACCELERATOR
MODEL NO. CA-2

FIGURE NO. 5.2

CA-2

6. ACCELERATOR TESTS AND ASSOCIATED EXPERIMENTS

6.1 PRELIMINARY TESTS WITH ONE PAIR OF ELECTRODES AND SEGMENTED METAL-CERAMIC MATRIX SIDEWALLS

The experimental tests were made utilizing the simple accelerator shown in Figure 2.12, with one pair of electrodes, the majority of the insulating material forming the channel consisting of uncooled firebrick. The anode was of cylindrical shape, domed at the top and water-cooled internally. (Material used was 10W3 copper Elkonite.) The diameter of the cylindrical portion was 3/4 inches (in the CA-1 accelerator, the anodes are of similar shape, differing only in that the diameter is 1 inch). The cathode was a 1 inch square tungsten block, about 5 inches long, without water cooling. It was not thought necessary to cool the cathode as the planned runs with cross-arc were not intended to much exceed one minute, and some radiation cooling from the exposed cathode surface was also expected.

The purposes of the experimental tests were twofold--to investigate the suitability of the electrode materials (copper and silver Elkonite anodes; tungsten or thoriated tungsten cathodes) for use in an air plasma environment, and to investigate the cooling efficiency and the electrical characteristics of the sidewall configuration discussed in Section 4.7 and shown in Figures 2.13, 2.14 and 2.15.

The duration of the test runs totaled approximately 10 minutes (including time with and without the cross-arc and the magnetic field). Total time with the cross-arc in operation (input powers ranging from 13.5 to 116 kw) was 2.4 minutes. The tests were terminated when arc attachment to a water fitting in the anode coolant supply circuit resulted in the failure of the fitting and a resultant water leak. The spurious arcing occurred probably because of erosion of the uncooled firebrick insulation used in this preliminary accelerator.

Measurements of the heat flux to the water-cooled sidewall were made with the arc jet alone. Equilibration required 2-3 minutes. It was not possible to allow sufficient time for equilibration with the cross-arc in operation due to the rapid erosion rate of the firebrick portions of the accelerator channel. An inspection of the rate of rise of coolant temperature in the two sidewall cooling circuits (one adjacent to the anode and the other to the cathode) revealed that the proportion received by each part did not change when the cross-arc was in operation. This indicates that no arc attachment to the sidewall bars occurred during these tests. The condition of the sidewall after the complete series of tests is shown in Figure 2.16. The results obtained during the tests are shown in Table 2.8.

Figure 2.5 shows the calculated current-voltage characteristic for the first pair of electrodes of the CA-1 accelerator at B = 0, B = 500 gauss and at the design point of 2000 gauss. These were calculated by the methods outlined in Section 3. The discrepancy between the experimental results and the theoretical predictions at low field strengths and low current levels might be due to arc constriction.

The fact, indicated in Table 2.8, that the measured thrust exceeded that calculated ($\Theta/hIB > 1$), is not unexpected because a considerable amount of erosion of the firebrick walls occurred and boosted the mass flow through the accelerator to a level considerably above the 0.01 pounds/second of air which was the inlet flow condition. This could cause internal thrust augmentation in a pressure gradient. Weight loss from the electrodes was small--the (uncooled) cathode losing 4 grams and the anode losing nothing during the complete series of tests.

Alternate possibilities for explanation of the high thrust measured are:

(a) The static pressure at the end of the accelerator was above ambient static.

(b) The accelerator channel was supporting a favorable pressure gradient, acting as a nozzle.

(c) The dynamometer was not reading correctly at this early date.

(d) There was an externally applied electromagnetic thrust from the electrical leads.

6.2 TESTS ON THE 500 KW ACCELERATOR MODEL CA-1

Four tests of accelerator CA-1 were performed. The test conditions and results are presented in Tables 2.6, 2.10, 2.11, 2.12, 4.1 and 4.2. Photographs of the accelerator before and after the tests appear in Figures 2.17 through 2.21 and Figure 2.25. In each test, the accelerator discharges were started with no applied magnetic field, to reduce the breakdown voltages in starting the electrode arcs. Then the magnetic field was increased while the electrode currents were maintained approximately constant.

For Test 1, which was of three minutes duration, the applied magnetic field was 0.05 webers/m^2 (500 gauss), the total applied current was 1000 amperes and the electric power input to the accelerator was 132 kw. The zirconia insulator between the sidewall cooling bars was cured during the test as indicated by the change in color of the initially pink ceramic to white. The only noticeable erosion occurred in the boron nitride electrode holders, with the most severe material loss occurring behind the first (upstream) anode. The initial condition of CA-1 is shown in Figure 2.21, and the condition after the first test in Figure 2.27. The thrust increment provided by the accelerator in Test 1 was expected to be about 2.5 newtons (9 ounces). Instrument limitations render measurement of such a low value of thrust highly uncertain. Therefore the thrust is indicated, in Table 2.12, as being of the order of the value obtained from the incremental change in thrust which occurred when the magnetic field was turned on.

Test 2 of CA-1 was of three minutes duration and was performed at an applied field of 0.1 webers/m^2 (1000 gauss) and an applied power of 199 kw. The thrust indicated in Table 12 for Test 2 is estimated to be accurate to within about 10%. The value was obtained by noting the change in total thrust when the accelerator was turned on and when it was turned off. Dead weight calibrations made during the test indicated that incremental thrust readings were in accord with the initial calibration in spite of the sizeable zero shift (equivalent to about 15 newtons) which occurred during the test. Additional erosion of the electrode holders occurred in Test 2, as shown in Figures 2.28 and 2.29. Some melting of the zirconia between the sidewall cooling bars was observed. Figure 2.29 shows a photograph of the accelerator after the second test with a mirror placed in the channel to afford a better view of the damaged section of the left sidewall. The diagrams in Figures 6.1 and 6.2 show the areas where sidewall erosion occurred. The erosion of the left sidewall (when looking upstream) was more severe than that of the right sidewall. The loss of insulator from the regions immediately adjacent to the cooling bars indicated that double arcing might have been occurring.

Test 3 was performed at a magnetic field of 0.1 webers/m^2 (1000 gauss), a total current of 1230 amperes, and an applied power of 257 kw. The test was terminated when a water leak developed after about a minute and one half of operation. The left sidewall was severely damaged in the area adjacent to the first three electrode pairs, as shown in Figure 2.25. The local melting of sidewall cooling bars which occurred is a clear indication that double arcing caused the failure. No additional erosion of the right sidewall, shown in Figure 6.3, occurred during the test. The right sidewall and the electrodes were coated with a residue of zirconia from the left sidewall. The electrode holders, which are shown in Figures 6.4 and 6.5, were not appreciably eroded during Test 3. This indicates that the wells formed upstream of the cathodes and downsteam of the anodes had reached a stable depth during Test 2. The deepest well was that behind the first anode. It extended slightly over one inch into the boron nitride block. The well was adjacent to the eroded area on the electrode itself which is shown in Figures 4.1 and 4.2. When cleaned, the electrodes were found to be in excellent condition. Some erosion occurred on the downstream side of each anode and at the tungsten-copper solder joint of each cathode.

Test 3 was terminated before pitot tube measurements could be made. The recorded thrust given in Table 2.11 is estimated to be accurate to within 10 percent. An inference of the amount of current which passed through the left sidewall may be drawn from the difference between the thrust observed and the theoretical thrust, resulting in an estimated current through the sidewall of about 440 amperes.

The double arcing of the accelerating discharge through the sidewall elements of accelerator CA-1 in the third test occurred after 92 seconds of operation. The applied power and electrode voltages were higher than in the preceding tests. It therefore appeared that either the high voltage or the increased power level resulted in double arcing. The voltages required at a given current and magnetic field level could be reduced by raising the enthalpy of the stream provided by the arc jet. Accordingly, the arc jet nozzle was modified by removing the stilling chamber and by making use of the constant area anode as the throat of the de Laval nozzle. This modification increased the net power into the stream to 55 kw at an applied power level of 156 kw (see configuration 3, Figure 7.1).

Following the third test, CA-1 was repaired and readied for testing. With the repaired accelerator and the modified arc jet nozzle, the fourth test of CA-1 was performed. The operating conditions were the same as those in Tests 1, 2 and 3 as given in Table 2.10, except that the net arc jet power was 55 kw. The data obtained are presented in Tables 2.11 and 2.12. The condition of CA-1 after the fourth test is shown in Figures 2.26, 4.3, 4.4 and 4.5. The arc jet was found to produce a stream having an average velocity of 9600 feet per second at a net power input of 55 kw. The accelerator provided a velocity increment of 4500 feet per second, assuming a fully expanded jet. If so, the average velocity of the stream at the accelerator exit was 14,100 feet per second indicated by the thrust stand measurement of the total momentum of the exhaust stream. The full design point current of over 2000 amperes was applied and the magnetic field of 1000 gauss was half of that planned for full power operation.

The increased power input in the arc jet in the fourth test did reduce the voltage requirements of the electrodes. In spite of this, double arcing occurred and caused failure of the right sidewall after 46 seconds of operation. The voltages across the electrodes were smaller than in either the second or the third tests, but the power level was higher. These facts combined with the time required for the double arcing to begin indicate that the failure was possibly associated with heating of the zirconia insulation between the sidewall elements. The conductivity of zirconia approaches that of the plasma at temperatures near its melting point. The CA-1 design apparently did not keep the insulator at a low enough temperature to prevent it from forming a conducting link between the sidewall elements.

Two of the thoriated tungsten cathode caps were separated from the copper electrode water jackets in the fourth test. (See Figures 4.3 and 4.4.) This appeared to be caused by arc attachment at the solder joint between the cap and the water jacket. Conical tungsten caps with a 60° included angle were used in subsequent tests to enhance arc attachment at the cathode tip.

6.3 TESTS ON THE 500 KW ACCELERATOR MODEL CA-2

Model CA-2 incorporated several improvements, including:

(a) The gaps between wall cooling elements were approximately 1/16 inches rather than 1/8 inches as in CA-1 in order to enhance the cooling f the insulating material placed between them.

(b) The insulating material was recessed so that its stream-side surface is 1/4 inches below that of the copper sidewall elements in order to reduce the heat flux to the insulator.

(c) Thoria was used as the insulator rather than zirconia as in CA-1 because it has a much greater electrical resistivity at a given temperature than zirconia.

(d) The sidewall elements were 0.5 inches in width, rather than 0.62 inches as in CA-1 in order to reduce the voltage drop between elements.

Two accelerator tests were performed using accelerator CA-2 with thoria insulation on the sidewalls. These tests will be denoted as the fifth and sixth tests, respectively. The tests' results are presented in Tables 2.6 and 4.1.

In the fifth test, which was performed at a total applied current of 1950 amperes and an applied magnetic field of 2000 gauss, a thrust increment of 28 newtons was observed. The sidewall failed almost simultaneously with the time at which the field reached 2000 gauss. The elapsed time from the point at which the magnetic field was increased from zero to the time at which arc attachment to the sidewall occurred was about 2 seconds. Motion pictures of the plasma stream at the accelerator exit and of the panel of voltmeters used to observe the voltage drops between sidewall elements as well as the current and voltage traces for the electrodes offer some evidence that the thrust reading was obtained before arc attachment. If that were the case, the corresponding velocity increment across the accelerator, assuming a fully expanded jet, would have been 21,000 feet per second and the exit velocity would have been 31,300 feet per second. However, the evidence that arc attachment occurred after a gross thrust of 28 newtons was observed is not conclusive.

The sixth test was performed with a total applied current of 2670 amperes and an initial applied magnetic field of 500 gauss. The recorded accelerator thrust was 5.3 newtons. Following 27 seconds of operation at 500 gauss, the magnetic field strength was increased until arc attachment occurred at about 700 gauss. The applied voltages across the electrodes were lower in the sixth test than in any of the preceding tests resulting from increased conductivity in the plasma core because of the increased ratio of applied current to applied magnetic field. The arc jet net power input to the stream was approximately 6 percent lower in the sixth test than in the fifth, however, the change in static enthalpy was negligible. The voltage across the first pair of electrodes was only 166 volts at the time when arc attachment occurred. The voltage drops between sidewall elements, however, were substantially higher than recorded in the fifth test.

Comparison of the conditions and results of the sixth test with those of previous tests indicates that one or more of the following factors contributed to the occurrance of double arcing in the sixth test:

(a) Closer spacing of the sidewall elements

(b) Recessing of the insulator

(c) Use of thoria rather than zirconia

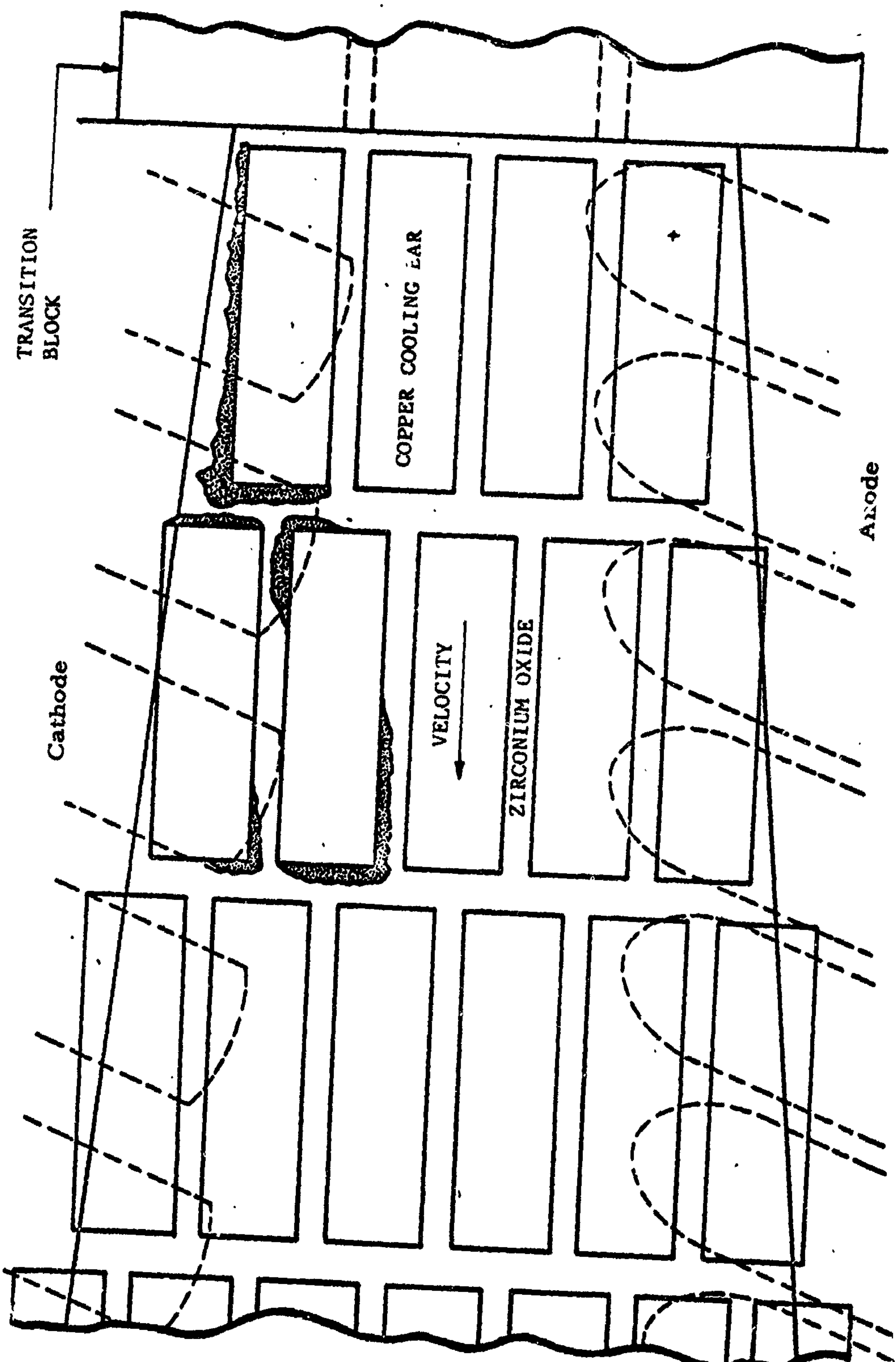

Figure 6.1 Schematic of left sidewall of CA-1 after Test 2

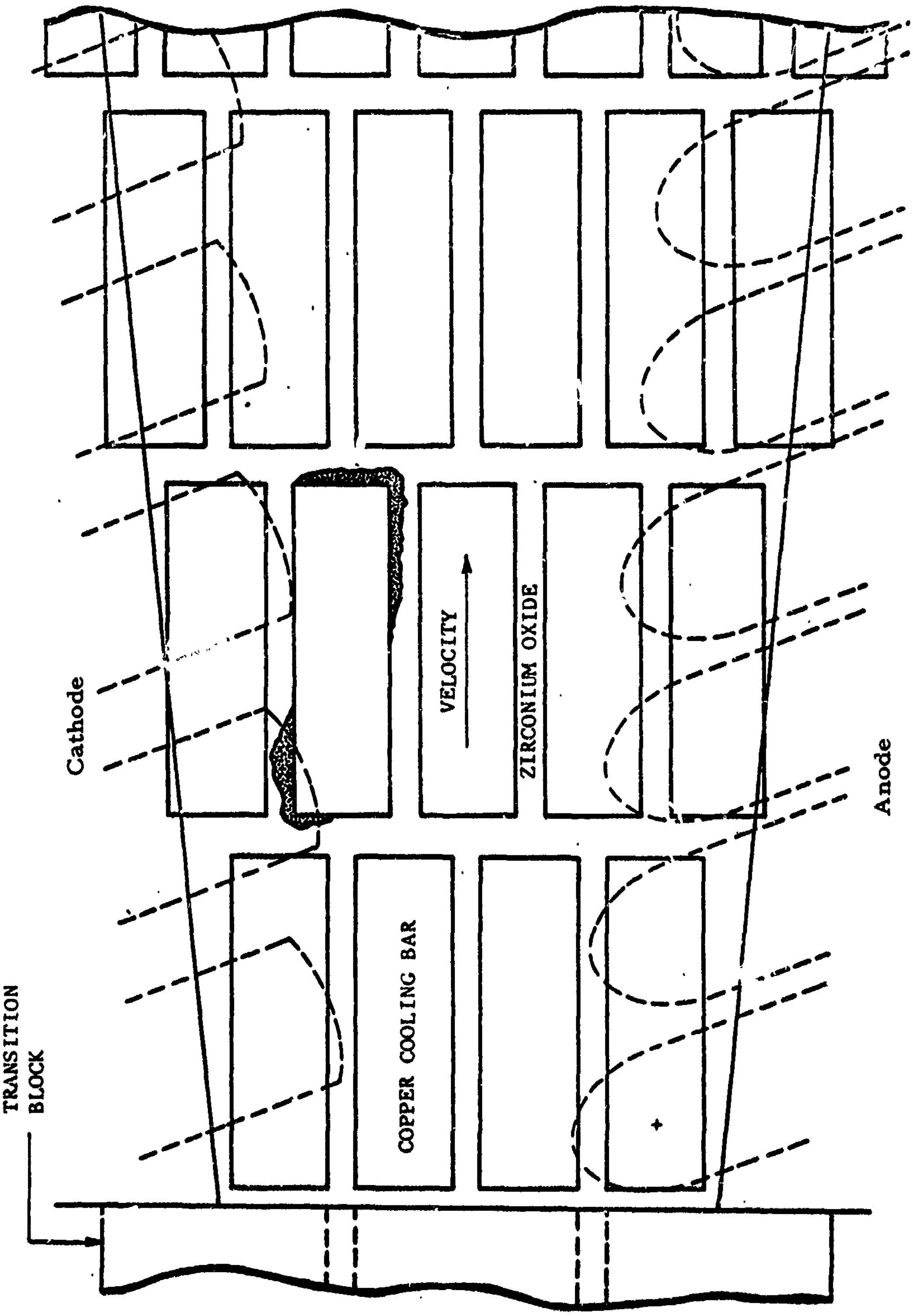

Figure 6.2 Schematic of right sidewall of CA-1 after Test 2

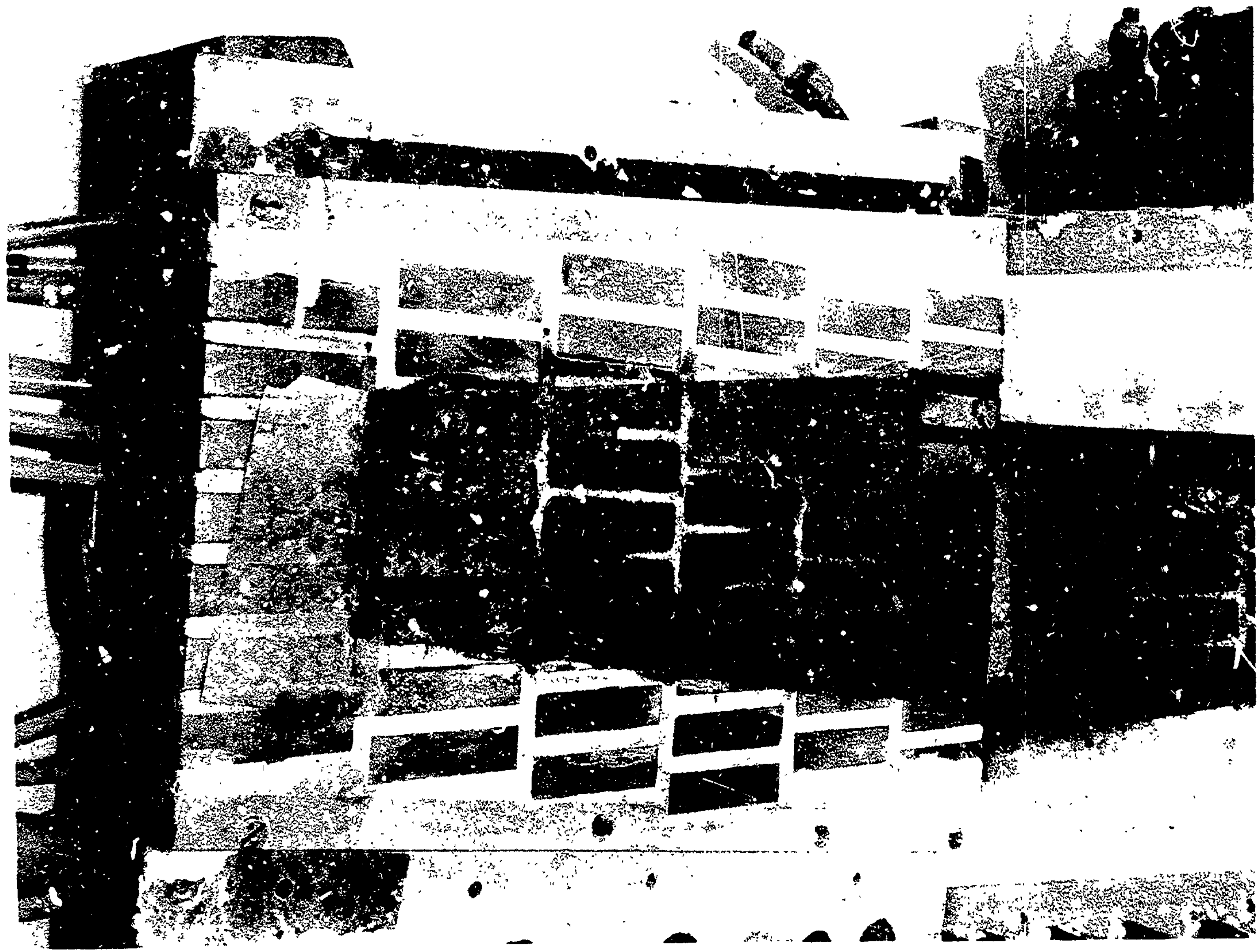

Figure 6.3 View of CA-1 right sidewall after third test

Figure 6.4 View of CA-1 anode holder after t rd test

Figure 6.5 View of CA-1 cathode holder after third test

7. PLASMA GENERATOR TESTS

The plasma generator, followed by a plenum chamber de Laval nozzle, serve to heat and pre-accelerate the flow. Since the general objective of the program is to accelerate air to 25,000 to 40,000 feet per second it is reasonable to pre-accelerate to the highest velocity achievable with the plasma generator and de Laval nozzle. This requires high enthalpy operation, which is compatible with the desire that the accelerator be fed with pre-ionized gas in order to reduce voltage requirements at the first electrode pair. In practice, the maximum enthalpy is limited by the capabilities of the arc head and the large losses sustained, particularly at the anode and in the de Laval nozzle throat. Variations in the length of plenum chamber and length of the supersonic portion of the nozzle had relatively small effects on losses. The variations made in plenum and nozzle configurations are shown in Figure 7.1. The power to the gas stream as measured and the velocity equivalent of thrust are shown in the following table:

Designation	Total Input (KW)	Power in gas (KW)	Power to gas (%)	H_T Exhaust Total Enthalpy (Btu/lb) //(j/Kg) x 10^{-7}	V (fps) //m/sec	$\frac{V^2}{2H_T}$ (%)
-1	172	59.2	33.2	5600//1.302	10,220//3115	37.2
-2	186	69.6	37.4	6600//1.535	11,280//3435	38.5
-3	156	55.5	35.6	5260//1.222	9,600//2930	35.1
-4	158	62.2	39.4	5890//1.370	(10,580)//3220	37.9

Most of the gain expected in eliminating the plenum chamber and shortening the nozzle in changing from -2 to -4 was apparently lost by reducing the (0.500 inch) throat diameter to match the anode exit (0.375 inch I.D.).

The enthalpy levels achieved were relatively disappointing. The de Laval losses (losses/component input) were around 50% and those in the arc head about 40%. The arc head was therefore delivering around 10,000 to 13,000 Btu/lb at the anode exit. On the basis of the data presented, the -2 plenum and nozzle configuration should probably have been utilized for all experiments. Not only is the efficiency indicated relatively high, but the contours are more suited to delivering of a shock-free uniform, unseparated flow. The -2 nozzle was designed for equilibrium flow to the throat and frozen flow thereafter.

The nozzle selection was confused by a tendency for the arc head to sometimes operate in a low-efficiency mode. This is probably a short-arc mode with large anode heat-transfer losses. This condition might have been caused by damage to the gas injection ring around the cathode. The problem was not investigated in detail because, in general, very little difficulty was experienced with the arc head. Its reliability did not interfere with accelerator testing.

At the beginning of the CA-1 tests it was decided to operate the arc head on two 80 KW rectifiers, utilizing the remainder on the electrodes. Maximum power input was thus limited to 175 KW to the arc head even for short duration runs. (In several early tests, 190 KW was obtained but could not be duplicated later). The arc head is believed capable of operation at 210 KW and delivering a net of 75 KW to the gas stream (35.7 percent efficiency and $H_T = 1.65 \times 10^7$ j/Kg).

In retrospect, it is believed that the plasma generator should have been powered at the maximum level to increase ionization in the gas input to the accelerator. This would reduce the voltage requirements of the first electrode pair and the danger of arc attachment to the side wall. This should have been done even at the cost of removing power supplies from downstream electrodes.

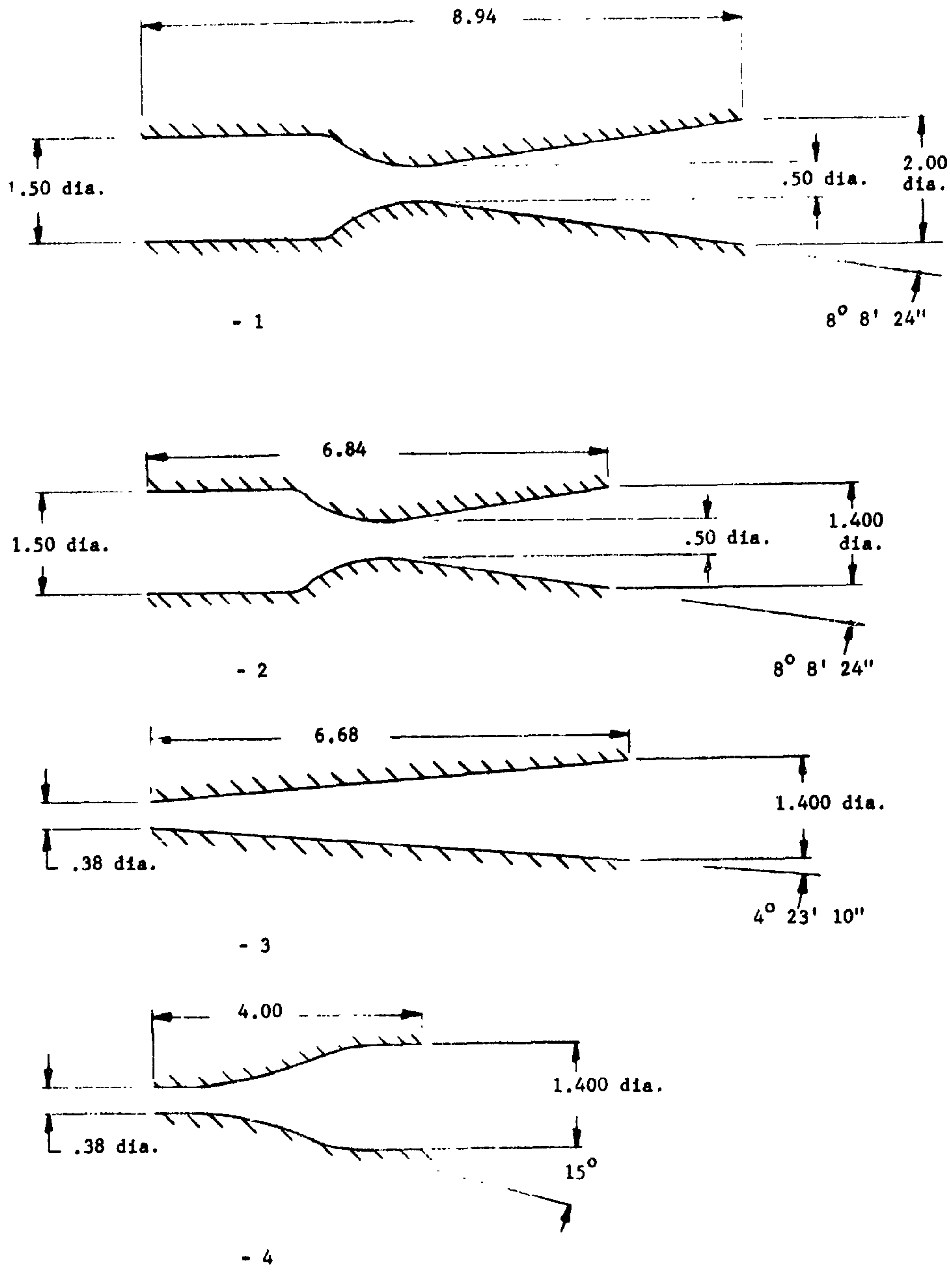

Figure 7.1. Plenum chamber and deLaval nozzle configurations

8. PLASMA INSTRUMENTATION

The following instruments were selected for use in the study of properties of the plasma flow stream:

Thrust dynamometer

Static pressure taps

Total (impact) pressure tube

Calorimeter

Ablation rake (carbon)

Microwave interferometer

Conductivity probe

Current density probe

Consideration was also given to the use of optical spectroscopy, Langmuir probes, Thomson scattering of coherent (laser) radiation, and a velocity meter, but practical considerations of schedule, cost and objectives limited attention to the above list. Measurements were handicapped by lack of success in operation of the accelerator. Most of the effort was directed to this objective.

8.1 THRUST AND STATIC PRESSURE

The thrust dynamometer was operated successfully after initial difficulties with zero shift were overcome. In order to resolve momentum average velocity changes through the accelerator, it is necessary to measure static pressures at both inlet and outlet. Static pressure measurements were made at the exit to the plasmajet de Laval nozzles initially used. Static pressure taps were not added to accelerator models CA-1 and CA-2, this being deferred in favor of attention to the sidewall problem. The thrust data presented include effects of both static pressure and the Lorentz forces. The dynamometer was made by mounting the plasmajet, accelerator and magnet assembly on a platform, suspending the latter as a ballistic pendulum on four wires and constraining movement with a small cantilever spring on which a bonded-wire strain gage was mounted. All electrical and hydraulic conduits were brought in straight and vertically to minimize spring and bourdon forces. Suspension wires were insulated against temperature changes. In this type of dynamometer it is important that the foundation (supports) do not change relative length or elevation between calibration and use in test. Magnetic forces are also a matter of concern, but no effect was detected. Fortunately the dynamometer can be calibrated under a force applied by a fine wire passing through an unsealed hole in the main test chamber. Calibrating forces can be applied, then, under any condition of operation. The dynamometer table and suspension wires can be seen in Figure 8. 1.

8.2 CALORIMETER AND IMPACT PRESSURE TUBE

These two instruments were combined into a single water cooled probe and mounted on a traversing mechanism. The device measures the heat transfer and total pressure recovery behind a nearly-normal shock wave over the tip of the tube. The instrument is well-suited to survey a steady accelerator jet stream for uniformity. Limited operation of the accelerator precluded collection of extensive data.

8.3 ABLATION RAKE

An ablation rake, consisting of a group of electrode carbon rods mounted in a water-cooled support, was also constructed for jet uniformity surveys. Due to lack of success in steady, high power operation of the accelerator the rake was not utilized.

8.4 MICROWAVE INTERFEROMETER

A 35 KMC (V band) microwave interferometer was installed at the test site to measure the free electron density in the accelerator jet. Wave guides were passed through the walls of the vacuum chamber for access to a short path through the jet. The apparatus was installed and operated during tests on the plasma generator and de Laval nozzle. In this experiment the jet was relatively cold. The free electron density and plasma frequency were low and an attenuation of only 2 db was measured. The apparatus was removed from the test area to avoid damage during laboratory remodeling. The equipment was not reinstalled pending steady, high power operation of the 500 KW accelerator. A description of the apparatus is contained in Appendix C.

8.5 PLASMA CONDUCTIVITY AND CURRENT DENSITY PROBES

These probes were studied for possible application to study of the physical properties of the plasma flow stream. Theory and description of the two types of probes are contained in Appendices D and E respectively. Problems with operation of the accelerator equipment discouraged the construction of these probes for use in the plasma stream.

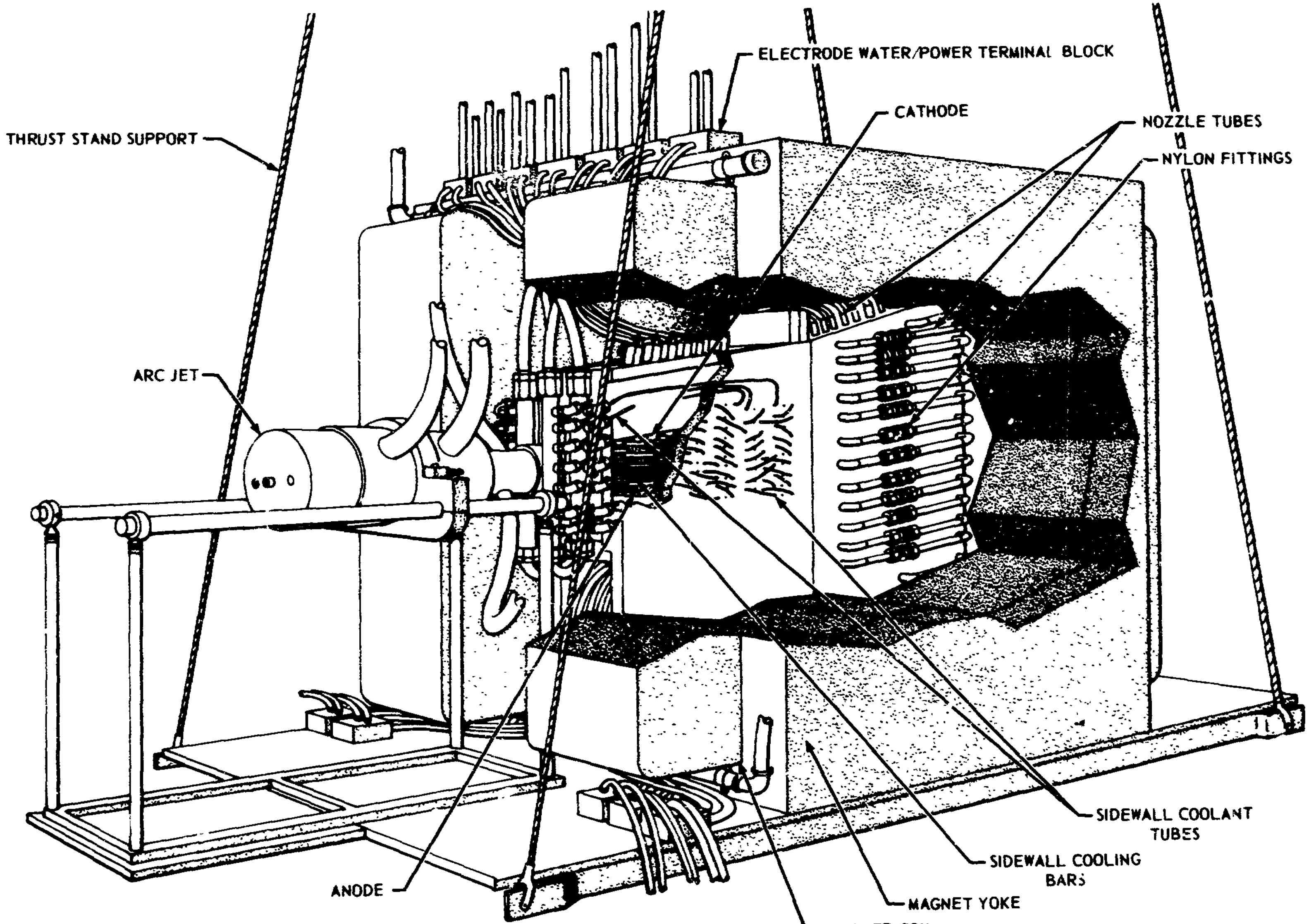

Figure 8.1 Cutaway sketch of accelerator CA1 and arc jet shown mounted on thrust stand

9. PRELIMINARY DESIGN AND RECOMMENDATIONS FOR DEVELOPMENT OF A 10 MW AIR PLASMA ACCELERATOR

9.1 A Preliminary Design

A specific design utilizing a simple power relation between velocity and enthalpy, has been selected for accelerating 0.0454 Kg/sec (0.166/sec) of air plasma from 6320 to 12,200 m/sec (40,000 ft/sec) and from a Mach number of 3 to 3.9 in 54.7 cm at a constant pressure of 4.5 Torr. An inlet stagnation enthalpy of 5×10^7 j/Kg is required. Segmented, water-cooled metal sidewalls and presently-available electrodes and electrode holders appear to be adequate. Design for further acceleration appears feasible. The aspect ratio of the channel is practical. Based on a constant width of 18.1 cm, the channel height varies from an initial 18.1 cm to 24 cm, thence back down to 19.2. The first 40 cm of the channel operates at approximately constant Mach number, the Mach number increasing in the last 15 cm.

The maximum arc column voltage gradient in the design is 6.9 volts/cm. Existing sidewalls will effectively withstand up to 50 volts/cm. The back e.m.f. gradient rises monotomically to 23.4 volts/cm.

The basic mechanical design elements, including insulators, electrodes, electrode holders, and sidewalls incorporated in the 500 Kw design appear suitable for use in the 10 MW design except perhaps that sidewall elements should be more strongly water-cooled.

Further information on the design based on the analysis of Reference 5 is as follows:

The design is based on relatively high inlet enthalpy which was found necessary to keep the accelerator length reasonably low. This dependence is very strong. The design is based on constant pressure to simplify calculations. In a real accelerator a favorable (negative) pressure gradient would improve boundary layer flow. Boundary layer and heat transfer effects can best be treated by iteration in design and the present method is a reasonable first step.

All units are MKS, except as noted.

A. Design Conditions

Fluid: Air plasma

$p = 4.5$ Torr

$H_1 = 3 \times 10^7$

$H_{T1} = 5 \times 10^7$ (21,500 Btu/lb)

$\mu_1 = 6320$ (for $\eta = 40\%$ for pre-accelerator)

$\mu_2 = 12,200$ (40,000 fps)

$T_1 = 5680^\circ$ K

$\rho_1 = 2.17 \times 10^{-4}$

$\dot{m} = 0.0454$ (0.1 lbs/sec)

Thermodynamic equilibrium in the gas and electrical properties, per Appendix C

[illegible] $= 1$ (optimum B-field)

$A_1 = 327 \times 10^{-4}$ or 18.1 cm x 18.1 cm (square)

A composite design is recommended. In the first section (to $x = 40$ cm) the design is for approximately constant Mach number, i.e., $r = 1/2$ in the equation:

$$u = u_1 \left(\frac{H}{H_1}\right)^r$$

and conditions at the exit (station 2') are such that:

$j_{2'} = 225,000$ $\rho_{2'} = 1.54 \times 10^{-4}$

$T_{2'} = 6900$ $A_{2'} = 403\ cm^2 = 18.1 \times 22.3\ cm$

$u_{2'} = 7300$ $H_{2'} = 4 \times 10^7$

From thispoint on, a value of r - 1, corresponding to a rising Mach number, can be used. Holding j at 225,000 to avoid electrode deterioration, the following parameters are calculated.

Length of second section = 14.7 cm. At station 2, the exit:

$H_2 = 6.68 \times 10^7$ $T_2 = 9650$

$\rho_2 = 1.07 \times 10^{-4}$ $A_2 = 348\ cm^2 = 18.1 \times 19.3\ cm$

Internal power required = 4.14 MW

Electrode fall power = 0.37 MW

Internal frequency = 60%

Plasma generator power (at 40% efficiency of investment in total enthalpy) = 5.68 MW.

Total power per above = 10.2 MW

Total arc current = 12,500 amperes.

The electrode voltages are:

Sta.	$\frac{\bar{V}}{h}$	$\frac{V_b}{h}$	h	$\bar{V} + V_b$	$\bar{V} + V_b + V_d$
1	2.7	1.8	18.1	81.5	111.5
2'	6.9	4.6	22.4	258	288
2	4.3	23.4	19.2	532	562

which voltages are in a reasona le range.

The applied magnetic field required varies from -150 gauss at the entrance to 2900 at the exit (at 55 cm).

The form of the accelerator is shown in Figure 9.1.

The nozzle added downstream is needed to carry the gases through the fringing field and expand the gases to the selected test-section conditions. This nozzle should be contoured as required.

The stagnation enthalpy at the exit is 14.1×10^7, equal to 60,000 Btu/lb, 53% of which is invested in directed kinetic energy.

This design is notable for having a practical aspect ratio, low arc column voltage and modest back emf.

A possible improvement, to simplify the power supplies and avoid arc lowdown is to design for constant voltage in the second section. This would call for rising current density, but this would remain within acceptable limits.

Extrapolating to the viscid flow case, a possible concern is the lack of back-emf generated in the boundary layer flow. The boundary layer must be maintained sufficiently cool to avoid short-circuiting through this region. Further study is required on heat transfer, radiation and boundary layer effects. The present model can serve as a basis for this study.

9.2 RECOMMENDED DEVELOPMENT PROGRAM

The following outline indicates recommendation for the course of a development program.

A. Theoretical studies

1 One-dimensional theory

a. Mach number reduction in first section

b. Design for constant or rising voltage

(1) Sidewall breakdown

(2) Arc blowdown

c. Stability and starting

d. Wall friction and heat losses

2. Slab theory (two-dimensional)

a. Boundary layer characteristics

b. Charge, momentum and energy transport

c. Short circuits through boundary layer

d. Nonuniform (core) heating

B. Critical Experiments

1. Selection of preheaters and preaccelerators to provide high enthalpy gases.

a. The Ducati plasma generator

b. The Ames constricted arc

c. Use of arc-holders and nonuniform heating across flow stream.

2. Methods for shaping the B-field for optimum performance.

3. Methods for ballasting electrodes for arbitrary control of current density.

4. Multiple electrodes developing single arc path

5. Blowdown of arcs in constant or rising-voltage design

C. Test of Full Scale Model by Pulse Method

1. 1 to 10 ms test duration

2. Simple uncooled configuration

3. Minimal materials problems

4. Condenser energy storage (for minimum cost)

5. Vacuum storage (for minimum cost)

6. Verification of configuration performance

7. Use of photographic and pulse instruments.

D. Design of Full Scale Water-Cooled Accelerator for Steady State Operation

It is visua'ized that Phases A and B would be run concurrently, leading to the selection of a design for Phase C. Results of these tests would, with the theoretical background, lead to this design of Phase D. It should be emphasized that the basic accelerator elements developed for the present program are believed suitable for the full scale application. It is proposed to improve the employment of these elements in an accelerator configuration by employing an improved mathematical model and test procedures as outlined above.

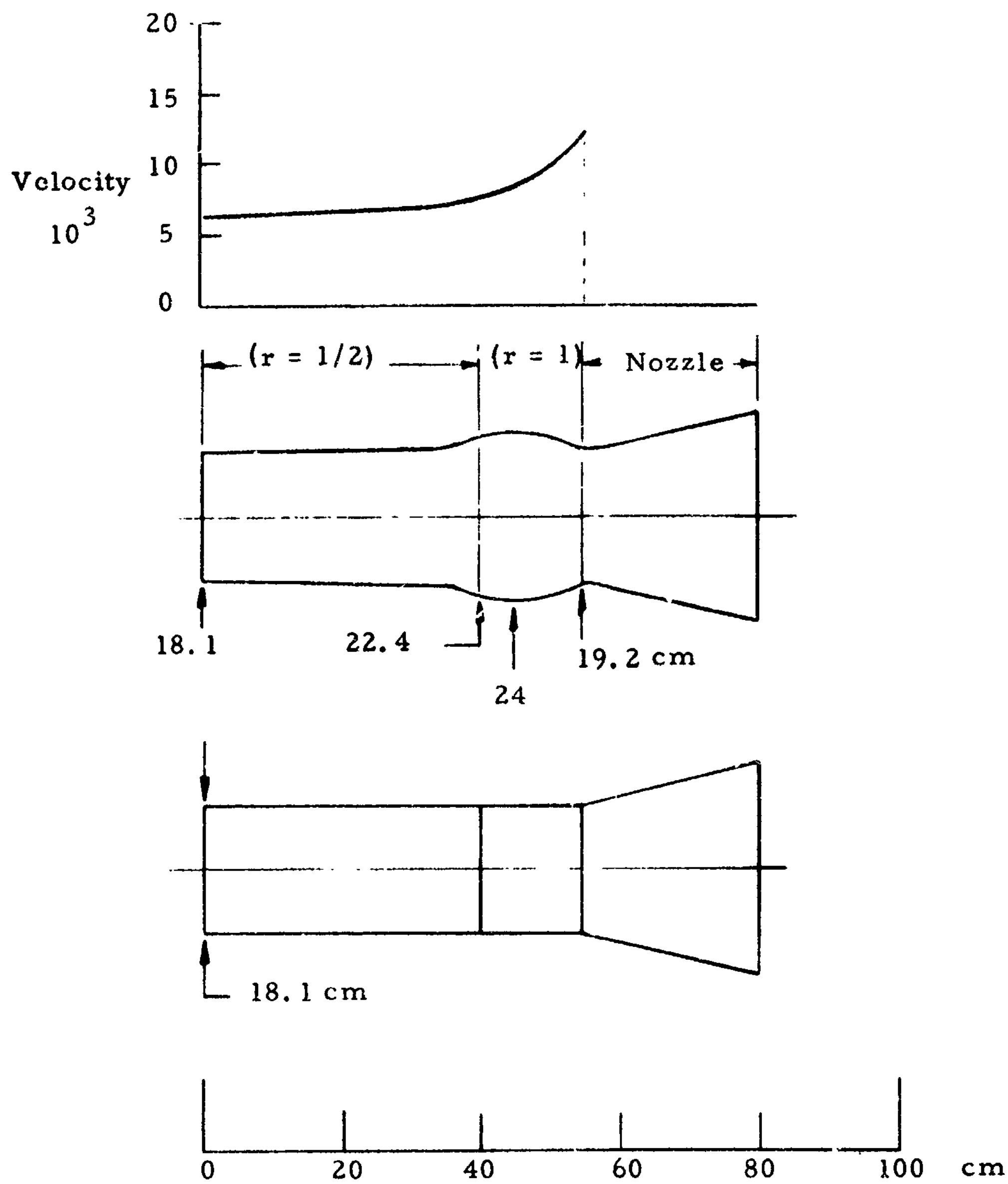

Figure 9.1. Contour of accelerator

REFERENCES

1. S. T. Demetriades, G. L. Hamilton, R. W. Ziemer, R. W. Jarl, and P. D. Lenn, "Three-Fluid Nonequilibrium Plasma Accelerators, Part I," ARS Preprint 2375-62, presented at ARS Electric Propulsion Conference, Berkeley, California, March 1962, Progress in Astronautics and Aeronautics AIAA Series, Vol. 9, Electric Propulsion Development, Academic Press, New York pp 461-511.

2. Northrop Space Laboratories Report NSL 62-113-10, Experimental and Analytical Investigations of Crossed-Field Plasma Accelerators, Final Report on Contract AF 33(657)-8558, ASD-TDR-63-307, May 1963.

3. P. D. Lenn, J. R. Bodoia, D. L. Ward, G. L. Hamilton, and S. T. Demetriades, "Three-Fluid Nonequilibrium Plasma Accelerators, Part II," AIAA Preprint 63047, presented at AIAA Electric Propulsion Conference, Colorado Springs, Colorado, March 1963.

4. Chance Vought Research Center Report No. RE-IR-14, "The Thermodynamic Properties of High Temperature Air."

5. R. C. Brumfield, "A Method for Optimizing the Design of Linear Crossed Field Accelerators", Internal Report No. 650, 15 March 1964, MHD Research, Inc.

APPENDIX A

THE ACCELERATOR FACILITY

The accelerator experiments were run in a facility installed in the Northrop Space Laboratory in Hawthorne, California. The following major equipment items were utilized in the experiments:

Vacuum test tanks: 8 feet diameter x 15 feet long, stainless steel with full diameter access, view ports and conduct flanges (water, power, microwave, and instrument leads) Figure 23.

Power supplies for arc head and accelerator:

6 A O Smith	80 KW, 80 V, 160 V, 320 V
3 Miller	40 KW, 80 V,
3 Miller	40 KW, 80 V, 160 V, 320 V.

Magnet power supply: 30 KW, 75 V, 400 amps. Westinghouse "Silicon welder" rectifier

Magnet: Bux-Schrader, water cooled
Pole faces, 4 and 6 inches high x 12 inches long,
10,000 gauss maximum at 4 inch gap.
10 inches between coils.

Vacuum pump: Roots - Connersville, 14,000 cfm, 3 stage. 0.5 torr minimum pressure with accelerator operating 0.1 torr at blank-off.

Dynamometer: Ballistic pendulum type carrying entire plasma generator, accelerator, magnet assembly. Restrained by small cantilever with strain gauge transducer. Calibrated by external force applied by wire through tank door, Figure 8.1

Gas-cooled system: water-cooled coils capable of absorbing up to 750 KW

Water-cooling system: Stored tap water. 300 gpm @ 250 psi.

APPENDIX B

INSTRUMENTS AND RECORDING

Control panel:

Water flow meters: Fischer-Porter for arc head, de Laval nozzle, magnet and calorimeter

Temperature recorder: MH 12 point

Pressure gauges: W&T 0-20 torr
$0\text{-}150^{\circ}F \pm 1/2^{\circ}F$ for copper-constantan thermocouples

Traversing mechanism:

Two-directional remotely controlled electrically-driven for jet survey. Capable of carrying the rake or combination calorimeter and stagnation pressure tube.

Control console for electrodes:

Texas Instrument chart recorder for voltage and current.

Sanborn Recorder for magnet current and thrust (strain gauge) recording.

Voltmeter panel for sidewall voltage monitoring. This was photographed at 24 frames per second on 16 mm film.

Temperature recorder: Brown Instrument Co.

APPENDIX C

MICROWAVE MEASUREMENTS

Microwave systems have been widely used to measure the properties of arc heated plasma. The theory has been developed and significant measurements have been made. The work of Jahn at California Institute of Technology, Ref. C1, and Nighan, Warder, Brodwin, and Cambel at Northwestern University, Ref. C2, are relevant to the present study.

The basic theory for a low loss system (Ref. C2) gives the electron number density and collision frequency in terms of the observed phase change and attenuation of an electromagnetic wave propagating through the plasma. Knowing the electron density and collision frequency one may calculate the so-called plasma dc conductivity which characterizes the plasma. The equations used are shown below.

$$N_e = \frac{\omega^2 e_o M_e}{e^2}\left[1 - \frac{C}{\omega^2}\left(\beta_o - \frac{\Delta\phi}{d}\right)^2\right]$$

$$\nu_c = \frac{ZC^2 \Delta\alpha}{\omega d}\left[\frac{\left(\beta_o - \Delta\phi/_d\right)}{1 - \frac{C^2}{\omega^2}\left(\beta_o - \Delta\phi/_d\right)^2}\right]$$

$$\sigma_{d.c.} = \frac{e^2 N_e}{M_e \nu_c}$$

where the following definitions hold

$\omega = 2\pi f$ where f is the microwave frequency in cps

$e_o = \frac{1}{36\pi} \times 10^{-9}$ farads/m, the free space dielectric constant

$M_c = 9.108 \times 10^{-31}$ Kg, the electron mass

$e = 1.6 \times 10^{-19}$ coulomb, the electronic charge

$C = 3 \times 10^{8}$ m/sec, the speed of light in a vacuum

$\beta_o = \frac{\omega}{c} \frac{rad}{m}$, the free space phase constant

$\Delta\Phi =$ change microwave phase in radians

d = width of plasma slab

ν_c = electron versus neutral collision frequency, sec^{-1}

σ = electrical conductivity in mhos/meter

To use these equations one simply has to determine the attenuation and phase shift introduced by the plasma on a microwave beam at frequency ω. The microwave circuit used is shown in the accompanying Figure C1. With the plasma jet in a large vacuum vessel, vacuum windows are used in the waveguide lines. The waveguide is then run through the walls of the chamber. Figures C3 - C5 indicate the microwave apparatus and installation in the vacuum tank.

Microwave Circuit

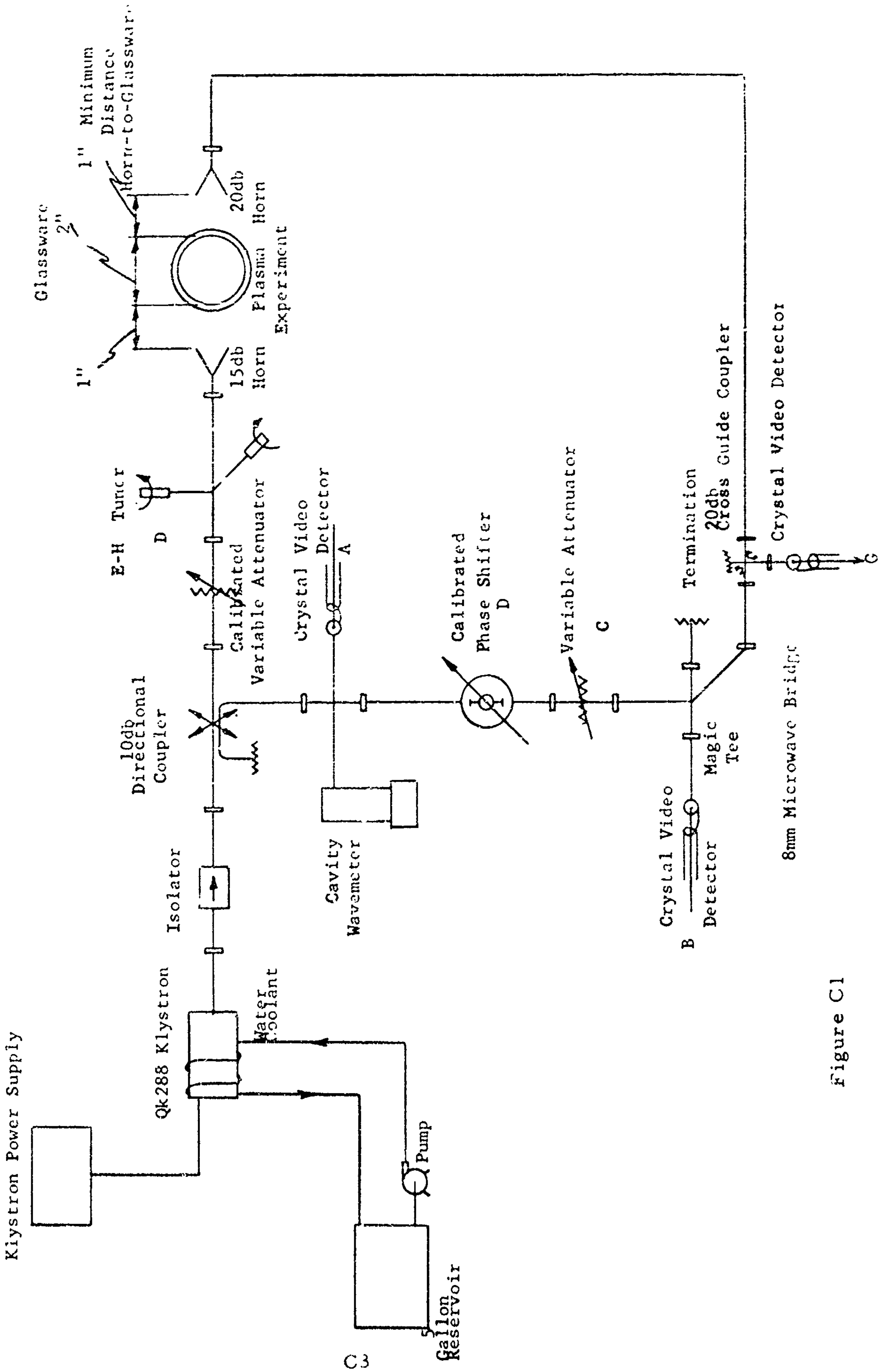

Figure C1

The procedure for use of the 8 mm microwave bridge is as follows:

1. Turn on the FXR filament switch. This will also start the pump.
2. After a 5 minute wait the high voltage may be turned on. The beam, repeller, and focus voltages should be adjusted to the values shown on the klystron data card. One must watch the beam current during this tune up procedure. If the beam current exceeds the rated value the cause of the over current must be corrected immediately.

To use the H. P. standing wave indicator as an amplitude detector at crystal video detector G, a 1 kc/sec square wave modulation should be applied to the repelier. The klystron tuning and voltages may now be adjusted for a maximum signal at crystal G.

The frequency may be determined at any time by tuning the cavity wavemeter for a response at crystal A.

The phase sensitive output of the bridge is obtained at crystal B. The display of the phase is smoothed by adding several filter capacitors across the oscilloscope input. This slows the response of the phase display so that the pump vibration and 1 kc/sec modulation is not seen. To balance the bridge the phase shifters and attenuator in the reference arm are adjusted for a minimum (null output) at crystal A. A calibration curve similar to the one shown, Figure C2, may now be obtained. Another possible mode of operation is recording the dial settings of the phase shifter before and after the balancing of the bridge, with changing plasma conditions, then referring to the phase shifter calibration charts.

f_o = 36.3 gc

Data taken with an air '·· ' path.
Voltages were taken as deflections on a 551 scope display with Type L preamp.
The crystal detector had a 10 K ohm termination.

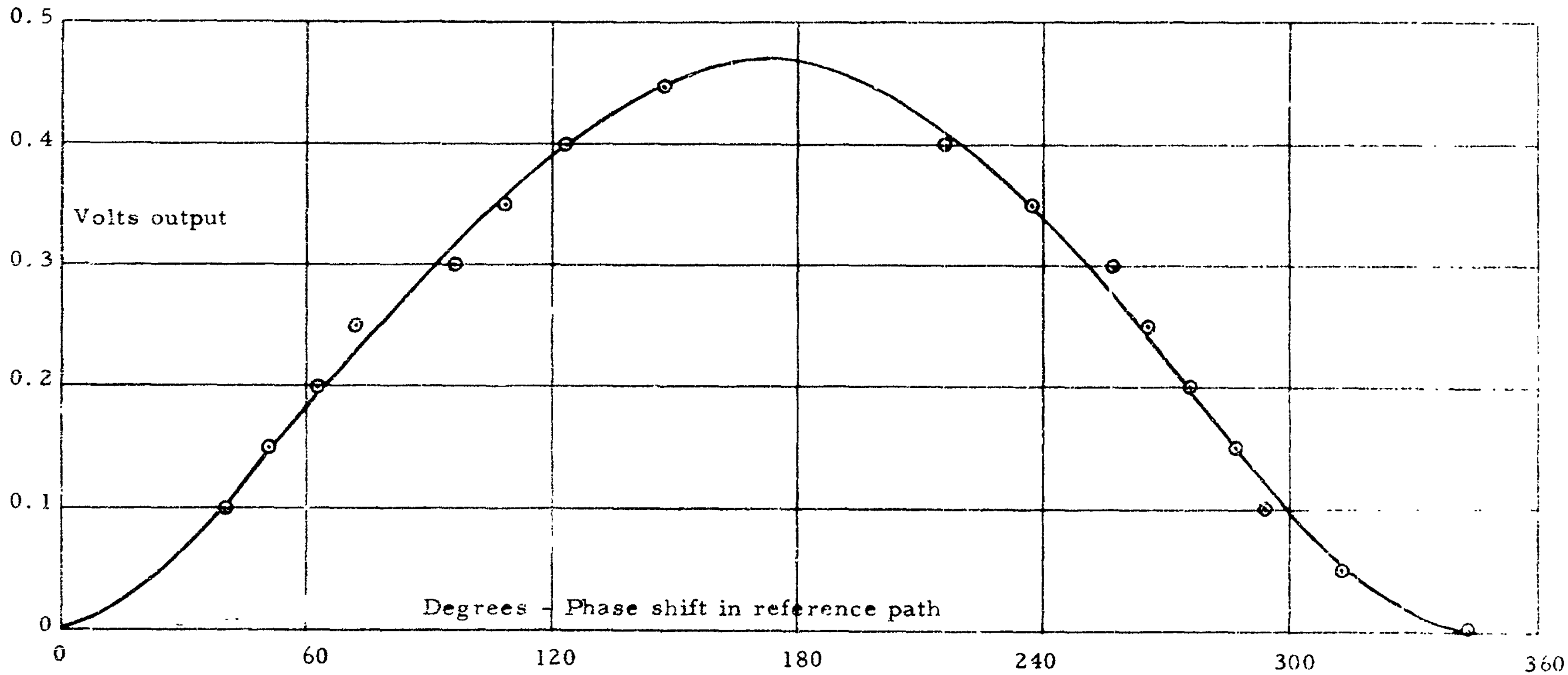

Figure C2
8 mm Interferometer Calibration Curve - Air Path

With the bridge balanced the plasma properties are determined as follows:

Phase is measured by allowing the input power to the arc to be run up to the maximum. When the flow is stabilized the bridge is balanced. Then as the arc input power is decreased in steps the bridge is constantly rebalanced noting the phase shifter dial settings corresponding to changes in flow conditions. Observing the bridge phase variations the number of maxima and minima passed through is easy to determine.

The attenuation constant is determined by noting the output level of the power monitor before the arc is turned on. Then at stabilized flow conditions the amount the output has decreased is recorded. With no plasma present this decrease may be reproduced by inserting the calibrated attenuator and recording the attenuation value.

The measurements described above were performed on three separate occasions on the arc jet at the Northrop facility. The data from two of the runs is inconclusive due to the unstable operation of the arc jet. The attenuation data is a good indicator of proper alignment of the microwave horns and the jet. If the attenuation of the microwave signal is steady and constant for the operating condition the flow conditions are well defined. In the unstable mode the microwave energy seemed to increase due to diffraction of the microwave beam around the plasma column.

For a microwave measurement 36" away from the arc jet the following values were obtained:

$f = 36.3$ gc/sec

$d = 0.14$ m, the thickness of the plasma slab

$\Delta \;=\; 1.13$ radians

$\Delta\alpha \;=\; 0.47$ nepers

The arc electrical input was 650 amperes at approximately 140 volts. For these experimental values one may calculate an electron number density of 3.3×10^{11} electron/cc, a collision frequency of 1×10^{11}/sec, and a conductivity of 9×10^{-2} mho/meter.

REFERENCES

C1 John, Robert G., "Interaction of Electromagnetic Waves with slightly Ionized Gases", Tech. Note No. 2, August 1960. California Institute of Technology, Pasadena, California.

C2 Nighan. Warder, Brodwin, and Cambel, "Microwave Diagnostics of Arc Heated Plasmas", Northwestern University, Evanston, Illinois.

APPENDIX D

PLASMA CONDUCTIVITY PROBE

A device has been studied which shows promise of a capability for measuring the electrical conductivity of a plasma with minimal disturbance to the flow. This device has the advantage of being based on experimentally verified theory (D1) and appears adaptable to the present requirement of measuring the effective conductivity of a plasma flow stream (D2). The probe configuration is shown in Figure D1.

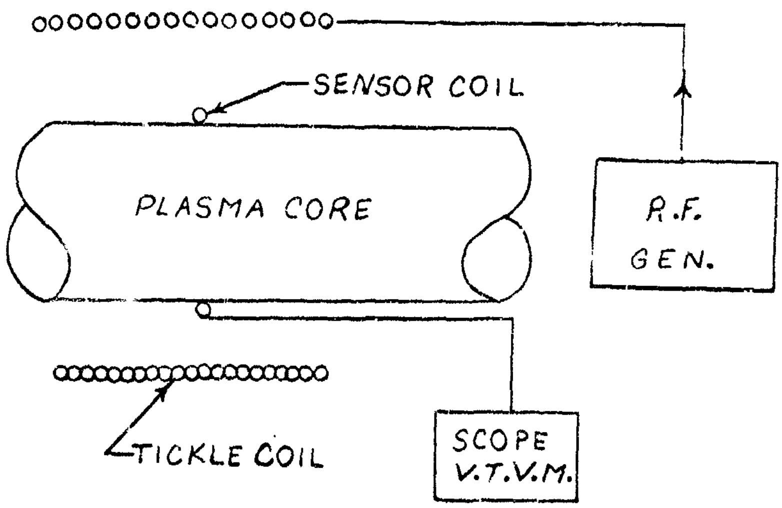

Basic Conductivity Measuring Device
Figure D1

High frequency current is passed through a solenoid-type tickle coil creating a high frequency magnetic field which penetrates the volume subtended by the tickle coil. Coaxial with the tickle coil is a sensor coil across which is induced a voltage dependent on the time rate of change of the magnetic flux through its cross section. When any conductor is present in the volume of the sensor coil, it is found that the voltage induced in the coil is decreased from the value obtained when no conductor is present by an amount dependent on the material's conductivity and the frequency of the magnetic field. Therefore, knowledge of the applied frequency and observation of the induced sensor coil voltage yields a measurement of the conductivity of the material coaxial with the sensor coil.

The theoretical principles upon which this device is based are presented below:

Coaxial with the plasma is a long solenoid carrying a weak rf current $\check{I}$. (The notation $\check{A}$ implies $\check{A} = A_o e^{i(\omega t + \theta)}$, with ω the angular frequency of the ac quantity and θ its phase).

The solenoid has n turns per unit length, so the magnetic induction in MKS units is given by

$$\check{B}_z = \mu_o n \check{I} \tag{1}$$

The electric field vector $\underline{E}$ is eliminated from Maxwell's equations by substitution. If the magnetic induction has a sinusoidal variation and if the plasma conductivity is uniform, the following expression for the behavior of the magnetic field in the plasma is obtained:

$$\nabla^2 \check{\underline{B}} - i \sigma \mu_o \omega \check{\underline{B}} = 0 \tag{2}$$

In a cylindrical geometry, where $\underset{\sim}{k}\check{B}_z \equiv \check{\underline{B}}$, equation (2) reduced to the well-known eddy current equation

$$\frac{d^2\check{B}_z}{dr^2} + \frac{1}{r}\frac{d\check{B}_z}{dr} - i\sigma\mu_o\,\omega\check{B}_z = 0 \qquad (3)$$

The solution for (3) is evaluated at the boundary where $r = R$, the outer radius of the plasma, with $\check{B}_z(R) = \check{B}_o$, and again at $r = O$, along the axis, where $B_z(O)$ is finite, to obtain

$$\check{B}_z(r) = B_o \frac{J_o(\sqrt{-i\sigma\mu_o\,\omega}\, r)}{J_o(\sqrt{-i\sigma\mu_o\,\omega}\, R)} \qquad (4)$$

The quantity J_o is the zeroth order Bessel function, in this case with a complex argument.

The distance which an electromagnetic wave penetrates into a conductor before falling to $1/e$ of its initial value is called the "penetration skin depth", δ, of the wave in the conductor, where

$\delta = \frac{2}{\sigma\mu_o\,\omega}$. Substitution of this relation in (4), and noting that

$-i = i^3$, yields

$$\check{B}_z(r) = B_o \frac{J_o(\sqrt{2}\; i^{3/2}/\delta\, r)}{J_o(\sqrt{2}\; i^{3/2}/\delta\, R)} \qquad (5)$$

Clearly the radial value of the magnetic induction is strongly dependent on the ratio R/δ. We take advantage of this in the technique for conductivity determination.

Integrating $\check{B}_z(r)$ over the sensor loop area yields the magnetic flux I.

$$\Phi = \int \underset{\sim}{B} \cdot \underset{\sim}{N}\, ds = \check{B}_o \pi R^2 \left(\frac{\delta}{\sqrt{2}R}\right) \frac{J_1\left(\frac{\sqrt{2}\, i^{3/2} R}{\delta}\right)}{J_o\left(\frac{\sqrt{2}\, i^{3/2} R}{\delta}\right)} i^{-3/2} \qquad (6)$$

This expression is easily handled in the notation of McLachlan[D5]:

$$\Phi = B_o \pi R^2 \left(\frac{\delta}{\sqrt{2}R}\right) \frac{M_1\left(\frac{\sqrt{2}\,R}{\delta}\right)}{M_o\left(\frac{\sqrt{2}\,R}{\delta}\right)} \exp\left[i\left(\theta_1 - \theta_o - \frac{\pi}{4}\right)\right], \qquad (7)$$

where

$$M_j(Z)_e\, i\theta_j(z) = J_j(Z i^{3/2}),$$

and

$$\theta_j(Z) \quad \tan^{-1} \frac{\mathrm{beij}(Z)}{\mathrm{berj}(Z)}$$

these functions are tabulated by McLachlan.

In the laboratory one observes the voltage induced on the sensor coil and calculates from this the magnetic flux. The radius, frequency, and permeability are known, so equation (7) can now be solved for the conductivity, σ.

Experimentally, it is convenient to make relative measurements. For a constant current the relation flux for two situation is written:

$$\left(\frac{\Phi}{\Phi}\right) = \frac{\delta}{\delta_o} \frac{M_1\left(\frac{\sqrt{2}\,R}{\delta}\right)}{M_o\left(\frac{\sqrt{2}\,R}{\delta}\right)} \frac{M_o\left(\frac{\sqrt{2}\,R}{\delta_o}\right)}{M_1\left(\frac{\sqrt{2}\,R}{\delta_o}\right)} C^{i\gamma} \qquad (8)$$

where

$$X = \left[\theta_1\left(\frac{\sqrt{2}\,R}{\delta}\right) - \theta_1\left(\frac{\sqrt{2}\,R}{\delta_o}\right) + \theta_o\left(\frac{\sqrt{2}\,R}{\delta_o}\right) - \theta_o\left(\frac{\sqrt{2}\,R}{\delta}\right)\right] \tag{9}$$

We measure the magnitude of this ratio:

$$\left|\frac{\Phi}{\Phi}\right| = \frac{\delta}{\delta_o}\ \frac{M_1\left(\frac{\sqrt{2}\,R}{\delta}\right)}{M_o\left(\frac{\sqrt{2}\,R}{\delta}\right)}\ \frac{M_o\left(\frac{\sqrt{2}\,R}{\delta_o}\right)}{M_1\left(\frac{\sqrt{2}\,R}{\delta_o}\right)} \tag{10}$$

The conductivity of the gas in the volume subtended by the solenoid prior to the ignition of the plasma is essentially zero; hence $\delta\,(\sigma = O)\ \ \infty$ and

$\frac{2R}{\delta_o} \rightarrow O$. Now, in general

$$M_j^2\,(Z) = \sum_{k=O}^{\infty}\left[\frac{(1/2\ Z)^{2j+4k}}{k!\,\Gamma(j+k+1)\,\Gamma(j+zk+1)}\right] \tag{11}$$

so we have

$$\frac{M_o\left(\frac{\sqrt{2}\,R}{\delta_o}\right)}{M_1\left(\frac{\sqrt{2}\,R}{\delta_o}\right)}\cdot\frac{1}{\delta_o} = \frac{\left[M_o\left(\frac{\sqrt{2}\,R}{\delta_o}\right)\right]\frac{1}{2}}{M_1\left(\frac{\sqrt{2}\,R}{\delta_o}\right)\Big/\frac{2}{\delta_o}} \tag{12}$$

Using (11), the following can be shown:

i) $\lim\limits_{z \to o} M_o(KZ) = 1$

ii) $\lim\limits_{z \to o} \frac{1}{k}\ M_1(kZ) = \frac{Z}{2}$

Therefore, when $\delta \to \infty$ ($\sigma_o = 0$) we set $\frac{\sqrt{2}}{\delta_o} = k$ in (12), and obtain

$$\frac{1}{\delta_o} \frac{M_o\left(\frac{\sqrt{2}\,R}{\delta_o}\right)}{M_1\left(\frac{\sqrt{2}\,R}{\delta_o}\right)} = \frac{2}{\sqrt{2}\,R} \tag{13}$$

Finally, for a measurement of flux relative to the flux observed with no plasma present, one obtains

$$\left|\frac{\Phi}{\Phi}\right| = \left(\frac{\delta}{2\,R}\right) \frac{M_1\left(\frac{\sqrt{2}\,R}{\delta}\right)}{M_o\left(\frac{\sqrt{2}\,R}{\delta}\right)} \tag{14}$$

The validity of the expression for the magnetic flux was established in an experiment [D4] shown schematically in Figure D2.

A sensor coil was wound about a glass tube and mounted coaxially with a larger solenoid. The solenoid was driven by a variable frequency signal generator and the voltage induced on the sensor coil was observed on an oscilloscope. A cylinder of copper representing an infinite conductivity, was placed in the glass tube and the output of the signal generator was adjusted until a particular voltage was induced on the sensor coil. The copper was then removed and another conductor inserted and the new voltage recorded. This process was repeated over a wide frequency range in order to allow measurements over a wide range in skin depth which was varied so that the ratio $2R/\delta$ covered the range of, roughly, one to seventy-five.

The results are plotted in Figure D3 in which the points are experimental. The solid line is the theoretical flux prediction, normalized to the value calculated for copper.

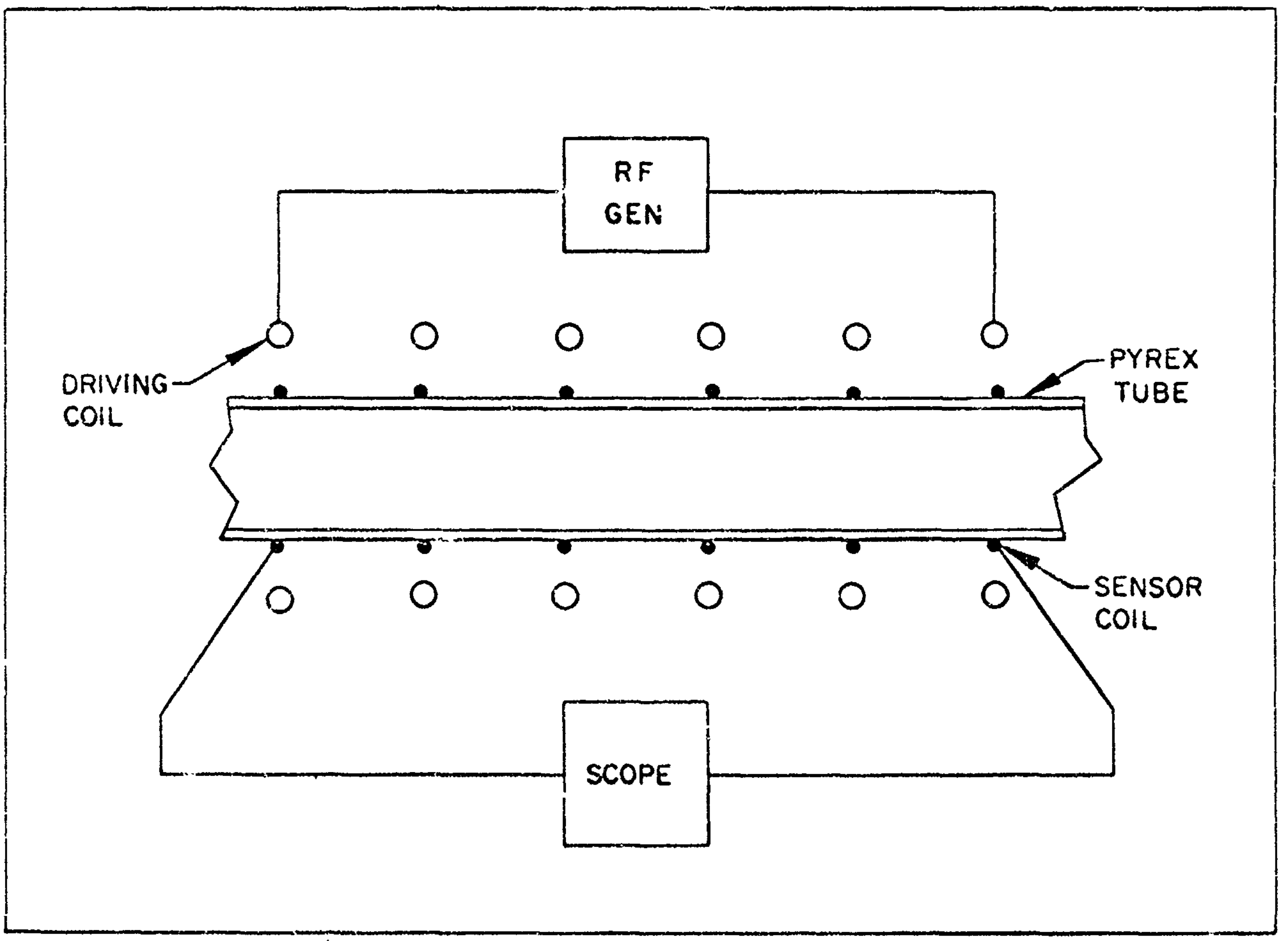

SCHEMATIC OF VERIFYING EXPERIMENT

Figure D2

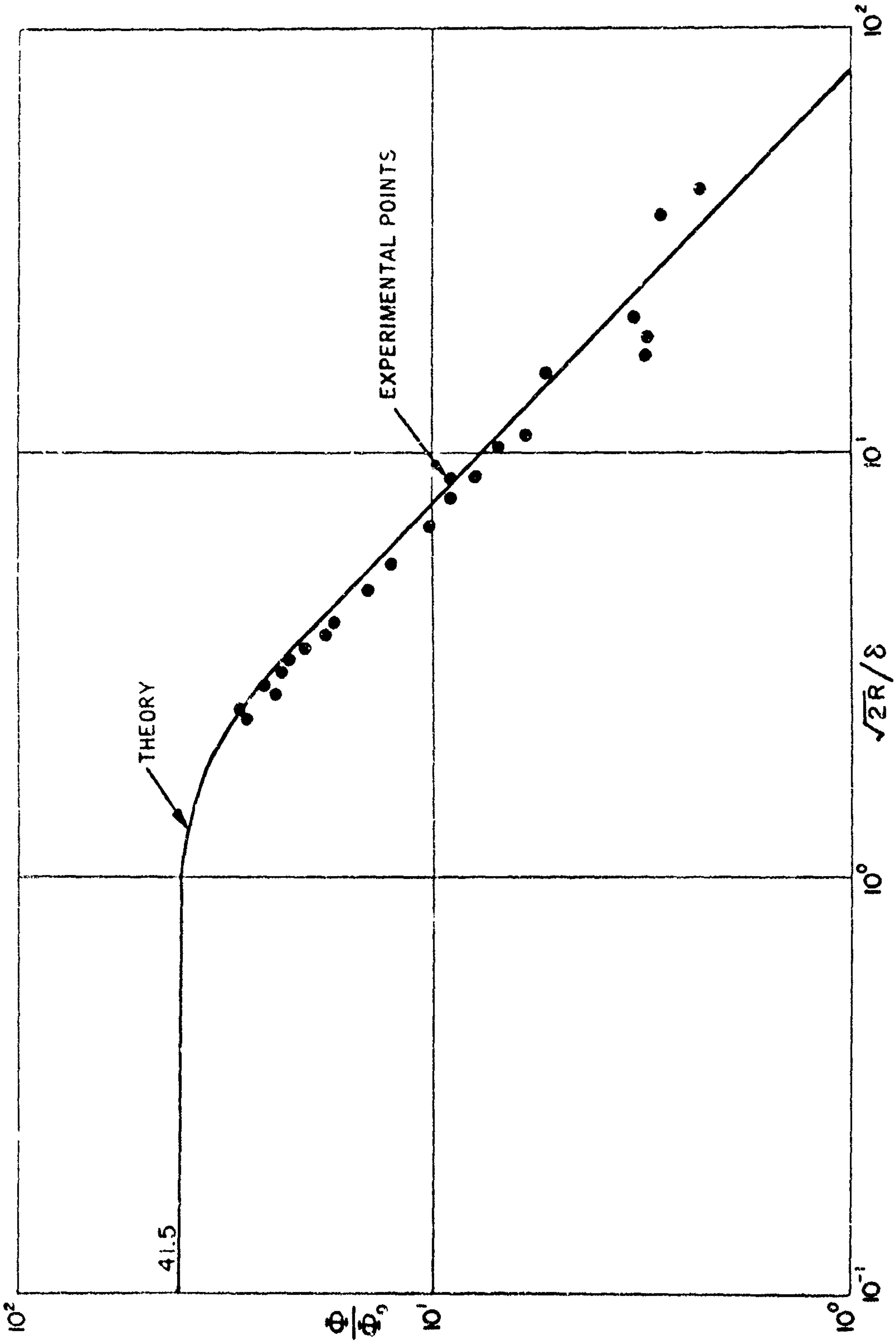

COMPARISON OF EXPERIMENT WITH THEORY

Figure D3
page D8

An immersible electrical conductivity probe based on the above theory, is shown in Figure D4.

A high-frequency current is passed through a tiny one-turn loop of wire resulting in the establishment of a high-frequency magnetic field within the loop. Coaxially positioned with this driver loop is a sensor coil which samples the magnetic field of the driver. The voltage induced in the sensor coil is indicated by a suitable voltmeter. Since the magnitude of the magnetic flux linking the sensor is dependent on the conductivity of the medium in which the probe is immersed, the induced voltage gives a measure of the conductivity of the medium. After a suitable calibration with materials of known conductivity, the voltmeter will read directly in "mhos per meter".

The spatial resolution of such a device is on the order of its diameter, hence detailed surveys of the plasma conductivity are possible.

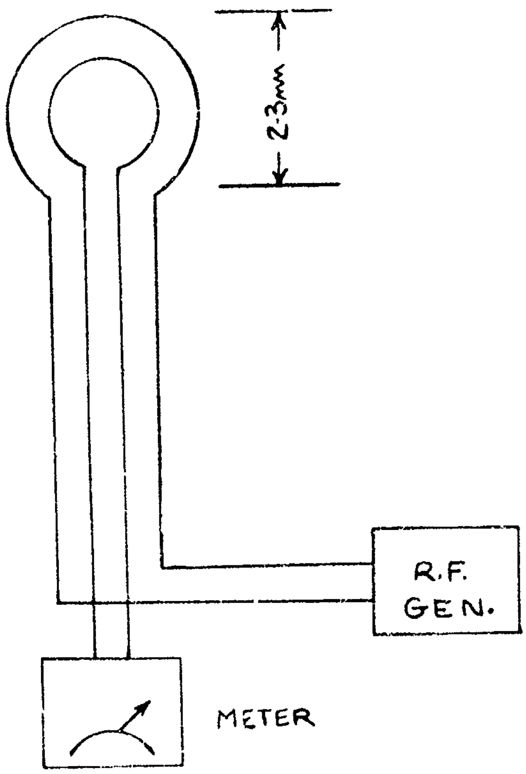

Immersible Conductivity Probe

Figure D4

page D10

APPENDIX D

REFERENCES

D1 Hollister, D. D., Bull. Amer. Phys. Soc., 7, 373 (1962).

D2 Rockman, Hollister, Sunderland, Final Report contract number AF 29(601)-5090; MHD Research, Inc., Newport Beach, Calif. Feb. 1963.

D3 McLachlan, N. W., "Bessel Functions for Engineers", Oxford University Press, London, Ed. 2, 1955.

D4 Hollister, D. D., Bull. Amer. Phys. Soc. 7, 441 (1962).

APPENDIX E

CURRENT DENSITY PROBE

A device known as the "j-probe" has been studied for application to measurements in the accelerator plasma.

The underlying principle of this device is Ampere's circuital law which states that the magnetomotive force (m. m. f.), i. e., the line integral of the magnetic field intensity H, around a closed contour, is 4π times the total current through the contour:

$$\oint \underset{\sim}{H} \cdot ds = 4\pi \int \underset{\sim}{J} \cdot d\underset{\sim}{s}, \text{ (emu)} \tag{1}$$

where $\underset{\sim}{J}$ is the current density.

Consider a single-turn planar loop of some suitable ferromagnetic material oriented so its plane is normal to the direction of current flow as in the accompanying sketch. If J is the magnetide of the average density of the current through the loop of inner diameter D then by equation (1) the m. m. f. around the loop is

$$\oint \underset{\sim}{H} \cdot d\underset{\sim}{s} = (\pi D)^2 J \tag{2}$$

Thus, the desired density is proportional to the m. m. f. and the problem is to devise means for sensing the latter quantity. There are several possible solutions, one of which is to employ the Hall effect.

If a plate of an appropriate conductor or semiconductor is inserted in the magnetic circuit the resulting Hall voltage is given by

$$V_H = K \frac{IB}{t} \tag{3}$$

where K is the Hall coefficient, I is the current through the plate, B is the magnetic induction, and t is the thickness of the plate in the direction of B.

The magnetic flux BA through the plate of area A normal to the field is related to the m. m. f. by

$$BA = \frac{1}{R} \oint \underset{\sim}{H} \cdot d\underset{\sim}{s} \tag{4}$$

in which R is the reluctance of the magnetic circuit. Assuming for simplicity that the reluctance of the circuit is primarily in the Hall plate of permeability μ, that is, the R $t/\mu A$, (4) gives

$$B \approx \frac{\mu}{t} \oint \underset{\sim}{H} \cdot d\underset{\sim}{s} \tag{5}$$

Substituting B from (5) into (3) and the m. m. f. from (2) into the result yields finally

$$J \approx \frac{t^2}{\mu K I (\pi D)^2} V_H \tag{6}$$

Thus, according to (6) the current density to be determined is proportional to the Hall voltage -- ignoring at first glance the variations of K and the circuit reluctance with the magnetic field.

In operation, the ring probe can be swept through the plasma flow stream to prevent over heating and current density measured as a function of position.

The experimental program did not progress to the point of making measurements with this probe.